

# Policy Representation via Diffusion Probability Model for Reinforcement Learning <sup>1</sup>

Long Yang<sup>1,\*</sup>, Zhixiong Huang<sup>2,\*</sup>, Fenghao Lei<sup>2</sup>, Yucun Zhong<sup>3</sup>, Yiming Yang<sup>4</sup>,  
Cong Fang<sup>1</sup>, Shiting Wen<sup>5</sup>, Binbin Zhou<sup>6</sup>, Zhouchen Lin<sup>1</sup>

<sup>1</sup>School of Artificial Intelligence, Peking University, Beijing, China

<sup>2</sup>College of Computer Science and Technology, Zhejiang University, China

<sup>3</sup>MOE Frontiers Science Center for Brain and Brain-Machine Integration & College of Computer Science, Zhejiang University, China.

<sup>4</sup>Institute of Automation Chinese Academy of Sciences Beijing, China

<sup>5</sup>School of Computer and Data Engineering, NingboTech University, China

<sup>6</sup>College of Computer Science and Technology, Hangzhou City University, China

{yanglong001, fangcong, zlin}@pku.edu.cn,  
{zx.huang, lfh, yucunzhong}@zju.edu.cn, {wensht}@nit.zju.edu.cn  
yangyiming2019@ia.ac.cn, bbzhou@hzcu.edu.cn

Code:<https://github.com/BellmanTimeHut/DIPO>

May 23, 2023

## Abstract

Popular reinforcement learning (RL) algorithms tend to produce a unimodal policy distribution, which weakens the expressiveness of complicated policy and decays the ability of exploration. The diffusion probability model is powerful to learn complicated multimodal distributions, which has shown promising and potential applications to RL.

In this paper, we formally build a theoretical foundation of policy representation via the diffusion probability model and provide practical implementations of diffusion policy for online model-free RL. Concretely, we character diffusion policy as a stochastic process induced by stochastic differential equations, which is a new approach to representing a policy. Then we present a convergence guarantee for diffusion policy, which provides a theory to understand the multimodality of diffusion policy. Furthermore, we propose the DIPO, which implements model-free online RL with **DI**ffusion **PO**licy. To the best of our knowledge, DIPO is the first algorithm to solve model-free online RL problems with the diffusion model. Finally, extensive empirical results show the effectiveness and superiority of DIPO on the standard continuous control Mujoco benchmark.

---

<sup>1\*</sup> L.Yang and Z.Huang share equal contributions.

# Contents

<b>1</b>	<b>Introduction</b>	<b>3</b>
1.1	Our Main Work . . . . .	3
1.2	Paper Organization . . . . .	4
<b>2</b>	<b>Reinforcement Learning</b>	<b>5</b>
<b>3</b>	<b>Motivation: A View from Policy Representation</b>	<b>5</b>
3.1	Policy Representation for Reinforcement Learning . . . . .	5
3.2	Diffusion Model is Powerful to Policy Representation . . . . .	6
<b>4</b>	<b>Diffusion Policy</b>	<b>7</b>
4.1	Stochastic Dynamics of Diffusion Policy . . . . .	7
4.2	Exponential Integrator Discretization for Diffusion Policy . . . . .	8
4.3	Convergence Analysis of Diffusion Policy . . . . .	9
<b>5</b>	<b>DIPO: Implementation of Diffusion Policy for Model-Free Online RL</b>	<b>10</b>
5.1	Training Loss of DIPO . . . . .	10
5.2	Playing Action of DIPO . . . . .	11
5.3	Policy Improvement of DIPO . . . . .	11
<b>6</b>	<b>Related Work</b>	<b>12</b>
6.1	Diffusion Models for Reinforcement Learning . . . . .	12
6.2	Generative Models for Policy Learning . . . . .	12
<b>7</b>	<b>Experiments</b>	<b>13</b>
7.1	Comparative Evaluation and Illustration . . . . .	13
7.2	State-Visiting Visualization . . . . .	14
7.3	Ablation Study . . . . .	15
<b>8</b>	<b>Conclusion</b>	<b>16</b>
<b>A</b>	<b>Review on Notations</b>	<b>25</b>
<b>B</b>	<b>Auxiliary Results</b>	<b>26</b>
B.1	Diffusion Probability Model (DPM). . . . .	26
B.2	Transition Probability for Ornstein-Uhlenbeck Process . . . . .	26
B.3	Exponential Integrator Discretization . . . . .	27
B.4	Fokker–Planck Equation . . . . .	27
B.5	Donsker-Varadhan Representation for KL-divergence . . . . .	28
B.6	Some Basic Results for Diffusion Policy . . . . .	28
<b>C</b>	<b>Implementation Details of DIPO</b>	<b>30</b>
C.1	DIPO: Model-Free Learning with Diffusion Policy . . . . .	31
C.2	Loss Function of DIPO . . . . .	31
C.3	Playing Actions of DIPO . . . . .	33

<b>D</b>	<b>Time Derivative of KL Divergence Between Difussion Policy and True Reverse Process</b>	<b>35</b>
D.1	Time Derivative of KL Divergence at Reverse Time $k = 0$	35
D.2	Auxiliary Results For Reverse Time $k = 0$	35
D.3	Proof for Result at Reverse Time $k = 0$	42
D.4	Proof for Result at Arbitrary Reverse Time $k$	44
<b>E</b>	<b>Proof of Theorem 4.3</b>	<b>45</b>
<b>F</b>	<b>Additional Details</b>	<b>48</b>
F.1	Proof of Lemma F.1	48
F.2	Proof of Lemma D.7	49
<b>G</b>	<b>Details and Discussions for multimodal Experiments</b>	<b>50</b>
G.1	Multimodal Environment	50
G.2	Plots Details of Visualization	51
G.3	Results Report	53
<b>H</b>	<b>Additional Experiments</b>	<b>55</b>
H.1	Hyper-parameters for MuJoCo	55
H.2	Additional Tricks for Implementation of DIPO	56
H.3	Details and Additional Reports for State-Visiting	57
H.4	Ablation Study on MLP and VAE	60

# 1 Introduction

Existing policy representations (e.g., Gaussian distribution) for reinforcement learning (RL) tend to output a unimodal distribution over the action space, which may be trapped in a locally optimal solution due to its limited expressiveness of complex distribution and may result in poor performance. Diffusion probability model [Sohl-Dickstein et al., 2015, Ho et al., 2020, Song et al., 2021] is powerful to learn complicated multimodal distributions, which has been applied to RL tasks (e.g., [Ajay et al., 2023, Reuss et al., 2023, Chi et al., 2023]).

Although the diffusion model (or diffusion policy) shows its promising and potential applications to RL tasks, previous works are all empirical or only consider offline RL settings. This raises some fundamental questions: How to character diffusion policy? How to show the expressiveness of diffusion policy? How to design a diffusion policy for online model-free RL? Those are the focuses of this paper.

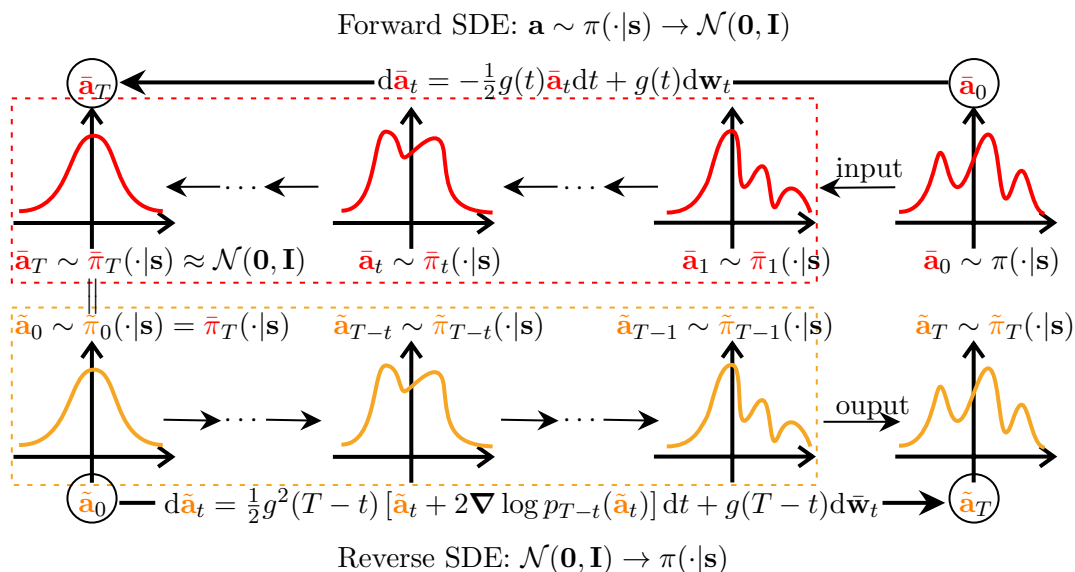


Figure 1: Diffusion Policy: Policy Representation via Stochastic Process. For a given state  $\mathbf{s}$ , the forward stochastic process  $\{\tilde{\mathbf{a}}_t|\mathbf{s}\}$  maps the input  $\tilde{\mathbf{a}}_0 =: \mathbf{a} \sim \pi(\cdot|\mathbf{s})$  to be a noise; then we recover the input by the stochastic process  $\{\tilde{\mathbf{a}}_t|\mathbf{s}\}$  that reverses the reversed SDE if we know the score function  $\nabla \log p_t(\cdot)$ , where  $p_t(\cdot)$  is the probability distribution of the forward process, i.e.,  $p_t(\cdot) = \tilde{\pi}_t(\cdot|\mathbf{s})$ .

## 1.1 Our Main Work

In this paper, we mainly consider diffusion policy from the next three aspects.

**Charactering Diffusion Policy as Stochastic Process.** We formulate diffusion policy as a stochastic process that involves two processes induced by stochastic differential equations (SDE), see Figure 1, where the forward process disturbs the input policy  $\pi$  to noise, then the reverse process infers the policy  $\pi$  according to a corresponding reverse SDE. Although this view is inspired by the score-based generative model [Song et al., 2021], we provide a brand new approach to represent a policy: via a stochastic process induced by SDE, neither via value function nor parametric function. Under this framework, the diffusion policy is flexible to

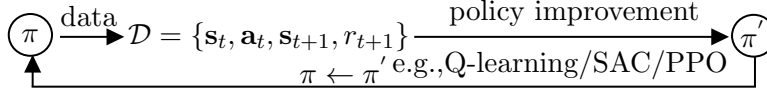


Figure 2: Standard Training Framework for Model-free Online RL.

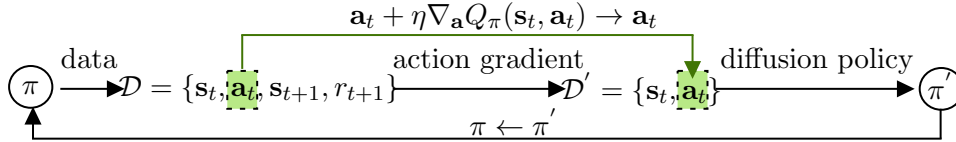


Figure 3: Framework of DIPO: Implementation for Model-free Online RL with **DI**ffusion **PO**licy.

generate actions according to numerical SDE solvers.

**Convergence Analysis of Diffusion Policy.** Under mild conditions, Theorem 4.3 presents a theoretical convergence guarantee for diffusion policy. The result shows that if the score estimator is sufficiently accurate, then diffusion policy efficiently infers the actions from any realistic policy that generates the training data. It is noteworthy that Theorem 4.3 also shows that diffusion policy is powerful to represent a multimodal distribution, which leads to sufficient exploration and better reward performance, Section 3 and Appendix G provide more discussions with numerical verifications for this view.

**Diffusion Policy for Model-free Online RL.** Recall the standard model-free online RL framework, see Figure 2, where the policy improvement produces a new policy  $\pi' \succeq \pi$  according to the data  $\mathcal{D}$ . However, Theorem 4.3 illustrates that the diffusion policy only fits the distribution of the policy  $\pi$  but does not improve the policy  $\pi$ . We can not embed the diffusion policy into the standard RL training framework, i.e., the policy improvement in Figure 2 can not be naively replaced by diffusion policy. To apply diffusion policy to model-free online RL task, we propose the DIPO algorithm, see Figure 3. The proposed DIPO considers a novel way for policy improvement, we call it **action gradient** that updates each  $\mathbf{a}_t \in \mathcal{D}$  along the gradient field (over the action space) of state-action value:

$$\mathbf{a}_t \leftarrow \mathbf{a}_t + \eta \nabla_{\mathbf{a}} Q_{\pi}(\mathbf{s}_t, \mathbf{a}_t),$$

where for a given state  $\mathbf{s}$ ,  $Q_{\pi}(\mathbf{s}, \mathbf{a})$  measures the reward performance over the action space  $\mathcal{A}$ . Thus, DIPO improves the policy according to the actions toward to better reward performance. To the best of our knowledge, this paper first presents the idea of action gradient, which provides an efficient way to make it possible to design a diffusion policy for online RL.

## 1.2 Paper Organization

Section 2 presents the background of reinforcement learning. Section 3 presents our motivation from the view of policy representation. Section 4 presents the theory of diffusion policy. Section 5 presents the practical implementation of diffusion policy for model-free online reinforcement learning. Section 7 presents the experiment results.

## 2 Reinforcement Learning

Reinforcement learning (RL) [Sutton and Barto, 2018] is formulated as *Markov decision process*  $\mathcal{M} = (\mathcal{S}, \mathcal{A}, \mathbb{P}(\cdot), r, \gamma, d_0)$ , where  $\mathcal{S}$  is the state space;  $\mathcal{A} \subset \mathbb{R}^p$  is the continuous action space;  $\mathbb{P}(\mathbf{s}'|\mathbf{s}, \mathbf{a})$  is the probability of state transition from  $\mathbf{s}$  to  $\mathbf{s}'$  after playing  $\mathbf{a}$ ;  $r(\mathbf{s}'|\mathbf{s}, \mathbf{a})$  denotes the reward that the agent observes when the state transition from  $\mathbf{s}$  to  $\mathbf{s}'$  after playing  $\mathbf{a}$ ;  $\gamma \in (0, 1)$  is the discounted factor, and  $d_0(\cdot)$  is the initial state distribution. A policy  $\pi$  is a probability distribution defined on  $\mathcal{S} \times \mathcal{A}$ , and  $\pi(\mathbf{a}|\mathbf{s})$  denotes the probability of playing  $\mathbf{a}$  in state  $\mathbf{s}$ . Let  $\{\mathbf{s}_t, \mathbf{a}_t, \mathbf{s}_{t+1}, r(\mathbf{s}_{t+1}|\mathbf{s}_t, \mathbf{a}_t)\}_{t \geq 0} \sim \pi$  be the trajectory sampled by the policy  $\pi$ , where  $\mathbf{s}_0 \sim d_0(\cdot)$ ,  $\mathbf{a}_t \sim \pi(\cdot|\mathbf{s}_t)$ ,  $\mathbf{s}_{t+1} \sim \mathbb{P}(\cdot|\mathbf{s}_t, \mathbf{a}_t)$ . The goal of RL is to find a policy  $\pi$  such that  $\pi_\star =: \arg \max_{\pi} \mathbb{E}_{\pi} [\sum_{t=0}^{\infty} \gamma^t r(\mathbf{s}_{t+1}|\mathbf{s}_t, \mathbf{a}_t)]$ .

## 3 Motivation: A View from Policy Representation

In this section, we clarify our motivation from the view of policy representation: diffusion model is powerful to policy representation, which leads to sufficient exploration and better reward performance.

### 3.1 Policy Representation for Reinforcement Learning

Value function and parametric function based are the main two approaches to represent policies, while diffusion policy expresses a policy via a stochastic process (shown in Figure 1) that is essentially difficult to the previous representation. In this section, we will clarify this view. Additionally, we will provide an empirical verification with a numerical experiment.

#### 3.1.1 Policy Representation via Value Function

A typical way to represent policy is  $\epsilon$ -greedy policy [Sutton and Barto, 1998] or *energy-based policy* [Sallans and Hinton, 2004, Peters et al., 2010],

$$\pi(\mathbf{a}|\mathbf{s}) = \begin{cases} \arg \max_{\mathbf{a}' \in \mathcal{A}} Q_{\pi}(\mathbf{s}, \mathbf{a}') & \text{w.p. } 1 - \epsilon; \\ \text{randomly play } \mathbf{a} \in \mathcal{A} & \text{w.p. } \epsilon; \end{cases} \quad \text{or } \pi(\mathbf{a}|\mathbf{s}) = \frac{\exp \{Q_{\pi}(\mathbf{s}, \mathbf{a})\}}{Z_{\pi}(\mathbf{s})}, \quad (1)$$

where

$$Q_{\pi}(\mathbf{s}, \mathbf{a}) =: \mathbb{E}_{\pi} \left[ \sum_{t=0}^{\infty} \gamma^t r(\mathbf{s}_{t+1}|\mathbf{s}_t, \mathbf{a}_t) | \mathbf{s}_0 = \mathbf{s}, \mathbf{a}_0 = \mathbf{a} \right],$$

the normalization term  $Z_{\pi}(\mathbf{s}) = \int_{\mathbb{R}^p} \exp \{Q_{\pi}(\mathbf{s}, \mathbf{a})\} d\mathbf{a}$ , and “w.p.” is short for “with probability”. The representation (1) illustrates a connection between policy and value function, which is widely used in *value-based methods* (e.g., SASRA [Rummery and Niranjan, 1994], Q-Learning [Watkins, 1989], DQN [Mnih et al., 2015]) and *energy-based methods* (e.g., SQL [Schulman et al., 2017a, Haarnoja et al., 2017, 2018a], SAC [Haarnoja et al., 2018b]).

#### 3.1.2 Policy Representation via Parametric Function

Instead of consulting a value function, the parametric policy is to represent a policy by a parametric function (e.g., neural networks), denoted as  $\pi_{\theta}$ , where  $\theta$  is the parameter. Policy gradient theorem [Sutton et al., 1999, Silver et al., 2014] plays a center role to learn  $\theta$ , which is fundamental in modern RL (e.g., TRPO [Schulman et al., 2015], DDPG [Lillicrap et al., 2016], PPO [Schulman et al., 2017b], IMPALA [Espeholt et al., 2018], et al).

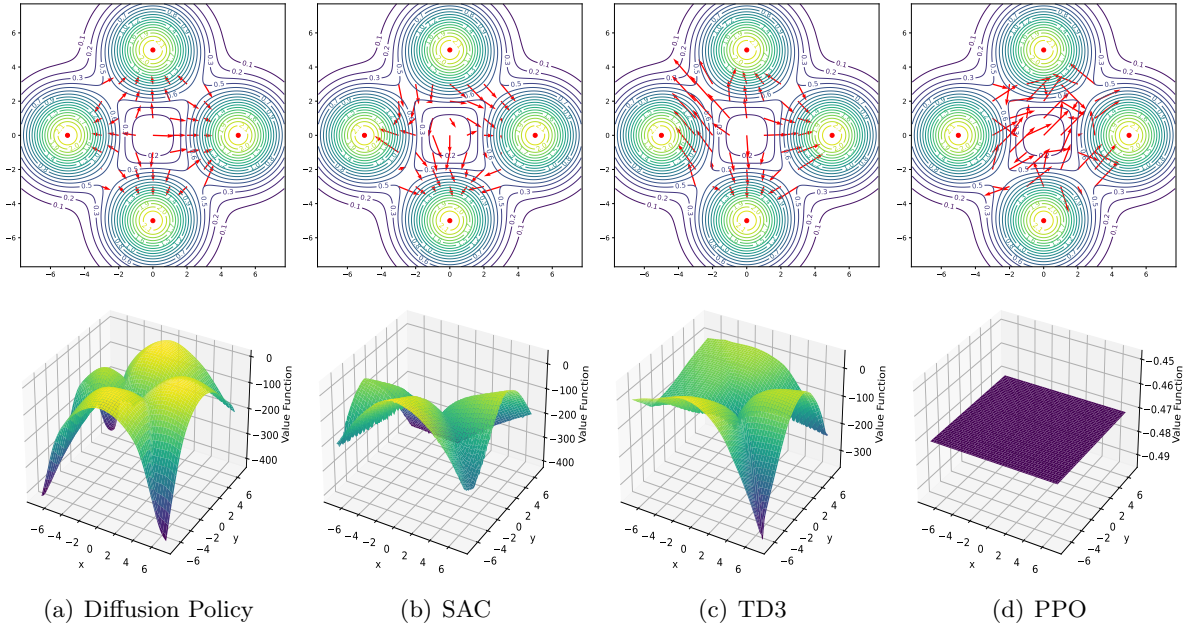


Figure 5: Policy representation comparison of different policies on multimodal environment.

### 3.1.3 Policy Representation via Stochastic Process

It is different from both value-based and parametric policy representation; the diffusion policy (see Figure 1) generates an action via a stochastic process, which is a fresh view for the RL community. The diffusion model with RL first appears in [Janner et al., 2022], where it proposes the *diffuser* that plans by iteratively refining trajectories, which is an essential offline RL method. Ajay et al. [2023], Reuss et al. [2023] model a policy as a return conditional diffusion model, Chen et al. [2023a], Wang et al. [2023], Chi et al. [2023] consider to generate actions via diffusion model. The above methods are all to solve offline RL problems. To the best of our knowledge, our proposed method is the first diffusion approach to online model-free reinforcement learning.

## 3.2 Diffusion Model is Powerful to Policy Representation

This section presents the diffusion model is powerful to represent a complex policy distribution. by two following aspects: 1) fitting a multimodal policy distribution is efficient for exploration; 2) empirical verification with a numerical experiment.

The Gaussian policy is widely used in RL, which is a unimodal distribution, and it plays actions around the region of its mean center with a higher probability, i.e., the red region  $A$  in Figure 4. The unimodal policy weakens the expressiveness of complicated policy and decays the agent’s ability to explore the environment. While for a multimodal policy, it plays actions among the different regions:  $A_1 \cup A_2 \cup A_3$ . Compared to the unimodal policy, the multimodal policy is powerful to explore the unknown world, making the agent

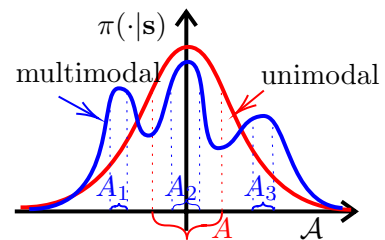


Figure 4: Unimodal Distribution vs Multimodal Distribution.

understand the environment efficiently and make a more reasonable decision.

We compare the ability of policy representation among SAC, TD3 [Fujimoto et al., 2018], PPO and diffusion policy on the “multi-goal” environment [Haarnoja et al., 2017] (see Figure 5), where the  $x$ -axis and  $y$ -axis are 2D states, the four red dots denote the states of the goal at  $(0, 5)$ ,  $(0, -5)$ ,  $(5, 0)$  and  $(-5, 0)$  symmetrically. A reasonable policy should be able to take actions uniformly to those four goal positions with the same probability, which characters the capacity of exploration of a policy to understand the environment. In Figure 5, the red arrowheads represent the directions of actions, and the length of the red arrowheads represents the size of the actions. Results show that diffusion policy accurately captures a multimodal distribution landscape, while both SAC, TD3, and PPO are not well suited to capture such a multimodality. From the distribution of action direction and length, we also know the diffusion policy keeps a more gradual and steady action size than the SAC, TD3, and PPO to fit the multimodal distribution. For more details about 2D/3D plots, environment, comparisons, and discussions, please refer to Appendix G.

## 4 Diffusion Policy

In this section, we present the details of diffusion policy from the following three aspects: its stochastic dynamic equation (shown in Figure 1), discretization implementation, and finite-time analysis of its performance for the policy representation.

### 4.1 Stochastic Dynamics of Diffusion Policy

Recall Figure 1, we know diffusion policy contains two processes: forward process and reverse process. We present its dynamic in this section.

**Forward Process.** To simplify the expression, we only consider  $g(t) = \sqrt{2}$ , which is parallel to the general setting in Figure 1. For any given state  $\mathbf{s}$ , the forward process produces a sequence  $\{(\bar{\mathbf{a}}_t|\mathbf{s})\}_{t=0:T}$  that starting with  $\bar{\mathbf{a}}_0 \sim \pi(\cdot|\mathbf{s})$ , and it follows the Ornstein-Uhlenbeck process (also known as Ornstein-Uhlenbeck SDE),

$$d\bar{\mathbf{a}}_t = -\bar{\mathbf{a}}_t dt + \sqrt{2}d\mathbf{w}_t. \quad (2)$$

Let  $\bar{\mathbf{a}}_t \sim \bar{\pi}_t(\cdot|\mathbf{s})$  be the evolution distribution along the Ornstein-Uhlenbeck flow (2). According to Proposition B.1 (see Appendix B.2), we know the conditional distribution of  $\bar{\mathbf{a}}_t|\bar{\mathbf{a}}_0$  is Gaussian,

$$\bar{\mathbf{a}}_t|\bar{\mathbf{a}}_0 \sim \mathcal{N}(e^{-t}\bar{\mathbf{a}}_0, (1 - e^{-2t})\mathbf{I}). \quad (3)$$

That implies the forward process (2) transforms policy  $\pi(\cdot|\mathbf{s})$  to the Gaussian noise  $\mathcal{N}(\mathbf{0}, \mathbf{I})$ .

**Reverse Process.** For any given state  $\mathbf{s}$ , if we reverse the stochastic process  $\{(\bar{\mathbf{a}}_t|\mathbf{s})\}_{t=0:T}$ , then we obtain a process that transforms noise into the policy  $\pi(\cdot|\mathbf{s})$ . Concretely, we model the policy as the process  $\{(\tilde{\mathbf{a}}_t|\mathbf{s})\}_{t=0:T}$  according to the next Ornstein-Uhlenbeck process (running forward in time),

$$d\tilde{\mathbf{a}}_t = (\tilde{\mathbf{a}}_t + 2\nabla \log p_{T-t}(\tilde{\mathbf{a}}_t)) dt + \sqrt{2}d\mathbf{w}_t, \quad (4)$$

where  $p_t(\cdot)$  is the probability density function of  $\bar{\pi}_t(\cdot|\mathbf{s})$ . Furthermore, according to [Anderson, 1982], with an initial action  $\tilde{\mathbf{a}}_0 \sim \bar{\pi}_T(\cdot|\mathbf{s})$ , the reverse process  $\{\tilde{\mathbf{a}}_t\}_{t=0:T}$  shares the same



---

**Algorithm 1:** Diffusion Policy with Exponential Integrator Discretization to Approximate  $\pi(\cdot|\mathbf{s})$

---

- 1: **input:** state  $\mathbf{s}$ , horizon  $T$ , reverse length  $K$ , step-size  $h = \frac{T}{K}$ , score estimators  $\hat{\mathbf{S}}(\cdot, \mathbf{s}, T - t)$ ;
  - 2: **initialization:** a random action  $\hat{\mathbf{a}}_0 \sim \mathcal{N}(\mathbf{0}, \mathbf{I})$ ;
  - 3: **for**  $k = 0, 1, \dots, K - 1$  **do**
  - 4:     a random  $\mathbf{z}_k \sim \mathcal{N}(\mathbf{0}, \mathbf{I})$ , set  $t_k = hk$ ;
  - 5:      $\hat{\mathbf{a}}_{t_{k+1}} = e^h \hat{\mathbf{a}}_{t_k} + (e^h - 1) \left( \hat{\mathbf{a}}_{t_k} + 2\hat{\mathbf{S}}(\hat{\mathbf{a}}_{t_k}, \mathbf{s}, T - t_k) \right) + \sqrt{e^{2h} - 1} \mathbf{z}_k$ ;
  - 6: **output:**  $\hat{\mathbf{a}}_{t_K}$ ;
- 

distribution as the time-reversed version of the forward process  $\{\tilde{\mathbf{a}}_{T-t}\}_{t=0:T}$ . That also implies for all  $t = 0, 1, \dots, T$ ,

$$\tilde{\pi}_t(\cdot|\mathbf{s}) = \bar{\pi}_{T-t}(\cdot|\mathbf{s}), \quad \text{if } \tilde{\mathbf{a}}_0 \sim \bar{\pi}_T(\cdot|\mathbf{s}). \quad (5)$$

**Score Matching.** The score function  $\nabla \log p_{T-t}(\cdot)$  defined in (4) is not explicit, we consider an estimator  $\hat{\mathbf{S}}(\cdot, \mathbf{s}, T - t)$  to approximate the score function at a given state  $\mathbf{s}$ . We consider the next problem,

$$\hat{\mathbf{S}}(\cdot, \mathbf{s}, T - t) =: \arg \min_{\hat{\mathbf{s}}(\cdot) \in \mathcal{F}} \mathbb{E}_{\mathbf{a} \sim \tilde{\pi}_t(\cdot|\mathbf{s})} \left[ \left\| \hat{\mathbf{s}}(\mathbf{a}, \mathbf{s}, t) - \nabla \log p_{T-t}(\mathbf{a}) \right\|_2^2 \right] \quad (6)$$

$$\stackrel{(5)}{=} \arg \min_{\hat{\mathbf{s}}(\cdot) \in \mathcal{F}} \mathbb{E}_{\mathbf{a} \sim \tilde{\pi}_t(\cdot|\mathbf{s})} \left[ \left\| \hat{\mathbf{s}}(\mathbf{a}, \mathbf{s}, t) - \nabla \log \tilde{\pi}_t(\mathbf{a}|\mathbf{s}) \right\|_2^2 \right], \quad (7)$$

where  $\mathcal{F}$  is the collection of function approximators (e.g., neural networks). We will provide the detailed implementations with a parametric function approximation later; please refer to Section 5 or Appendix C.2.

## 4.2 Exponential Integrator Discretization for Diffusion Policy

In this section, we consider the implementation of the reverse process (4) with exponential integrator discretization [Zhang, 2022, Lee et al., 2023]. Let  $h > 0$  be the step-size, assume reverse length  $K = \frac{T}{h} \in \mathbb{N}$ , and  $t_k =: hk$ ,  $k = 0, 1, \dots, K$ . Then we give a partition on the interval  $[0, T]$  as follows,  $0 = t_0 < t_1 < \dots < t_k < t_{k+1} < \dots < t_K = T$ . Furthermore, we take the discretization to the reverse process (4) according to the following equation,

$$d\hat{\mathbf{a}}_t = \left( \hat{\mathbf{a}}_t + 2\hat{\mathbf{S}}(\hat{\mathbf{a}}_{t_k}, \mathbf{s}, T - t_k) \right) dt + \sqrt{2} d\mathbf{w}_t, \quad t \in [t_k, t_{k+1}], \quad (8)$$

where it runs initially from  $\hat{\mathbf{a}}_0 \sim \mathcal{N}(\mathbf{0}, \mathbf{I})$ . By Itô integration to the two sides of (8) on the  $k$ -th interval  $[t_k, t_{k+1}]$ , we obtain the exact solution of the SDE (8), for each  $k = 0, 1, 2, \dots, K - 1$ ,

$$\hat{\mathbf{a}}_{t_{k+1}} = e^h \hat{\mathbf{a}}_{t_k} + \left( e^h - 1 \right) \left( \hat{\mathbf{a}}_{t_k} + 2\hat{\mathbf{S}}(\hat{\mathbf{a}}_{t_k}, \mathbf{s}, T - t_k) \right) + \sqrt{e^{2h} - 1} \mathbf{z}_k, \quad \mathbf{z}_k \sim \mathcal{N}(\mathbf{0}, \mathbf{I}). \quad (9)$$

For the derivation from the SDE (8) to the iteration (9), please refer to Appendix B.3, and we have shown the implementation in Algorithm 1.

### 4.3 Convergence Analysis of Diffusion Policy

In this section, we present the convergence analysis of diffusion policy, we need the following notations and assumptions before we further analyze. Let  $\rho(\mathbf{x})$  and  $\mu(\mathbf{x})$  be two smooth probability density functions on the space  $\mathbb{R}^p$ , the Kullback–Leibler (KL) divergence and relative Fisher information (FI) from  $\mu(\mathbf{x})$  to  $\rho(\mathbf{x})$  are defined as follows,

$$\text{KL}(\rho\|\mu) = \int_{\mathbb{R}^p} \rho(\mathbf{x}) \log \frac{\rho(\mathbf{x})}{\mu(\mathbf{x})} d\mathbf{x}, \quad \text{FI}(\rho\|\mu) = \int_{\mathbb{R}^p} \rho(\mathbf{x}) \left\| \nabla \log \left( \frac{\rho(\mathbf{x})}{\mu(\mathbf{x})} \right) \right\|_2^2 d\mathbf{x}.$$

**Assumption 4.1** (Lipschitz Score Estimator and Policy). *The score estimator is  $L_s$ -Lipschitz over action space  $\mathcal{A}$ , and the policy  $\pi(\cdot|\mathbf{s})$  is  $L_p$ -Lipschitz over action space  $\mathcal{A}$ , i.e., for any  $\mathbf{a}, \mathbf{a}' \in \mathcal{A}$ , the following holds,*

$$\|\hat{\mathbf{S}}(\mathbf{a}, \mathbf{s}, t) - \hat{\mathbf{S}}(\mathbf{a}', \mathbf{s}, t)\| \leq L_s \|\mathbf{a} - \mathbf{a}'\|, \quad \|\nabla \log \pi(\mathbf{a}|\mathbf{s}) - \nabla \log \pi(\mathbf{a}'|\mathbf{s})\| \leq L_p \|\mathbf{a} - \mathbf{a}'\|.$$

**Assumption 4.2** (Policy with  $\nu$ -LSI Setting). *The policy  $\pi(\cdot|\mathbf{s})$  satisfies  $\nu$ -Log-Sobolev inequality (LSI) that defined as follows, there exists constant  $\nu > 0$ , for any probability distribution  $\mu(\mathbf{x})$  such that*

$$\text{KL}(\mu\|\pi) \leq \frac{1}{2\nu} \text{FI}(\mu\|\pi).$$

Assumption 4.1 is a standard setting for Langevin-based algorithms (e.g., [Wibisono and Yang, 2022, Vempala and Wibisono, 2019]), and we extend it with RL notations. Assumption 4.2 presents the policy distribution class that we are concerned, which contains many complex distributions that are not restricted to be log-concave, e.g. any slightly smoothed bound distribution admits the condition (see [Ma et al., 2019, Proposition 1]).

**Theorem 4.3** (Finite-time Analysis of Diffusion Policy). *For a given state  $\mathbf{s}$ , let  $\{\tilde{\pi}_t(\cdot|\mathbf{s})\}_{t=0:T}$  and  $\{\hat{\pi}_t(\cdot|\mathbf{s})\}_{t=0:T}$  be the distributions along the flow (2) and (4) correspondingly, where  $\{\tilde{\pi}_t(\cdot|\mathbf{s})\}_{t=0:T}$  starts at  $\tilde{\pi}_0(\cdot|\mathbf{s}) = \pi(\cdot|\mathbf{s})$  and  $\{\hat{\pi}_t(\cdot|\mathbf{s})\}_{t=0:T}$  starts at  $\hat{\pi}_0(\cdot|\mathbf{s}) = \tilde{\pi}_T(\cdot|\mathbf{s})$ . Let  $\hat{\pi}_k(\cdot|\mathbf{s})$  be the distribution of the iteration (9) at the  $k$ -th time  $t_k = hk$ , i.e.,  $\hat{\mathbf{a}}_{t_k} \sim \hat{\pi}_k(\cdot|\mathbf{s})$  denotes the diffusion policy (see Algorithm 1) at the time  $t_k = hk$ . Let  $\{\hat{\pi}_k(\cdot|\mathbf{s})\}_{k=0:K}$  be starting at  $\hat{\pi}_0(\cdot|\mathbf{s}) = \mathcal{N}(\mathbf{0}, \mathbf{I})$ , under Assumption 4.1 and 4.2, let the reverse length  $K \geq T \cdot \max\{\tau_0^{-1}, \mathbf{T}_0^{-1}, 12L_s, \nu\}$ , where constants  $\tau_0$  and  $\mathbf{T}_0$  will be special later. Then the KL-divergence between diffusion policy  $\hat{\pi}_K(\cdot|\mathbf{s})$  and input policy  $\pi(\cdot|\mathbf{s})$  is upper-bounded as follows,*

$$\text{KL}(\hat{\pi}_K(\cdot|\mathbf{s})\|\pi(\cdot|\mathbf{s})) \leq \underbrace{e^{-\frac{9}{4}\nu h K} \text{KL}(\mathcal{N}(\mathbf{0}, \mathbf{I})\|\pi(\cdot|\mathbf{s}))}_{\text{convergence of forward process (2)}} + \underbrace{\left(64pL_s\sqrt{5/\nu}\right)h}_{\text{errors from discretization (9)}} + \frac{20}{3}\epsilon_{\text{score}},$$

$$\text{where } \epsilon_{\text{score}} = \underbrace{\sup_{(k,t) \in [K] \times [t_k, t_{k+1}]} \left\{ \log \mathbb{E}_{\mathbf{a} \sim \tilde{\pi}_t(\cdot|\mathbf{s})} \left[ \exp \left\| \hat{\mathbf{S}}(\mathbf{a}, \mathbf{s}, T - hk) - \nabla \log \tilde{\pi}_t(\mathbf{a}|\mathbf{s}) \right\|_2^2 \right] \right\}}_{\text{errors from score matching (7)}}.$$

Theorem 4.3 illustrates that the errors involve the following three terms. The first error involves  $\text{KL}(\mathcal{N}(\mathbf{0}, \mathbf{I})\|\pi(\cdot|\mathbf{s}))$  that represents how close the distribution of the input policy  $\pi$  is to the standard Gaussian noise, which is bounded by the exponential convergence rate of Ornstein-Uhlenbeck flow (2) [Bakry et al., 2014, Wibisono and Jog, 2018, Chen et al., 2023c]. The second error is sourced from exponential integrator discretization implementation (9), which scales with the discretization step-size  $h$ . The discretization error term implies a first-order convergence rate with respect to the discretization step-size  $h$  and scales polynomially

on other parameters. The third error is sourced from score matching (7), which represents how close the score estimator  $\hat{\mathbf{S}}$  is to the score function  $\nabla \log p_{T-t}(\cdot)$  defined in (4). That implies for the practical implementation, the error from score matching could be sufficiently small if we find a good score estimator  $\hat{\mathbf{S}}$ .

Furthermore, for any  $\epsilon > 0$ , if we find a good score estimator that makes the score matching error satisfy  $\epsilon_{\text{score}} < \frac{1}{20}\epsilon$ , the step-size  $h = \mathcal{O}\left(\frac{\epsilon\sqrt{\nu}}{pL_s}\right)$ , and reverse length  $K = \frac{9}{4\nu h} \log \frac{3\text{KL}(\mathcal{N}(\mathbf{0}, \mathbf{I})\|\pi(\cdot|\mathbf{s}))}{\epsilon}$ , then Theorem 4.3 implies the output of diffusion policy ( $\hat{\pi}_K(\cdot|\mathbf{s})$ ) makes a sufficient close to the input policy  $\pi(\cdot|\mathbf{s})$  with the measurement by  $\text{KL}(\hat{\pi}_K(\cdot|\mathbf{s})\|\pi(\cdot|\mathbf{s})) \leq \epsilon$ .

## 5 DIPO: Implementation of Diffusion Policy for Model-Free Online RL

In this section, we present the details of DIPO, which is an implementation of **DI**ffusion **P**olicy for model-free reinforcement learning. According to Theorem 4.3, diffusion policy only fits the current policy  $\pi$  that generates the training data (denoted as  $\mathcal{D}$ ), but it does not improve the policy  $\pi$ . It is different from traditional policy-based RL algorithms, we can not improve a policy according to the policy gradient theorem since diffusion policy is not a parametric function but learns a policy via a stochastic process. Thus, we need a new way to implement policy improvement, which is nontrivial. We have presented the framework of DIPO in Figure 3, and shown the key steps of DIPO in Algorithm 2. For the detailed implementation, please refer to Algorithm 3 (see Appendix C).

### 5.1 Training Loss of DIPO

It is intractable to directly apply the formulation (7) to estimate the score function since  $\nabla \log p_t(\cdot) = \nabla \log \bar{\pi}_t(\cdot|\mathbf{s})$  is unknown, which is sourced from the initial distribution  $\bar{\mathbf{a}}_0 \sim \pi(\cdot|\mathbf{s})$  is unknown. According to denoising score matching [Vincent, 2011, Hyvärinen, 2005], a practical way is to solve the next optimization problem (10). For any given  $\mathbf{s} \in \mathcal{S}$ ,

$$\min_{\phi} \mathcal{L}(\phi) = \min_{\hat{\mathbf{s}}_{\phi} \in \mathcal{F}} \int_0^T \omega(t) \mathbb{E}_{\bar{\mathbf{a}}_0 \sim \pi(\cdot|\mathbf{s})} \mathbb{E}_{\bar{\mathbf{a}}_t | \bar{\mathbf{a}}_0} \left[ \left\| \hat{\mathbf{s}}_{\phi}(\bar{\mathbf{a}}_t, \mathbf{s}, t) - \nabla \log \varphi_t(\bar{\mathbf{a}}_t | \bar{\mathbf{a}}_0) \right\|_2^2 \right] dt, \quad (10)$$

where  $\omega(t) : [0, T] \rightarrow \mathbb{R}_+$  is a positive weighting function;  $\varphi_t(\bar{\mathbf{a}}_t | \bar{\mathbf{a}}_0) = \mathcal{N}(e^{-t}\bar{\mathbf{a}}_0, (1 - e^{-2t})\mathbf{I})$  denotes the transition kernel of the forward process (3);  $\mathbb{E}_{\bar{\mathbf{a}}_t | \bar{\mathbf{a}}_0}[\cdot]$  denotes the expectation with respect to  $\varphi_t(\bar{\mathbf{a}}_t | \bar{\mathbf{a}}_0)$ ; and  $\phi$  is the parameter needed to be learned. Then, according to Theorem C.1 (see Appendix C.2), we rewrite the objective (10) as follows,

$$\mathcal{L}(\phi) = \mathbb{E}_{k \sim \mathcal{U}(\{1, 2, \dots, K\}), \mathbf{z} \sim \mathcal{N}(\mathbf{0}, \mathbf{I}), (\mathbf{s}, \mathbf{a}) \sim \mathcal{D}} \left[ \left\| \mathbf{z} - \epsilon_{\phi}(\sqrt{\bar{\alpha}_k} \mathbf{a} + \sqrt{1 - \bar{\alpha}_k} \mathbf{z}, \mathbf{s}, k) \right\|_2^2 \right], \quad (11)$$

where  $\mathcal{U}(\cdot)$  denotes uniform distribution,

$$\epsilon_{\phi}(\cdot, \cdot, k) = -\sqrt{1 - \bar{\alpha}_k} \hat{\mathbf{s}}_{\phi}(\cdot, \cdot, T - t_k),$$

and  $\bar{\alpha}_k$  will be special. The objective (11) provides a way to learn  $\phi$  from samples; see line 14-16 in Algorithm 2.

---

**Algorithm 2:** (DIPO) Model-Free Reinforcement Learning with **DI**ffusion **PO**licy

---

```

1: initialize  $\phi$ , critic network  $Q_\psi$ ;  $\{\alpha_i\}_{i=0}^K$ ;  $\bar{\alpha}_k = \prod_{i=1}^k \alpha_i$ ; step-size  $\eta$ ;
2: repeat
3:   dataset  $\mathcal{D} \leftarrow \emptyset$ ; initialize  $\mathbf{s}_0 \sim d_0(\cdot)$ ;
4:   #update experience
5:   for  $t = 0, 1, \dots, T$  do
6:     play  $\mathbf{a}_t$  follows (12);  $\mathbf{s}_{t+1} \sim \mathbb{P}(\cdot | \mathbf{s}_t, \mathbf{a}_t)$ ;  $\mathcal{D} \leftarrow \mathcal{D} \cup \{\mathbf{s}_t, \mathbf{a}_t, \mathbf{s}_{t+1}, r(\mathbf{s}_{t+1} | \mathbf{s}_t, \mathbf{a}_t)\}$ ;
7:     #update value function
8:     repeat  $N$  times
9:       sample  $(\mathbf{s}_t, \mathbf{a}_t, \mathbf{s}_{t+1}, r(\mathbf{s}_{t+1} | \mathbf{s}_t, \mathbf{a}_t)) \sim \mathcal{D}$  i.i.d; take gradient descent on  $\ell_Q(\psi)$  (14);
10:    #action gradient
11:    for  $t = 0, 1, \dots, T$  do
12:      replace each action  $\mathbf{a}_t \in \mathcal{D}$  follows  $\mathbf{a}_t \leftarrow \mathbf{a}_t + \eta \nabla_{\mathbf{a}} Q_\psi(\mathbf{s}_t, \mathbf{a})|_{\mathbf{a}=\mathbf{a}_t}$ ;
13:    #update policy
14:    repeat  $N$  times
15:      sample  $(\mathbf{s}, \mathbf{a})$  from  $\mathcal{D}$  i.i.d, sample index  $k \sim \mathcal{U}(\{1, \dots, K\})$ ,  $\mathbf{z} \sim \mathcal{N}(\mathbf{0}, \mathbf{I})$ ;
16:      take gradient decent on the loss  $\ell_d(\phi) = \|\mathbf{z} - \epsilon_\phi(\sqrt{\bar{\alpha}_k} \mathbf{a} + \sqrt{1 - \bar{\alpha}_k} \mathbf{z}, \mathbf{s}, k)\|_2^2$ ;
17:    until the policy performs well in the environment.

```

---

## 5.2 Playing Action of DIPO

Replacing the score estimator  $\hat{\mathbf{S}}$  (defined in Algorithm 1) according to  $\hat{\epsilon}_\phi$ , after some algebras (see Appendix C.3), we rewrite diffusion policy (i.e., Algorithm 1) as follows,

$$\hat{\mathbf{a}}_{k+1} = \frac{1}{\sqrt{\alpha_k}} \left( \hat{\mathbf{a}}_k - \frac{1 - \alpha_k}{\sqrt{1 - \bar{\alpha}_k}} \epsilon_\phi(\hat{\mathbf{a}}_k, \mathbf{s}, k) \right) + \sqrt{\frac{1 - \alpha_k}{\alpha_k}} \mathbf{z}_k, \quad (12)$$

where  $k = 0, 1, \dots, K - 1$  runs forward in time, the noise  $\mathbf{z}_k \sim \mathcal{N}(\mathbf{0}, \mathbf{I})$ . The agent plays the last (output) action  $\hat{\mathbf{a}}_K$ .

## 5.3 Policy Improvement of DIPO

According to (11), we know that only the state-action pairs  $(\mathbf{s}, \mathbf{a}) \in \mathcal{D}$  are used to learn a policy. That inspires us that if we design a method that transforms a given pair  $(\mathbf{s}, \mathbf{a}) \in \mathcal{D}$  to be a “better” pair, then we use the “better” pair to learn a new diffusion policy  $\pi'$ , then  $\pi' \succeq \pi$ . About “better” state-action pair should maintain a higher reward performance than the originally given pair  $(\mathbf{s}, \mathbf{a}) \in \mathcal{D}$ . We break our key idea into two steps: **1**) first, we regard the reward performance as a function with respect to actions,  $J_\pi(\mathbf{a}) = \mathbb{E}_{\mathbf{s} \sim d_0(\cdot)}[Q_\pi(\mathbf{s}, \mathbf{a})]$ , which quantifies how the action  $\mathbf{a}$  affects the performance; **2**) then, we update all the actions  $\mathbf{a} \in \mathcal{D}$  through the direction  $\nabla_{\mathbf{a}} J_\pi(\mathbf{a})$  by gradient ascent method:

$$\mathbf{a} \leftarrow \mathbf{a} + \eta \nabla_{\mathbf{a}} J_\pi(\mathbf{a}) = \mathbf{a} + \eta \mathbb{E}_{\mathbf{s} \sim d_0(\cdot)}[\nabla_{\mathbf{a}} Q_\pi(\mathbf{s}, \mathbf{a})], \quad (13)$$

where  $\eta > 0$  is step-size, and we call  $\nabla_{\mathbf{a}} J_\pi(\mathbf{a})$  as **action gradient**. To implement (13) from samples, we need a neural network  $Q_\psi$  to estimate  $Q_\pi$ . Recall  $\{\mathbf{s}_t, \mathbf{a}_t, \mathbf{s}_{t+1}, r(\mathbf{s}_{t+1} | \mathbf{s}_t, \mathbf{a}_t)\}_{t \geq 0} \sim \pi$ , we train the parameter  $\psi$  by minimizing the following Bellman residual error,

$$\ell_Q(\psi) = (r(\mathbf{s}_{t+1} | \mathbf{s}_t, \mathbf{a}_t) + \gamma Q_\psi(\mathbf{s}_{t+1}, \mathbf{a}_{t+1}) - Q_\psi(\mathbf{s}_t, \mathbf{a}_t))^2. \quad (14)$$

Finally, we consider each pair  $(\mathbf{s}_t, \mathbf{a}_t) \in \mathcal{D}$ , and replace the action  $\mathbf{a}_t \in \mathcal{D}$  as follows,

$$\mathbf{a}_t \leftarrow \mathbf{a}_t + \eta \nabla_{\mathbf{a}} Q_{\psi}(\mathbf{s}_t, \mathbf{a})|_{\mathbf{a}=\mathbf{a}_t}. \quad (15)$$

## 6 Related Work

Due to the diffusion model being a fast-growing field, this section only presents the work that relates to reinforcement learning, a recent work [Yang et al., 2022] provides a comprehensive survey on the diffusion model. In this section, first, we review recent advances in diffusion models with reinforcement learning. Then, we review the generative models for reinforcement learning.

### 6.1 Diffusion Models for Reinforcement Learning

The diffusion model with RL first appears in [Janner et al., 2022], where it proposes the diffuser that plans by iteratively refining trajectories, which is an essential offline RL method. Later Ajay et al. [2023] model a policy as a return conditional diffusion model, Chen et al. [2023a], Wang et al. [2023], Chi et al. [2023] consider to generate actions via diffusion model. SE(3)-diffusion fields [Urain et al., 2023] consider learning data-driven SE(3) cost functions as diffusion models. Pearce et al. [2023] model the imitating human behavior with diffusion models. Reuss et al. [2023] propose score-based diffusion policies for the goal-conditioned imitation learning problems. ReorientDiff [Mishra and Chen, 2023] presents a reorientation planning method that utilizes a diffusion model-based approach. StructDiffusion [Liu et al., 2022] is an object-centric transformer with a diffusion model, based on high-level language goals, which constructs structures out of a single RGB-D image. Brehmer et al. [2023] propose an equivariant diffuser for generating interactions (EDGI), which trains a diffusion model on an offline trajectory dataset, where EDGI learns a world model and planning in it as a conditional generative modeling problem follows the diffuser [Janner et al., 2022]. DALL-E-Bot [Kapelyukh et al., 2022] explores the web-scale image diffusion models for robotics. AdaptDiffuser [Liang et al., 2023] is an evolutionary planning algorithm with diffusion, which is adapted to unseen tasks.

The above methods are all to solve offline RL problems, to the best of our knowledge, the proposed DIPO is the first diffusion approach to solve online model-free RL problems. The action gradient plays a critical way to implement DIPO, which never appears in existing RL literature. In fact, the proposed DIPO shown in Figure 3 is a general training framework for RL, where we can replace the diffusion policy with any function fitter (e.g., MLP or VAE).

### 6.2 Generative Models for Policy Learning

In this section, we mainly review the generative models, including VAE [Kingma and Welling, 2013], GAN [Goodfellow et al., 2020], Flow [Rezende and Mohamed, 2015], and GFlowNet [Bengio et al., 2021a,b] for policy learning. Generative models are mainly used in cloning diverse behaviors [Pomerleau, 1988], imitation learning [Osa et al., 2018], goal-conditioned imitation learning [Argall et al., 2009], or offline RL [Levine et al., 2020], a recent work [Yang et al., 2023] provides a foundation presentation for the generative models for policy learning.

**VAE for Policy Learning.** Lynch et al. [2020], Ajay et al. [2021] have directly applied auto-encoding variational Bayes (VAE) [Kingma and Welling, 2013] and VQ-VAE [Van Den Oord et al., 2017] model behavioral priors. Mandlekar et al. [2020] design the low-level

policy that is conditioned on latent from the CVAE. [Pertsch et al. \[2021\]](#) joint the representation of skill embedding and skill prior via a deep latent variable model. [Mees et al. \[2022\]](#), [Rosete-Beas et al. \[2023\]](#) consider seq2seq CVAE [\[Lynch et al., 2020, Wang et al., 2022\]](#) to model of conditioning the action decoder on the latent plan allows the policy to use the entirety of its capacity for learning unimodal behavior.

**GAN for Imitation Learning.** GAIL [\[Ho and Ermon, 2016\]](#) considers the Generative Adversarial Networks (GANs) [\[Goodfellow et al., 2020\]](#) to imitation learning. These methods consist of a generator and a discriminator, where the generator policy learns to imitate the experts’ behaviors, and the discriminator distinguishes between real and fake trajectories, which models the imitation learning as a distribution matching problem between the expert policy’s state-action distribution and the agent’s policy [\[Fu et al., 2018, Wang et al., 2021\]](#). For several advanced results and applications, please refer to [\[Chen et al., 2023b, Deka et al., 2023, Rafailov et al., Taranovic et al., 2023\]](#).

**Flow and GFlowNet Model for Policy Learning.** [Singh et al. \[2020\]](#) consider normalizing flows [\[Rezende and Mohamed, 2015\]](#) for the multi-task RL tasks. [Li et al. \[2023a\]](#) propose diverse policy optimization, which consider the GFlowNet [\[Bengio et al., 2021a,b\]](#) for the structured action spaces. [Li et al. \[2023b\]](#) propose CFlowNets that combines GFlowNet with continuous control. Stochastic GFlowNet [\[Pan et al., 2023\]](#) learns a model of the environment to capture the stochasticity of state transitions. [Malkin et al. \[2022\]](#) consider training a GFlowNet with trajectory balance.

**Other Methods.** Decision Transformer (DT) [\[Chen et al., 2021\]](#) model the offline RL tasks as a conditional sequence problem, which does not learn a policy follows the traditional methods (e.g., [Sutton \[1988\]](#), [Sutton and Barto \[1998\]](#)). Those methods with DT belong to the task-agnostic behavior learning methods, which is an active direction in policy learning (e.g., [\[Cui et al., 2023, Brohan et al., 2022, Zheng et al., 2022, Konan et al., 2023, Kim et al., 2023\]](#)). Energy-based models [\[LeCun et al., 2006\]](#) are also modeled as conditional policies [\[Florence et al., 2022\]](#) or applied to inverse RL [\[Liu et al., 2021\]](#). Autoregressive model [\[Vaswani et al., 2017, Brown et al., 2020\]](#) represents the policy as the distribution of action, where it considers the distribution of the whole trajectory [\[Reed et al., 2022, Shafiq et al., 2022\]](#).

## 7 Experiments

In this section, we aim to cover the following three issues: How does DIPO compare to the widely used RL algorithms (SAC, PPO, and TD3) on the standard continuous control benchmark? How to show and illustrate the empirical results? How does the diffusion model compare to VAE [\[Kingma and Welling, 2013\]](#) and multilayer perceptron (MLP) for learning distribution? How to choose the reverse length  $K$  of DIPO for the reverse inference?

### 7.1 Comparative Evaluation and Illustration

We provide an evaluation on MuJoCo tasks [\[Todorov et al., 2012\]](#). Figure 6 shows the reward curves for SAC, PPO, TD3, and DIPO on MuJoCo tasks. To demonstrate the robustness of the proposed DIPO, we train DIPO with the same hyperparameters for all those 5 tasks, where we provide the hyperparameters in Table 3, see Appendix H.1. For each algorithm, we plot the average return of 5 independent trials as the solid curve and plot the standard deviation across 5 same seeds as the transparent shaded region. We evaluate all the methods with  $10^6$  iterations. Results show that the proposed DIPO achieves the best score across all those 5 tasks, and DIPO learns much faster than SAC, PPO, and TD3 on the tasks of Ant-3v

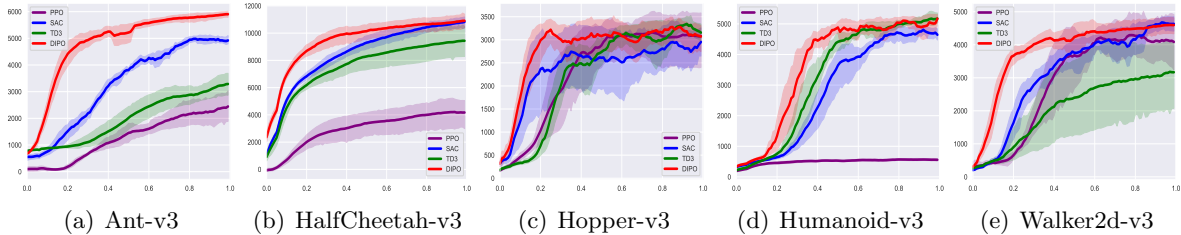


Figure 6: Average performances on MuJoCo Gym environments with  $\pm$  std shaded, where the horizontal axis of coordinate denotes the iterations ( $\times 10^6$ ), the plots smoothed with a window of 10.

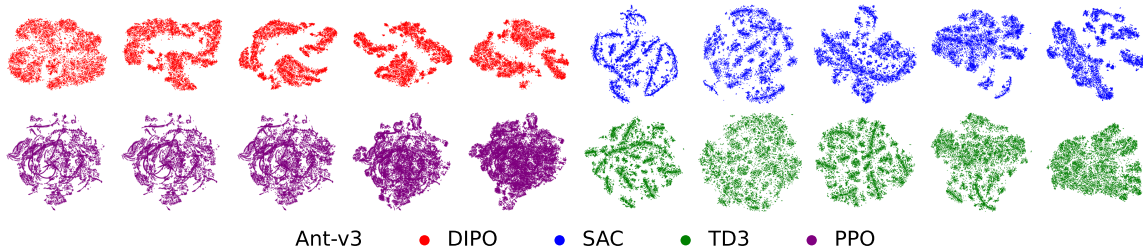


Figure 7: State-visiting visualization by each algorithm on the Ant-v3 task, where states get dimension reduction by t-SNE. The points with different colors represent the states visited by the policy with the style. The distance between points represents the difference between states.

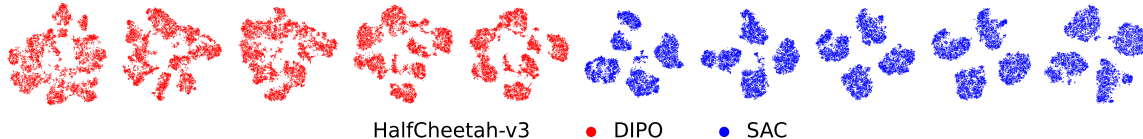


Figure 8: State-visiting visualization for comparison between DIPO and SAC on HalfCheetah-v3.

and Walker2d-3v. Although the asymptotic reward performance of DIPO is similar to baseline algorithms on other 3 tasks, the proposed DIPO achieves better performance at the initial iterations, we will try to illustrate some insights for such empirical results of HalfCheetah-v3 in Figure 8, for more discussions, see Appendix H.

## 7.2 State-Visiting Visualization

From Figure 6, we also know that DIPO achieves the best initial reward performance among all the 5 tasks, a more intuitive illustration has been shown in Figure 7 and 8, where we only consider Ant-v3 and HalfCheetah-v3; for more discussions and observations, see Appendix H.3. We show the state-visiting region to compare both the exploration and final reward performance, where we use the same t-SNE [Van der Maaten and Hinton, 2008] to transfer the high-dimensional states visited by all the methods for 2D visualization. Results of Figure 7 show that the DIPO explores a wider range of state-visiting, covering TD3, SAC, and PPO. Furthermore, from Figure 7, we also know DIPO achieves a more dense state-visiting at the final period, which is a reasonable result since after sufficient training, the agent identifies and

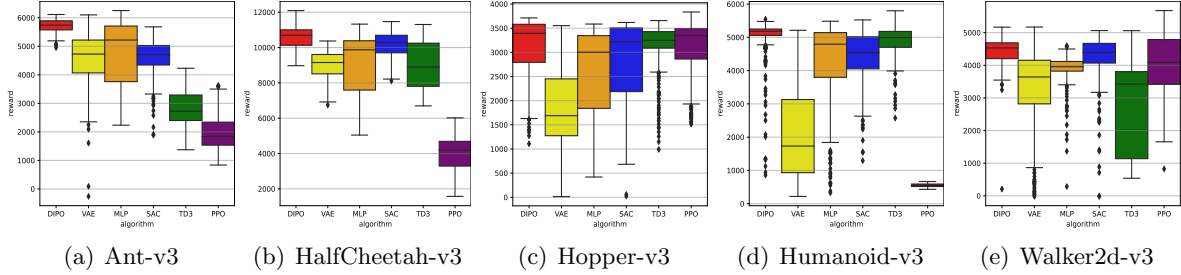


Figure 9: Reward Performance Comparison to VAE and MLP with DIPO, SAC, PPO and TD3.

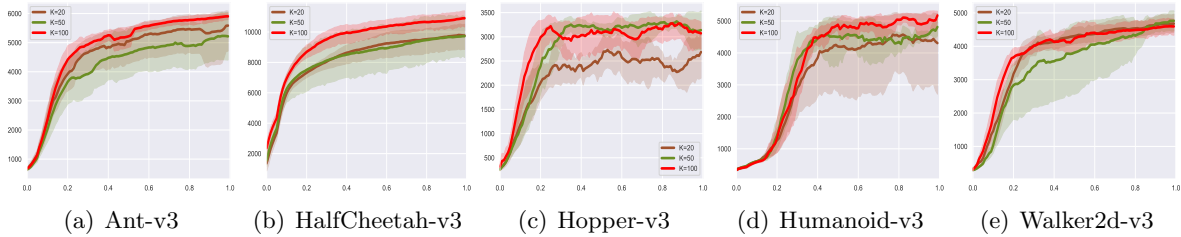


Figure 10: Learning curves with different reverse lengths  $K = 20, 50, 100$ .

Reverse length	Ant-v3	HalfCheetah-v3	Hopper-v3	Humanoid-v3	Walker2d-v3
$K = 100$	<b>5622.30</b> $\pm$ 487.09	<b>10472.31</b> $\pm$ 654.96	3123.14 $\pm$ 636.23	<b>4878.41</b> $\pm$ 822.03	<b>4409.18</b> $\pm$ 469.06
$K = 50$	4877.41 $\pm$ 1010.35	9198.20 $\pm$ 1738.25	<b>3214.83</b> $\pm$ 491.15	4513.39 $\pm$ 1075.94	4199.34 $\pm$ 1062.31
$K = 20$	5288.77 $\pm$ 970.35	9343.69 $\pm$ 986.82	2511.63 $\pm$ 837.03	4294.79 $\pm$ 1583.48	<b>4467.20</b> $\pm$ 368.13

Table 1: Average return over final 6E5 iterations with different reverse lengths  $K = 20, 50, 100$ , and maximum value is bolded for each task.

avoids the "bad" states, and plays actions transfer to "good" states. On the contrary, PPO shows an aimless exploration in the Ant-v3 task, which partially explains why PPO is not so good in the Ant-v3 task.

From Figure 8 we know, at the initial time, DIPO covers more regions than SAC in the HalfCheetah-v3, which results in DIPO obtaining a better reward performance than SAC. This result coincides with the results of Figure 5, which demonstrates that DIPO is efficient for exploration, which leads DIPO to better reward performance. While we also know that SAC starts with a narrow state visit that is similar to the final state visit, and SAC performs with the same reward performance with DIPO at the final, which implies SAC runs around the "good" region at the beginning although SAC performs a relatively worse initial reward performance than DIPO. Thus, the result of Figure 8 partially explains why DIPO performs better than SAC at the initial iterations but performs with same performance with SAC at the final for the HalfCheetah-v3 task.

### 7.3 Ablation Study

In this section, we consider the ablation study to compare the diffusion model with VAE and MLP for policy learning, and show a trade-off on the reverse length  $K$  for reverse inference.



### 7.3.1 Comparison to VAE and MLP

Both VAE and MLP are widely used to learn distribution in machine learning, a fundamental question is: why must we consider the diffusion model to learn a policy distribution? what the reward performance is if we use VAE and MLP to model a policy distribution? We show the answer in Figure 9, where the VAE (or MLP) is the result we replace the diffusion policy of DIPO (see Figure 3) with VAE (or MLP), i.e., we consider VAE (or MLP)+action gradient for the tasks. Results show that the diffusion model is more powerful than VAE and MLP for learning a distribution. This implies the diffusion model is an expressive and flexible family to model a distribution, which is also consistent with the field of the generative model.

### 7.3.2 Comparison with Different Reverse Lengths

Reverse length  $K$  is an important parameter for the diffusion model, which not only affects the reward performance but also affects the training time, we show the results in Figure 10 and Table 1. The results show that the reverse time  $K = 100$  returns a better reward performance than other cases (except Hopper-v3 task). Longer reverse length consumes more reverse time for inference, we hope to use less time for reverse time for action inference. However, a short reverse length  $K = 20$  decays the reward performance among (except Walker2d-v3 task), which implies a trade-off between reward performance and reverse length  $K$ . In practice, we set  $K = 100$  throughout this paper.

## 8 Conclusion

We have formally built a theoretical foundation of diffusion policy, which shows a policy representation via the diffusion probability model and which is a new way to represent a policy via a stochastic process. Then, we have shown a convergence analysis for diffusion policy, which provides a theory to understand diffusion policy. Furthermore, we have proposed an implementation for model-free online RL with a diffusion policy, named DIPO. Finally, extensive empirical results show the effectiveness of DIPO among the Mujoco tasks.

## References

- Anurag Ajay, Aviral Kumar, Pulkit Agrawal, Sergey Levine, and Ofir Nachum. Opal: Offline primitive discovery for accelerating offline reinforcement learning. In *International Conference on Learning Representations (ICLR)*, 2021. (Cited on page 12.)
- Anurag Ajay, Yilun Du, Abhi Gupta, Joshua Tenenbaum, Tommi Jaakkola, and Pulkit Agrawal. Is conditional generative modeling all you need for decision-making? In *International Conference on Learning Representations (ICLR)*, 2023. (Cited on pages 3, 6, and 12.)
- Brian DO Anderson. Reverse-time diffusion equation models. *Stochastic Processes and their Applications*, 12(3):313–326, 1982. (Cited on pages 7 and 26.)
- Brenna D Argall, Sonia Chernova, Manuela Veloso, and Brett Browning. A survey of robot learning from demonstration. *Robotics and autonomous systems*, 57(5):469–483, 2009. (Cited on page 12.)
- Dominique Bakry, Ivan Gentil, Michel Ledoux, et al. *Analysis and geometry of Markov diffusion operators*, volume 103. Springer, 2014. (Cited on page 9.)

- Emmanuel Bengio, Moksh Jain, Maksym Korablyov, Doina Precup, and Yoshua Bengio. Flow network based generative models for non-iterative diverse candidate generation. *Advances in Neural Information Processing Systems (NeurIPS)*, 34:27381–27394, 2021a. (Cited on pages 12 and 13.)
- Yoshua Bengio, Salem Lahlou, Tristan Deleu, Edward J Hu, Mo Tiwari, and Emmanuel Bengio. Gflownet foundations. *arXiv preprint arXiv:2111.09266*, 2021b. (Cited on pages 12 and 13.)
- Johann Brehmer, Joey Bose, Pim De Haan, and Taco Cohen. Edgi: Equivariant diffusion for planning with embodied agents. In *Workshop on Reincarnating Reinforcement Learning at ICLR*, 2023. (Cited on page 12.)
- Anthony Brohan, Noah Brown, Justice Carbajal, Yevgen Chebotar, Joseph Dabis, Chelsea Finn, Keerthana Gopalakrishnan, Karol Hausman, Alex Herzog, Jasmine Hsu, Julian Ibarz, Brian Ichter, Alex Irpan, Tomas Jackson, Sally Jesmonth, Nikhil Joshi, Ryan Julian, Dmitry Kalashnikov, Yuheng Kuang, Isabel Leal, Kuang-Huei Lee, Sergey Levine, Yao Lu, Utsav Malla, Deeksha Manjunath, Igor Mordatch, Ofir Nachum, Carolina Parada, Jodilyn Peralta, Emily Perez, Karl Pertsch, Jornell Quiambao, Kanishka Rao, Michael Ryoo, Grecia Salazar, Pannag Sanketi, Kevin Sayed, Jaspiar Singh, Sumedh Sontakke, Austin Stone, Clayton Tan, Huong Tran, Vincent Vanhoucke, Steve Vega, Quan Vuong, Fei Xia, Ted Xiao, Peng Xu, Sichun Xu, Tianhe Yu, and Brianna Zitkovich. Rt-1: Robotics transformer for real-world control at scale. In *arXiv preprint arXiv:2212.06817*, 2022. (Cited on page 13.)
- Tom Brown, Benjamin Mann, Nick Ryder, Melanie Subbiah, Jared D Kaplan, Prafulla Dhariwal, Arvind Neelakantan, Pranav Shyam, Girish Sastry, Amanda Askell, et al. Language models are few-shot learners. *Advances in neural information processing systems (NeurIPS)*, 33:1877–1901, 2020. (Cited on page 13.)
- Hongrui Chen, Holden Lee, and Jianfeng Lu. Improved analysis of score-based generative modeling: User-friendly bounds under minimal smoothness assumptions. *arXiv preprint arXiv:2211.01916*, 2022. (Cited on page 29.)
- Huayu Chen, Cheng Lu, Chengyang Ying, Hang Su, and Jun Zhu. Offline reinforcement learning via high-fidelity generative behavior modeling. In *International Conference on Learning Representations (ICLR)*, 2023a. (Cited on pages 6 and 12.)
- Jinyin Chen, Shulong Hu, Haibin Zheng, Changyou Xing, and Guomin Zhang. Gail-pt: An intelligent penetration testing framework with generative adversarial imitation learning. *Computers & Security*, 126:103055, 2023b. (Cited on page 13.)
- Lili Chen, Kevin Lu, Aravind Rajeswaran, Kimin Lee, Aditya Grover, Misha Laskin, Pieter Abbeel, Aravind Srinivas, and Igor Mordatch. Decision transformer: Reinforcement learning via sequence modeling. *Advances in neural information processing systems (NeurIPS)*, 34:15084–15097, 2021. (Cited on page 13.)
- Sitan Chen, Sinho Chewi, Jerry Li, Yuanzhi Li, Adil Salim, and Anru R Zhang. Sampling is as easy as learning the score: theory for diffusion models with minimal data assumptions. In *International Conference on Learning Representations (ICLR)*, 2023c. (Cited on page 9.)
- Cheng Chi, Siyuan Feng, Yilun Du, Zhenjia Xu, Eric Cousineau, Benjamin Burchfiel, and Shuran Song. Diffusion policy: Visuomotor policy learning via action diffusion. *arXiv preprint arXiv:2303.04137*, 2023. (Cited on pages 3, 6, and 12.)

- Kai Lai Chung and Ruth J Williams. *Introduction to stochastic integration*, volume 2. Springer, 1990. (Cited on page 27.)
- Zichen Jeff Cui, Yibin Wang, Nur Muhammad, Lerrel Pinto, et al. From play to policy: Conditional behavior generation from uncurated robot data. *International Conference on Learning Representations (ICLR)*, 2023. (Cited on page 13.)
- Ankur Deka, Changliu Liu, and Katia P Sycara. Arc-actor residual critic for adversarial imitation learning. In *Conference on Robot Learning (CORL)*, pages 1446–1456. PMLR, 2023. (Cited on page 13.)
- Monroe D Donsker and SR Srinivasa Varadhan. Asymptotic evaluation of certain markov process expectations for large time. iv. *Communications on pure and applied mathematics*, 36(2):183–212, 1983. (Cited on page 28.)
- Lasse Espeholt, Hubert Soyer, Remi Munos, Karen Simonyan, Vlad Mnih, Tom Ward, Yotam Doron, Vlad Firoiu, Tim Harley, Iain Dunning, et al. Impala: Scalable distributed deep-rl with importance weighted actor-learner architectures. In *International conference on machine learning (ICML)*, pages 1407–1416. PMLR, 2018. (Cited on page 5.)
- Pete Florence, Corey Lynch, Andy Zeng, Oscar A Ramirez, Ayzaan Wahid, Laura Downs, Adrian Wong, Johnny Lee, Igor Mordatch, and Jonathan Tompson. Implicit behavioral cloning. In *Conference on Robot Learning (CORL)*, pages 158–168. PMLR, 2022. (Cited on page 13.)
- Adriaan Daniël Fokker. Die mittlere energie rotierender elektrischer dipole im strahlungsfeld. *Annalen der Physik*, 348(5):810–820, 1914. (Cited on page 27.)
- Justin Fu, Katie Luo, and Sergey Levine. Learning robust rewards with adversarial inverse reinforcement learning. In *International Conference on Learning Representations (ICLR)*, 2018. (Cited on page 13.)
- Scott Fujimoto, Herke Hoof, and David Meger. Addressing function approximation error in actor-critic methods. In *International conference on machine learning (ICML)*, pages 1587–1596. PMLR, 2018. (Cited on page 7.)
- Ian Goodfellow, Jean Pouget-Abadie, Mehdi Mirza, Bing Xu, David Warde-Farley, Sherjil Ozair, Aaron Courville, and Yoshua Bengio. Generative adversarial networks. *Communications of the ACM*, 63(11):139–144, 2020. (Cited on pages 12 and 13.)
- Tuomas Haarnoja, Haoran Tang, Pieter Abbeel, and Sergey Levine. Reinforcement learning with deep energy-based policies. In *International conference on machine learning (ICML)*, pages 1352–1361. PMLR, 2017. (Cited on pages 5, 7, and 50.)
- Tuomas Haarnoja, Vitchyr Pong, Aurick Zhou, Murtaza Dalal, Pieter Abbeel, and Sergey Levine. Composable deep reinforcement learning for robotic manipulation. In *2018 IEEE international conference on robotics and automation (ICRA)*, pages 6244–6251. IEEE, 2018a. (Cited on page 5.)
- Tuomas Haarnoja, Aurick Zhou, Pieter Abbeel, and Sergey Levine. Soft actor-critic: Off-policy maximum entropy deep reinforcement learning with a stochastic actor. In *International conference on machine learning (ICML)*, pages 1861–1870. PMLR, 2018b. (Cited on page 5.)

- Hado Hasselt. Double q-learning. *Advances in Neural Information Processing Systems (NeurIPS)*, 23, 2010. (Cited on page 56.)
- Ulrich G Haussmann and Etienne Pardoux. Time reversal of diffusions. *The Annals of Probability*, pages 1188–1205, 1986. (Cited on page 26.)
- Jonathan Ho and Stefano Ermon. Generative adversarial imitation learning. *Advances in neural information processing systems (NeurIPS)*, 29, 2016. (Cited on page 13.)
- Jonathan Ho, Ajay Jain, and Pieter Abbeel. Denoising diffusion probabilistic models. *Advances in Neural Information Processing Systems (NeurIPS)*, 33:6840–6851, 2020. (Cited on pages 3, 26, 33, and 34.)
- Aapo Hyvärinen. Estimation of non-normalized statistical models by score matching. *Journal of Machine Learning Research (JMLR)*, 6(4), 2005. (Cited on page 10.)
- Michael Janner, Yilun Du, Joshua Tenenbaum, and Sergey Levine. Planning with diffusion for flexible behavior synthesis. In *International Conference on Machine Learning (ICML)*, 2022. (Cited on pages 6 and 12.)
- Ivan Kapelyukh, Vitalis Vosylius, and Edward Johns. Dall-e-bot: Introducing web-scale diffusion models to robotics. In *CoRL 2022 Workshop on Pre-training Robot Learning*, 2022. (Cited on page 12.)
- Changyeon Kim, Jongjin Park, Jinwoo Shin, Honglak Lee, Pieter Abbeel, and Kimin Lee. Preference transformer: Modeling human preferences using transformers for rl. In *The Eleventh International Conference on Learning Representations (ICLR)*, 2023. (Cited on page 13.)
- Dongjun Kim, Seungjae Shin, Kyungwoo Song, Wanmo Kang, and Il-Chul Moon. Soft truncation: A universal training technique of score-based diffusion model for high precision score estimation. In *Proceedings of the 39th International Conference on Machine Learning (ICML)*, volume 162, pages 11201–11228, 2022. (Cited on page 26.)
- Diederik P Kingma and Max Welling. Auto-encoding variational bayes. *arXiv preprint arXiv:1312.6114*, 2013. (Cited on pages 12 and 13.)
- Andrei Kolmogoroff. Über die analytischen methoden in der wahrscheinlichkeitsrechnung. *Mathematische Annalen*, 104:415–458, 1931. (Cited on page 27.)
- Sachin G Konan, Esmaeil Seraj, and Matthew Gombolay. Contrastive decision transformers. In *Conference on Robot Learning (CORL)*, pages 2159–2169. PMLR, 2023. (Cited on page 13.)
- Yann LeCun, Sumit Chopra, Raia Hadsell, Marc’Aurelio Ranzato, and Fu Jie Huang. A tutorial on energy-based learning. *Predicting Structured Data*, 1:0, 2006. (Cited on page 13.)
- Holden Lee, Jianfeng Lu, and Yixin Tan. Convergence of score-based generative modeling for general data distributions. In *International Conference on Algorithmic Learning Theory (ALT)*, pages 946–985. PMLR, 2023. (Cited on page 8.)
- Sergey Levine, Aviral Kumar, George Tucker, and Justin Fu. Offline reinforcement learning: Tutorial, review, and perspectives on open problems. *arXiv preprint arXiv:2005.01643*, 2020. (Cited on page 12.)

- Wenhao Li, Baoxiang Wang, Shanchao Yang, and Hongyuan Zha. Diverse policy optimization for structured action space. In *Proceedings of the 22th International Conference on Autonomous Agents and MultiAgent Systems (AAMAS)*, 2023a. (Cited on page 13.)
- Yinchuan Li, Shuang Luo, Haozhi Wang, and Hao Jianye. Cflownets: Continuous control with generative flow networks. In *The Eleventh International Conference on Learning Representations (ICLR)*, 2023b. (Cited on page 13.)
- Zhixuan Liang, Yao Mu, Mingyu Ding, Fei Ni, Masayoshi Tomizuka, and Ping Luo. Adaptdiffuser: Diffusion models as adaptive self-evolving planners. *arXiv preprint arXiv:2302.01877*, 2023. (Cited on page 12.)
- Timothy P Lillicrap, Jonathan J Hunt, Alexander Pritzel, Nicolas Heess, Tom Erez, Yuval Tassa, David Silver, and Daan Wierstra. Continuous control with deep reinforcement learning. In *International Conference on Learning Representations (ICLR)*, 2016. (Cited on page 5.)
- Minghuan Liu, Tairan He, Minkai Xu, and Weinan Zhang. Energy-based imitation learning. In *Proceedings of the 20th International Conference on Autonomous Agents and MultiAgent Systems (AAMAS)*, pages 809–817, 2021. (Cited on page 13.)
- Weiyu Liu, Tucker Hermans, Sonia Chernova, and Chris Paxton. Structdiffusion: Object-centric diffusion for semantic rearrangement of novel objects. In *Workshop on Language and Robotics at CoRL*, 2022. (Cited on page 12.)
- Corey Lynch, Mohi Khansari, Ted Xiao, Vikash Kumar, Jonathan Tompson, Sergey Levine, and Pierre Sermanet. Learning latent plans from play. In *Conference on robot learning (CORL)*, pages 1113–1132. PMLR, 2020. (Cited on pages 12 and 13.)
- Yi-An Ma, Yuansi Chen, Chi Jin, Nicolas Flammarion, and Michael I Jordan. Sampling can be faster than optimization. *Proceedings of the National Academy of Sciences*, 116(42): 20881–20885, 2019. (Cited on page 9.)
- Nikolay Malkin, Moksh Jain, Emmanuel Bengio, Chen Sun, and Yoshua Bengio. Trajectory balance: Improved credit assignment in gflownets. In *Advances in Neural Information Processing Systems*, 2022. (Cited on page 13.)
- Ajay Mandlekar, Danfei Xu, Roberto Martín-Martín, Silvio Savarese, and Li Fei-Fei. Learning to generalize across long-horizon tasks from human demonstrations. In *Robotics: Science and Systems (RSS)*, 2020. (Cited on page 12.)
- Oier Mees, Lukas Hermann, and Wolfram Burgard. What matters in language conditioned robotic imitation learning over unstructured data. *IEEE Robotics and Automation Letters*, 7(4):11205–11212, 2022. (Cited on page 13.)
- Utkarsh A Mishra and Yongxin Chen. Reorientdiff: Diffusion model based reorientation for object manipulation. *arXiv preprint arXiv:2303.12700*, 2023. (Cited on page 12.)
- Diganta Misra. Mish: A self regularized non-monotonic activation function. *arXiv preprint arXiv:1908.08681*, 2019. (Cited on page 56.)

- Volodymyr Mnih, Koray Kavukcuoglu, David Silver, Andrei A Rusu, Joel Veness, Marc G Bellemare, Alex Graves, Martin Riedmiller, Andreas K Fidjeland, Georg Ostrovski, et al. Human-level control through deep reinforcement learning. *nature*, 518(7540):529–533, 2015. (Cited on page 5.)
- Takayuki Osa, Joni Pajarinen, Gerhard Neumann, J Andrew Bagnell, Pieter Abbeel, Jan Peters, et al. An algorithmic perspective on imitation learning. *Foundations and Trends® in Robotics*, 7(1-2):1–179, 2018. (Cited on page 12.)
- Ling Pan, Dinghuai Zhang, Moksh Jain, Longbo Huang, and Yoshua Bengio. Stochastic generative flow networks. *arXiv preprint arXiv:2302.09465*, 2023. (Cited on page 13.)
- Tim Pearce, Tabish Rashid, Anssi Kanervisto, Dave Bignell, Mingfei Sun, Raluca Georgescu, Sergio Valcarcel Macua, Shan Zheng Tan, Ida Momennejad, Katja Hofmann, et al. Imitating human behaviour with diffusion models. In *International Conference on Learning Representations (ICLR)*, 2023. (Cited on page 12.)
- Karl Pertsch, Youngwoon Lee, and Joseph Lim. Accelerating reinforcement learning with learned skill priors. In *Conference on robot learning (CORL)*, pages 188–204, 2021. (Cited on page 13.)
- Jan Peters, Katharina Mulling, and Yasemin Altun. Relative entropy policy search. In *Proceedings of the AAAI Conference on Artificial Intelligence*, volume 24, pages 1607–1612, 2010. (Cited on page 5.)
- VM Planck. Über einen satz der statistischen dynamik und seine erweiterung in der quantentheorie. *Sitzungsberichte der Preussischen Akademie der Wissenschaften zu Berlin*, 24: 324–341, 1917. (Cited on page 27.)
- Dean A Pomerleau. Alvin: An autonomous land vehicle in a neural network. *Advances in neural information processing systems (NeurIPS)*, 1, 1988. (Cited on page 12.)
- Rafael Rafailov, Victor Koley, Kyle Beltran Hatch, John D Martin, Mariano Phielipp, Jiajun Wu, and Chelsea Finn. Model-based adversarial imitation learning as online fine-tuning. In *Workshop on Reincarnating Reinforcement Learning at ICLR 2023*. (Cited on page 13.)
- Scott Reed, Konrad Zolna, Emilio Parisotto, Sergio Gómez Colmenarejo, Alexander Novikov, Gabriel Barth-maroon, Mai Giménez, Yury Sulsky, Jackie Kay, Jost Tobias Springenberg, Tom Eccles, Jake Bruce, Ali Razavi, Ashley Edwards, Nicolas Heess, Yutian Chen, Raia Hadsell, Oriol Vinyals, Mahyar Bordbar, and Nando de Freitas. A generalist agent. *Transactions on Machine Learning Research (TMLR)*, 2022. ISSN 2835-8856. (Cited on page 13.)
- Moritz Reuss, Maximilian Li, Xiaogang Jia, and Rudolf Lioutikov. Goal-conditioned imitation learning using score-based diffusion policies. *arXiv preprint arXiv:2304.02532*, 2023. (Cited on pages 3, 6, and 12.)
- Danilo Rezende and Shakir Mohamed. Variational inference with normalizing flows. In *International conference on machine learning (ICML)*, pages 1530–1538, 2015. (Cited on pages 12 and 13.)
- Hannes Risken and Hannes Risken. *Fokker-planck equation*. Springer, 1996. (Cited on page 27.)

- Erick Rosete-Beas, Oier Mees, Gabriel Kalweit, Joschka Boedecker, and Wolfram Burgard. Latent plans for task-agnostic offline reinforcement learning. In *Conference on Robot Learning (CORL)*, pages 1838–1849, 2023. (Cited on page 13.)
- Gavin A Rummery and Mahesan Niranjan. *On-line Q-learning using connectionist systems*, volume 37. University of Cambridge, Department of Engineering, 1994. (Cited on page 5.)
- Brian Sallans and Geoffrey E Hinton. Reinforcement learning with factored states and actions. *The Journal of Machine Learning Research (JMLR)*, 5:1063–1088, 2004. (Cited on page 5.)
- Simo Särkkä and Arno Solin. *Applied stochastic differential equations*, volume 10. Cambridge University Press, 2019. (Cited on pages 26 and 27.)
- John Schulman, Sergey Levine, Pieter Abbeel, Michael Jordan, and Philipp Moritz. Trust region policy optimization. In *International conference on machine learning (ICML)*, pages 1889–1897. PMLR, 2015. (Cited on page 5.)
- John Schulman, Xi Chen, and Pieter Abbeel. Equivalence between policy gradients and soft q-learning. *arXiv preprint arXiv:1704.06440*, 2017a. (Cited on page 5.)
- John Schulman, Filip Wolski, Prafulla Dhariwal, Alec Radford, and Oleg Klimov. Proximal policy optimization algorithms. *arXiv preprint arXiv:1707.06347*, 2017b. (Cited on page 5.)
- Nur Muhammad Shafiullah, Zichen Cui, Ariuntuya Arty Altanzaya, and Lerrel Pinto. Behavior transformers: Cloning  $k$  modes with one stone. *Advances in neural information processing systems (NeurIPS)*, 35:22955–22968, 2022. (Cited on page 13.)
- David Silver, Guy Lever, Nicolas Heess, Thomas Degris, Daan Wierstra, and Martin Riedmiller. Deterministic policy gradient algorithms. In *International conference on machine learning (ICML)*, pages 387–395. Pmlr, 2014. (Cited on page 5.)
- Avi Singh, Huihan Liu, Gaoyue Zhou, Albert Yu, Nicholas Rhinehart, and Sergey Levine. Parrot: Data-driven behavioral priors for reinforcement learning. In *International Conference on Learning Representations (ICLR)*, 2020. (Cited on page 13.)
- Jascha Sohl-Dickstein, Eric Weiss, Niru Maheswaranathan, and Surya Ganguli. Deep unsupervised learning using nonequilibrium thermodynamics. In *International Conference on Machine Learning (ICML)*, pages 2256–2265. PMLR, 2015. (Cited on pages 3 and 26.)
- Yang Song, Jascha Sohl-Dickstein, Diederik P Kingma, Abhishek Kumar, Stefano Ermon, and Ben Poole. Score-based generative modeling through stochastic differential equations. In *International Conference on Learning Representations (ICLR)*, 2021. (Cited on pages 3, 26, and 34.)
- Richard S Sutton. Learning to predict by the methods of temporal differences. *Machine learning*, 3:9–44, 1988. (Cited on page 13.)
- Richard S Sutton and Andrew G Barto. *Reinforcement learning: An introduction*. MIT press, 1998. (Cited on pages 5 and 13.)
- Richard S Sutton and Andrew G Barto. *Reinforcement learning: An introduction*. MIT press, 2018. (Cited on page 5.)

- Richard S Sutton, David McAllester, Satinder Singh, and Yishay Mansour. Policy gradient methods for reinforcement learning with function approximation. *Advances in neural information processing systems (NeurIPS)*, 12, 1999. (Cited on page 5.)
- Aleksandar Taranovic, Andras Gabor Kupcsik, Niklas Freymuth, and Gerhard Neumann. Adversarial imitation learning with preferences. In *The Eleventh International Conference on Learning Representations (ICLR)*, 2023. (Cited on page 13.)
- Emanuel Todorov, Tom Erez, and Yuval Tassa. Mujoco: A physics engine for model-based control. In *2012 IEEE/RSJ International Conference on Intelligent Robots and Systems*, pages 5026–5033. IEEE, 2012. doi: 10.1109/IROS.2012.6386109. (Cited on page 13.)
- Julen Urain, Niklas Funk, Georgia Chalvatzaki, and Jan Peters. Se(3)-diffusionfields: Learning cost functions for joint grasp and motion optimization through diffusion. In *2018 IEEE international conference on robotics and automation (ICRA)*, 2023. (Cited on page 12.)
- Aaron Van Den Oord, Oriol Vinyals, et al. Neural discrete representation learning. *Advances in neural information processing systems (NeurIPS)*, 30, 2017. (Cited on page 12.)
- Laurens Van der Maaten and Geoffrey Hinton. Visualizing data using t-sne. *Journal of machine learning research (JMLR)*, 9(11), 2008. (Cited on pages 14 and 57.)
- Ashish Vaswani, Noam Shazeer, Niki Parmar, Jakob Uszkoreit, Llion Jones, Aidan N Gomez, Lukasz Kaiser, and Illia Polosukhin. Attention is all you need. *Advances in neural information processing systems (NeurIPS)*, 30, 2017. (Cited on pages 13 and 56.)
- Santosh Vempala and Andre Wibisono. Rapid convergence of the unadjusted langevin algorithm: Isoperimetry suffices. In *Advances in neural information processing systems (NeurIPS)*, volume 32, 2019. (Cited on pages 9, 25, and 29.)
- Pascal Vincent. A connection between score matching and denoising autoencoders. *Neural computation*, 23(7):1661–1674, 2011. (Cited on page 10.)
- Lirui Wang, Xiangyun Meng, Yu Xiang, and Dieter Fox. Hierarchical policies for cluttered-scene grasping with latent plans. *IEEE Robotics and Automation Letters*, 7(2):2883–2890, 2022. (Cited on page 13.)
- Yunke Wang, Chang Xu, Bo Du, and Honglak Lee. Learning to weight imperfect demonstrations. In *International Conference on Machine Learning (ICML)*, pages 10961–10970. PMLR, 2021. (Cited on page 13.)
- Zhendong Wang, Jonathan J Hunt, and Mingyuan Zhou. Diffusion policies as an expressive policy class for offline reinforcement learning. In *International Conference on Learning Representations (ICLR)*, 2023. (Cited on pages 6 and 12.)
- Christopher John Cornish Hellaby Watkins. *Learning from delayed rewards*. PhD thesis, King’s College, Cambridge, 1989. (Cited on page 5.)
- Andre Wibisono and Varun Jog. Convexity of mutual information along the ornstein-uhlenbeck flow. In *2018 International Symposium on Information Theory and Its Applications (ISITA)*, pages 55–59. IEEE, 2018. (Cited on page 9.)



- Andre Wibisono and Kaylee Yingxi Yang. Convergence in kl divergence of the inexact langevin algorithm with application to score-based generative models. *arXiv preprint arXiv:2211.01512*, 2022. (Cited on pages 9, 28, and 44.)
- Ling Yang, Zhilong Zhang, Yang Song, Shenda Hong, Runsheng Xu, Yue Zhao, Yingxia Shao, Wentao Zhang, Bin Cui, and Ming-Hsuan Yang. Diffusion models: A comprehensive survey of methods and applications. *arXiv preprint arXiv:2209.00796*, 2022. (Cited on page 12.)
- Sherry Yang, Ofir Nachum, Yilun Du, Jason Wei, Pieter Abbeel, and Dale Schuurmans. Foundation models for decision making: Problems, methods, and opportunities. *arXiv preprint arXiv:2303.04129*, 2023. (Cited on page 12.)
- Chen Yongxin Zhang, Qinsheng. Fast sampling of diffusion models with exponential integrator. In *International Conference on Learning Representations (ICLR)*, 2022. (Cited on page 8.)
- Qinqing Zheng, Amy Zhang, and Aditya Grover. Online decision transformer. In *International Conference on Machine Learning (ICML)*, pages 27042–27059. PMLR, 2022. (Cited on page 13.)

## A Review on Notations

This section reviews some notations and integration by parts formula, using the notations consistent with [Vempala and Wibisono, 2019].

Given a smooth function  $f : \mathbb{R}^n \rightarrow \mathbb{R}$ , its **gradient**  $\nabla f : \mathbb{R}^n \rightarrow \mathbb{R}^n$  is the vector of partial derivatives:

$$\nabla f(\mathbf{x}) = \left( \frac{\partial f(\mathbf{x})}{\partial x_1}, \dots, \frac{\partial f(\mathbf{x})}{\partial x_n} \right)^\top.$$

The **Hessian**  $\nabla^2 f : \mathbb{R}^n \rightarrow \mathbb{R}^{n \times n}$  is the matrix of second partial derivatives:

$$\nabla^2 f(\mathbf{x}) = \left( \frac{\partial^2 f(\mathbf{x})}{\partial x_i \partial x_j} \right)_{1 \leq i, j \leq n}.$$

The **Laplacian**  $\Delta f : \mathbb{R}^n \rightarrow \mathbb{R}$  is the trace of its Hessian:

$$\Delta f(\mathbf{x}) = \text{Tr}(\nabla^2 f(\mathbf{x})) = \sum_{i=1}^n \frac{\partial^2 f(\mathbf{x})}{\partial x_i^2}.$$

Given a smooth vector field  $\mathbf{p} = (p_1, \dots, p_n) : \mathbb{R}^n \rightarrow \mathbb{R}^n$ , its **divergence** is  $\text{div} \cdot \mathbf{p} : \mathbb{R}^n \rightarrow \mathbb{R}$ :

$$(\text{div} \cdot \mathbf{p})(\mathbf{x}) = \sum_{i=1}^n \frac{\partial p_i(\mathbf{x})}{\partial x_i}. \quad (16)$$

When the variable of a function is clear and without causing ambiguity, we also denote the above notation as follows,

$$\text{div} \cdot (\mathbf{p}(\mathbf{x})) =: (\text{div} \cdot \mathbf{p})(\mathbf{x}) = \sum_{i=1}^n \frac{\partial p_i(\mathbf{x})}{\partial x_i}. \quad (17)$$

In particular, the divergence of the gradient is the Laplacian:

$$(\text{div} \cdot \nabla f)(\mathbf{x}) = \sum_{i=1}^n \frac{\partial^2 f(\mathbf{x})}{\partial x_i^2} = \Delta f(\mathbf{x}). \quad (18)$$

Let  $\rho(\mathbf{x})$  and  $\mu(\mathbf{x})$  be two smooth probability density functions on the space  $\mathbb{R}^p$ , the Kullback–Leibler (KL) divergence and relative Fisher information (FI) from  $\mu(\mathbf{x})$  to  $\rho(\mathbf{x})$  are defined as follows,

$$\text{KL}(\rho \parallel \mu) = \int_{\mathbb{R}^p} \rho(\mathbf{x}) \log \frac{\rho(\mathbf{x})}{\mu(\mathbf{x})} d\mathbf{x}, \quad \text{FI}(\rho \parallel \mu) = \int_{\mathbb{R}^p} \rho(\mathbf{x}) \left\| \nabla \log \frac{\rho(\mathbf{x})}{\mu(\mathbf{x})} \right\|_2^2 d\mathbf{x}. \quad (19)$$

Before we further analyze, we need the integration by parts formula. For any function  $f : \mathbb{R}^p \rightarrow \mathbb{R}$  and vector field  $\mathbf{v} : \mathbb{R}^p \rightarrow \mathbb{R}^p$  with sufficiently fast decay at infinity, we have the following **integration by parts** formula:

$$\int_{\mathbb{R}^p} \langle \mathbf{v}(\mathbf{x}), \nabla f(\mathbf{x}) \rangle d\mathbf{x} = - \int_{\mathbb{R}^p} f(\mathbf{x}) (\text{div} \cdot \mathbf{v})(\mathbf{x}) d\mathbf{x}. \quad (20)$$

## B Auxiliary Results

### B.1 Diffusion Probability Model (DPM).

This section reviews some basic background about the diffusion probability model (DPM). For a given (but unknown)  $p$ -dimensional data distribution  $q(\mathbf{x}_0)$ , DPM [Sohl-Dickstein et al., 2015, Ho et al., 2020, Song et al., 2021] is a latent variable generative model that learns a parametric model to approximate the distribution  $q(\mathbf{x}_0)$ . To simplify the presentation in this section, we only focus on the continuous-time diffusion [Song et al., 2021]. The mechanism of DPM contains two processes, *forward process* and *reverse process*; we present them as follows.

**Forward Process.** The forward process produces a sequence  $\{\mathbf{x}_t\}_{t=0:T}$  that perturbs the initial  $\mathbf{x}_0 \sim q(\cdot)$  into a Gaussian noise, which follows the next stochastic differential equation (SDE),

$$d\mathbf{x}_t = \mathbf{f}(\mathbf{x}_t, t)dt + g(t)d\mathbf{w}_t, \quad (21)$$

where  $\mathbf{f}(\cdot, \cdot)$  is the drift term,  $g(\cdot)$  is the diffusion term, and  $\mathbf{w}_t$  is the standard Wiener process.

**Reverse Process.** According to Anderson [1982], Haussmann and Pardoux [1986], there exists a corresponding reverse SDE that exactly coincides with the solution of the forward SDE (21):

$$d\mathbf{x}_t = [\mathbf{f}(\mathbf{x}_t, t) - g^2(t)\nabla \log p_t(\mathbf{x}_t)] d\bar{t} + g(t)d\bar{\mathbf{w}}_t, \quad (22)$$

where  $d\bar{t}$  is the backward time differential,  $d\bar{\mathbf{w}}_t$  is a standard Wiener process flowing backward in time, and  $p_t(\mathbf{x}_t)$  is the marginal probability distribution of the random variable  $\mathbf{x}_t$  at time  $t$ .

Once the *score function*  $\nabla \log p_t(\mathbf{x}_t)$  is known for each time  $t$ , we can derive the reverse diffusion process from SDE (22) and simulate it to sample from  $q(\mathbf{x}_0)$  [Song et al., 2021].

### B.2 Transition Probability for Ornstein-Uhlenbeck Process

**Proposition B.1.** *Consider the next SDEs,*

$$d\mathbf{x}_t = -\frac{1}{2}\beta(t)\mathbf{x}_t dt + g(t)d\mathbf{w}_t,$$

where  $\beta(\cdot)$  and  $g(\cdot)$  are real-valued functions. Then, for a given  $\mathbf{x}_0$ , the conditional distribution of  $\mathbf{x}_t|\mathbf{x}_0$  is a Gaussian distribution, i.e.,

$$\mathbf{x}_t|\mathbf{x}_0 \sim \mathcal{N}(\mathbf{x}_t|\boldsymbol{\mu}_t, \boldsymbol{\Sigma}_t),$$

where

$$\begin{aligned} \boldsymbol{\mu}_t &= \exp\left\{-\frac{1}{2}\int_0^t \beta(s)ds\right\} \mathbf{x}_0, \\ \boldsymbol{\Sigma}_t &= \exp\left\{-\int_0^t \beta(s)ds\right\} \left(\int_0^t \exp\left\{\int_0^\tau \beta(s)ds\right\} g^2(\tau)d\tau\right) \mathbf{I}. \end{aligned}$$

*Proof.* See [Kim et al., 2022, A.1] or [Särkkä and Solin, 2019, Chapter 6.1].  $\square$

### B.3 Exponential Integrator Discretization

The next Proposition B.2 provides a fundamental way for us to derivate the exponential integrator discretization (9).

**Proposition B.2.** *For a given state  $\mathbf{s}$ , we consider the following continuous time process, for  $t \in [t_k, t_{k+1}]$ ,*

$$d\mathbf{x}_t = \left( \mathbf{x}_t + 2\hat{\mathbf{S}}(\mathbf{x}_{t_k}, \mathbf{s}, T - t_k) \right) dt + \sqrt{2}d\mathbf{w}_t. \quad (23)$$

Then with Itô integration [Chung and Williams, 1990],

$$\mathbf{x}_t - \mathbf{x}_{t_k} = (e^{t-t_k} - 1) \left( \mathbf{x}_{t_k} + 2\hat{\mathbf{S}}(\mathbf{x}_{t_k}, \mathbf{s}, T - t_k) \right) + \sqrt{2} \int_{t_k}^t e^{t'-t_k} d\mathbf{w}_{t'},$$

where  $t \in [t_k, t_{k+1}]$ , and  $t_k = hk$ .

*Proof.* See [Särkkä and Solin, 2019, Chapter 6.1]. □

Recall SDE (8), according to Proposition B.2, we know the next SDE

$$d\hat{\mathbf{a}}_t = \left( \hat{\mathbf{a}}_t + 2\hat{\mathbf{S}}(\hat{\mathbf{a}}_{t_k}, \mathbf{s}, T - t_k) \right) dt + \sqrt{2}d\mathbf{w}_t, \quad t \in [t_k, t_{k+1}] \quad (24)$$

formulates the exponential integrator discretization as follows,

$$\hat{\mathbf{a}}_{t_{k+1}} - \hat{\mathbf{a}}_{t_k} = (e^{t_{k+1}-t_k} - 1) \left( \hat{\mathbf{a}}_{t_k} + 2\hat{\mathbf{S}}(\hat{\mathbf{a}}_{t_k}, \mathbf{s}, T - t_k) \right) + \sqrt{2} \int_{t_k}^{t_{k+1}} e^{t'-t_k} d\mathbf{w}_{t'} \quad (25)$$

$$= (e^h - 1) \left( \hat{\mathbf{a}}_{t_k} + 2\hat{\mathbf{S}}(\hat{\mathbf{a}}_{t_k}, \mathbf{s}, T - t_k) \right) + \sqrt{e^{2h} - 1}\mathbf{z}, \quad (26)$$

where last equation holds due to Wiener process is a stationary process with independent increments, i.e., the following holds,

$$\begin{aligned} \sqrt{2} \int_{t_k}^{t_{k+1}} e^{t'-t_k} d\mathbf{w}_{t'} &= \sqrt{2} \int_0^{t_{k+1}} e^{t'-t_k} d\mathbf{w}_{t'} - \sqrt{2} \int_0^{t_k} e^{t'-t_k} d\mathbf{w}_{t'} \\ &= \sqrt{e^{2h} - 1}\mathbf{z}, \end{aligned}$$

where  $\mathbf{z} \sim \mathcal{N}(\mathbf{0}, \mathbf{I})$ .

Then, we rewrite (26) as follows,

$$\hat{\mathbf{a}}_{t_{k+1}} = e^h \hat{\mathbf{a}}_{t_k} + (e^h - 1) \left( \hat{\mathbf{a}}_{t_k} + 2\hat{\mathbf{S}}(\hat{\mathbf{a}}_{t_k}, \mathbf{s}, T - t_k) \right) + \sqrt{e^{2h} - 1}\mathbf{z},$$

which concludes the iteration defined in (9).

### B.4 Fokker–Planck Equation

The Fokker–Planck equation is named after Adriaan Fokker and Max Planck, who described it in 1914 and 1917 [Fokker, 1914, Planck, 1917]. It is also known as the Kolmogorov forward equation, after Andrey Kolmogorov, who independently discovered it in 1931 [Kolmogoroff, 1931]. For more history and background about Fokker–Planck equation, please refer to [Risken and Risken, 1996] or [https://en.wikipedia.org/wiki/Fokker%E2%80%93Planck\\_equation#cite\\_note-1](https://en.wikipedia.org/wiki/Fokker%E2%80%93Planck_equation#cite_note-1).

For an Itô process driven by the standard Wiener process  $\mathbf{w}_t$  and described by the stochastic differential equation

$$d\mathbf{x}_t = \boldsymbol{\mu}(\mathbf{x}_t, t)dt + \boldsymbol{\Sigma}(\mathbf{x}_t, t)d\mathbf{w}_t, \quad (27)$$

where  $\mathbf{x}_t$  and  $\boldsymbol{\mu}(\mathbf{x}_t, t)$  are  $N$ -dimensional random vectors,  $\boldsymbol{\Sigma}(\mathbf{x}_t, t)$  is an  $n \times m$  matrix and  $\mathbf{w}_t$  is an  $m$ -dimensional standard Wiener process, the probability density  $p(\mathbf{x}, t)$  for  $\mathbf{x}_t$  satisfies the Fokker–Planck equation

$$\frac{\partial p(\mathbf{x}, t)}{\partial t} = - \sum_{i=1}^N \frac{\partial}{\partial x_i} [\mu_i(\mathbf{x}, t)p(\mathbf{x}, t)] + \sum_{i=1}^N \sum_{j=1}^N \frac{\partial^2}{\partial x_i \partial x_j} [D_{ij}(\mathbf{x}, t)p(\mathbf{x}, t)], \quad (28)$$

with drift vector  $\boldsymbol{\mu} = (\mu_1, \dots, \mu_N)$  and diffusion tensor  $\mathbf{D}(\mathbf{x}, t) = \frac{1}{2}\boldsymbol{\Sigma}\boldsymbol{\Sigma}^\top$ , i.e.

$$D_{ij}(\mathbf{x}, t) = \frac{1}{2} \sum_{k=1}^M \sigma_{ik}(\mathbf{x}, t)\sigma_{jk}(\mathbf{x}, t),$$

and  $\sigma_{ij}$  denotes the  $(i, j)$ -th element of the matrix  $\boldsymbol{\Sigma}$ .

## B.5 Donsker-Varadhan Representation for KL-divergence

**Proposition B.3** ([Donsker and Varadhan, 1983]). *Let  $\rho, \mu$  be two probability distributions on the measure space  $(\mathcal{X}, \mathcal{F})$ , where  $\mathcal{X} \in \mathbb{R}^p$ . Then*

$$\text{KL}(\rho\|\mu) = \sup_{f:\mathcal{X}\rightarrow\mathbb{R}} \left\{ \int_{\mathbb{R}^p} \rho(\mathbf{x})f(\mathbf{x})d\mathbf{x} - \log \int_{\mathbb{R}^p} \mu(\mathbf{x}) \exp(f(\mathbf{x}))d\mathbf{x} \right\}.$$

The Donsker-Varadhan representation for KL-divergence implies for any  $f(\cdot)$ ,

$$\text{KL}(\rho\|\mu) \geq \int_{\mathbb{R}^p} \rho(\mathbf{x})f(\mathbf{x})d\mathbf{x} - \log \int_{\mathbb{R}^p} \mu(\mathbf{x}) \exp(f(\mathbf{x}))d\mathbf{x}, \quad (29)$$

which is useful later.

## B.6 Some Basic Results for Diffusion Policy

**Proposition B.4.** *Let  $\pi(\cdot|\mathbf{s})$  satisfy  $\nu$ -Log-Sobolev inequality (LSI) (see Assumption 4.2), the initial random action  $\bar{\mathbf{a}}_0 \sim \pi(\cdot|\mathbf{s})$ , and  $\bar{\mathbf{a}}_t$  evolves according to the following Ornstein-Uhlenbeck process,*

$$d\bar{\mathbf{a}}_t = -\bar{\mathbf{a}}_t dt + \sqrt{2}d\mathbf{w}_t. \quad (30)$$

*Let  $\bar{\mathbf{a}}_t \sim \bar{\pi}_t(\cdot|\mathbf{s})$  be the evolution along the Ornstein-Uhlenbeck flow (30), then  $\bar{\pi}_t(\cdot|\mathbf{s})$  is  $\nu_t$ -LSI, where*

$$\nu_t = \frac{\nu}{\nu + (1 - \nu)e^{-2t}}.$$

*Proof.* See [Wibisono and Yang, 2022, Lemma 6]. □

**Proposition B.5.** *Under Assumption 4.1, then  $\nabla \log \tilde{\pi}_t(\cdot|\mathbf{s})$  is  $L_p e^t$ -Lipschitz on the time interval  $[0, T_0]$ , where the policy  $\tilde{\pi}_t(\cdot|\mathbf{s})$  is the evolution along the flow (4), and the time  $T_0$  is defined as follows,*

$$T_0 =: \sup_{t \geq 0} \left\{ t : 1 - e^{-2t} \leq \frac{e^{-t}}{L_p} \right\}.$$

*Proof.* [Chen et al., 2022, Lemma 13]. □

The positive scalar  $T_0$  is well-defined, i.e.,  $T_0$  always exists. In fact, let  $1 - e^{-2t} \leq \frac{e^{-t}}{L_p} \geq 0$ , then the following holds,

$$e^{-t} \geq \sqrt{\frac{1}{L_p^2} + 4} - \frac{1}{L_p},$$

then

$$T_0 = \log \left( \frac{1}{4} \left( \sqrt{\frac{1}{L_p^2} + 4} + \frac{1}{L_p} \right) \right).$$

**Proposition B.6.** ([Vempala and Wibisono, 2019, Lemma 10]) *Let  $\rho(\mathbf{x})$  be a probability distribution function on  $\mathbb{R}^p$ , and let  $f(\mathbf{x}) = -\log \rho(\mathbf{x})$  be a  $L$ -smooth, i.e., there exists a positive constant  $L$  such that  $-L\mathbf{I} \preceq \nabla^2 f(\mathbf{x}) \preceq L\mathbf{I}$  for all  $\mathbf{x} \in \mathbb{R}^p$ . Furthermore, let  $\rho(\mathbf{x})$  satisfy the LSI condition with constant  $\nu > 0$ , i.e., for any probability distribution  $\mu(\mathbf{x})$ ,  $\text{KL}(\mu||\rho) \leq \frac{1}{2\nu} \text{FI}(\mu||\rho)$ . Then for any distribution  $\mu(\mathbf{x})$ , the following equation holds,*

$$\mathbb{E}_{\mathbf{x} \sim \mu(\cdot)} [\|\nabla \log \rho(\mathbf{x})\|_2^2] = \int_{\mathbb{R}^p} \mu(\mathbf{x}) \|\nabla \log \rho(\mathbf{x})\|_2^2 d\mathbf{x} \leq \frac{4L^2}{\nu} \text{KL}(\mu||\rho) + 2pL.$$

## C Implementation Details of DIPO

In this section, we provide all the details of our implementation for DIPO.

---

### Algorithm 3: (DIPO): Model-Free Learning with Diffusion Policy

---

- 1: Initialize parameter  $\phi$ , critic networks  $Q_\psi$ , target networks  $Q_{\psi'}$ , length  $K$ ;
- 2: Initialize  $\{\beta_i\}_{i=1}^K$ ;  $\alpha_i =: 1 - \beta_i$ ,  $\bar{\alpha}_k =: \prod_{i=1}^k \alpha_i$ ,  $\sigma_k =: \sqrt{\frac{1 - \bar{\alpha}_{k-1}}{1 - \bar{\alpha}_k}} \beta_k$ ;
- 3: Initialize  $\psi' \leftarrow \psi$ ,  $\phi' \leftarrow \phi$ ;
- 4: **repeat**
- 5:    **#update experience with diffusion policy**
- 6:    dataset  $\mathcal{D}_{\text{env}} \leftarrow \emptyset$ ; initial state  $\mathbf{s}_0 \sim d_0(\cdot)$ ;
- 7:    **for**  $t = 0, 1, \dots, T$  **do**
- 8:      initial  $\hat{\mathbf{a}}_K \sim \mathcal{N}(\mathbf{0}, \mathbf{I})$ ;
- 9:      **for**  $k = K, \dots, 1$  **do**
- 10:         $\mathbf{z}_k \sim \mathcal{N}(\mathbf{0}, \mathbf{I})$ , if  $k > 1$ ; else  $\mathbf{z}_k = \mathbf{0}$ ;
- 11:         $\hat{\mathbf{a}}_{k-1} \leftarrow \frac{1}{\sqrt{\alpha_k}} \left( \hat{\mathbf{a}}_k - \frac{\beta_k}{\sqrt{1 - \bar{\alpha}_k}} \epsilon_\phi(\hat{\mathbf{a}}_k, \mathbf{s}, k) \right) + \sigma_k \mathbf{z}_k$ ;
- 12:      **end for**
- 13:       $\mathbf{a}_t \leftarrow \hat{\mathbf{a}}_0$ ;  $\mathbf{s}_{t+1} \sim \mathbb{P}(\cdot | \mathbf{s}_t, \mathbf{a}_t)$ ;  $\mathcal{D}_{\text{env}} \leftarrow \mathcal{D}_{\text{env}} \cup \{\mathbf{s}_t, \mathbf{a}_t, \mathbf{s}_{t+1}, r(\mathbf{s}_{t+1} | \mathbf{s}_t, \mathbf{a}_t)\}$ ;
- 14:    **end for**
- 15:    **#update value function**
- 16:    **for** each mini-batch data **do**
- 17:      sample mini-batch  $\mathcal{D}$  from  $\mathcal{D}_{\text{env}}$  with size  $N$ ,  $\mathcal{D} = \{\mathbf{s}_j, \mathbf{a}_j, \mathbf{s}_{j+1}, r(\mathbf{s}_{j+1} | \mathbf{s}_j, \mathbf{a}_j)\}_{j=1}^N$ ;
- 18:      take gradient descent as follows

$$\psi \leftarrow \psi - \eta_\psi \nabla_\psi \frac{1}{N} \sum_{j=1}^N \left( r(\mathbf{s}_{j+1} | \mathbf{s}_j, \mathbf{a}_j) + \gamma Q_{\psi'}(\mathbf{s}_{j+1}, \mathbf{a}_{j+1}) - Q_\psi(\mathbf{s}_j, \mathbf{a}_j) \right)^2;$$

- 19:    **end for**
- 20:    **#improve experience through action**
- 21:    **for**  $t = 0, 1, \dots, T$  **do**
- 22:      replace the action  $\mathbf{a}_t \in \mathcal{D}_{\text{env}}$  as follows

$$\mathbf{a}_t \leftarrow \mathbf{a}_t + \eta_a \nabla_{\mathbf{a}} Q_\psi(\mathbf{s}_t, \mathbf{a}) \Big|_{\mathbf{a}=\mathbf{a}_t};$$

- 23:    **end for**
- 24:    **#update diffusion policy**
- 25:    **for** each pair **do**
- 26:      sample a pair  $(\mathbf{s}, \mathbf{a}) \sim \mathcal{D}_{\text{env}}$  uniformly;  $k \sim \text{Uniform}(\{1, \dots, K\})$ ;  $\mathbf{z} \sim \mathcal{N}(\mathbf{0}, \mathbf{I})$ ;
- 27:      take gradient descent as follows

$$\phi \leftarrow \phi - \eta_\phi \nabla_\phi \left\| \mathbf{z} - \epsilon_\phi \left( \sqrt{\bar{\alpha}_k} \mathbf{a} + \sqrt{1 - \bar{\alpha}_k} \mathbf{z}, \mathbf{s}, k \right) \right\|_2^2;$$

- 28:    **end for**
  - 29:    soft update  $\psi' \leftarrow \rho \psi' + (1 - \rho) \psi$ ;
  - 30:    soft update  $\phi' \leftarrow \rho \phi' + (1 - \rho) \phi$ ;
  - 31: **until** the policy performs well in the real environment.
-

## C.1 DIPO: Model-Free Learning with Diffusion Policy

Our source code follows the Algorithm 3.

## C.2 Loss Function of DIPO

In this section, we provide the details of [#update diffusion policy](#) presented in Algorithm 3. We present the derivation of the loss of score matching (10) and present the details of updating the diffusion from samples. First, the next Theorem C.1 shows an equivalent version of the loss defined in (10), then we present the learning details from samples.

### C.2.1 Conditional Sampling Version of Score Matching

**Theorem C.1.** *For give a partition on the interval  $[0, T]$ ,  $0 = t_0 < t_1 < \dots < t_k < t_{k+1} < \dots < t_K = T$ , let  $\alpha_0 = e^{-2T}$ ,  $\alpha_k = e^{2(-t_{k+1}+t_k)}$ , and  $\bar{\alpha}_{k-1} = \prod_{k'=0}^k \alpha_{k'}$ . Setting  $\omega(t)$  according to the next (36), then the objective (10) follows the next expectation version,*

$$\mathcal{L}(\phi) = \mathbb{E}_{k \sim \mathcal{U}([K]), \mathbf{z}_k \sim \mathcal{N}(\mathbf{0}, \mathbf{I}), \bar{\mathbf{a}}_0 \sim \pi(\cdot | \mathbf{s})} \left[ \mathbf{z}_k - \epsilon_\phi \left( \sqrt{\bar{\alpha}_k} \bar{\mathbf{a}}_0 + \sqrt{1 - \bar{\alpha}_k} \mathbf{z}_k, \mathbf{s}, k \right) \right], \quad (31)$$

where  $[K] =: \{1, 2, \dots, K\}$ ,  $\mathcal{U}(\cdot)$  denotes uniform distribution, the parametic funciton

$$\epsilon_\phi(\cdot, \cdot, \cdot) : \mathcal{A} \times \mathcal{S} \times [K] \rightarrow \mathbb{R}^p$$

shares the parameter  $\phi$  according to:

$$\epsilon_\phi(\cdot, \cdot, k) = -\sqrt{1 - \bar{\alpha}_k} \hat{\mathbf{s}}_\phi(\cdot, \cdot, T - t_k).$$

*Proof.* According to (3), and Proposition B.1, we know  $\varphi_t(\bar{\mathbf{a}}_t | \bar{\mathbf{a}}_0) = \mathcal{N}(e^{-t} \bar{\mathbf{a}}_0, (1 - e^{-2t}) \mathbf{I})$ , then

$$\nabla \log \varphi_t(\bar{\mathbf{a}}_t | \bar{\mathbf{a}}_0) = -\frac{\bar{\mathbf{a}}_t - e^{-t} \bar{\mathbf{a}}_0}{1 - 2e^{-t}} = -\frac{\mathbf{z}_t}{\sqrt{1 - 2e^{-t}}}, \quad (32)$$

where  $\mathbf{z}_t \sim \mathcal{N}(\mathbf{0}, \mathbf{I})$ ,

Let  $\sigma_t = \sqrt{1 - e^{-2t}}$ , according to (3), we know

$$\bar{\mathbf{a}}_t = e^{-t} \bar{\mathbf{a}}_0 + \left( \sqrt{1 - e^{-2t}} \right) \mathbf{z}_t = e^{-t} \bar{\mathbf{a}}_0 + \sigma_t \mathbf{z}_t, \quad (33)$$

where  $\mathbf{z}_t \sim \mathcal{N}(\mathbf{0}, \mathbf{I})$ .

Recall (10), we obtain

$$\begin{aligned} \mathcal{L}(\phi) &= \int_0^T \omega(t) \mathbb{E}_{\bar{\mathbf{a}}_0 \sim \pi(\cdot | \mathbf{s})} \mathbb{E}_{\bar{\mathbf{a}}_t | \bar{\mathbf{a}}_0} \left[ \|\hat{\mathbf{s}}_\phi(\bar{\mathbf{a}}_t, \mathbf{s}, t) - \nabla \log \varphi_t(\bar{\mathbf{a}}_t | \bar{\mathbf{a}}_0)\|_2^2 \right] dt \\ &\stackrel{(32)}{=} \int_0^T \frac{\omega(t)}{\sigma_t^2} \mathbb{E}_{\bar{\mathbf{a}}_0 \sim \pi(\cdot | \mathbf{s})} \mathbb{E}_{\bar{\mathbf{a}}_t | \bar{\mathbf{a}}_0} \left[ \|\sigma_t \hat{\mathbf{s}}_\phi(\bar{\mathbf{a}}_t, \mathbf{s}, t) + \mathbf{z}_t\|_2^2 \right] dt \end{aligned} \quad (34)$$

$$\stackrel{t \leftarrow T-t}{=} \int_0^T \frac{\omega(T-t)}{\sigma_{T-t}^2} \mathbb{E}_{\bar{\mathbf{a}}_0 \sim \pi(\cdot | \mathbf{s})} \mathbb{E}_{\bar{\mathbf{a}}_{T-t} | \bar{\mathbf{a}}_0} \left[ \|\sigma_{T-t} \hat{\mathbf{s}}_\phi(\bar{\mathbf{a}}_{T-t}, \mathbf{s}, T-t) + \mathbf{z}_{T-t}\|_2^2 \right] dt. \quad (35)$$

Furthermore, we define an indicator function  $\mathbb{I}_{t'}(t)$  as follows,

$$\mathbb{I}_{t'}(t) =: \begin{cases} 1, & \text{if } t' = t; \\ 0, & \text{if } t' \neq t. \end{cases}$$



Let the weighting function be defined as follows, for any  $t \in [0, T]$ ,

$$\omega(t) = \frac{1}{K} \sum_{k=1}^K \left(1 - e^{-2(T-t)}\right) \mathbb{I}_{T-t_k}(t), \quad (36)$$

where we give a partition on the interval  $[0, T]$  as follows,

$$0 = t_0 < t_1 < \dots < t_k < t_{k+1} < \dots < t_K = T.$$

Then, we rewrite (34) as follows,

$$\mathcal{L}(\phi) = \frac{1}{K} \sum_{k=1}^K \mathbb{E}_{\bar{\mathbf{a}}_0 \sim \pi(\cdot|\mathbf{s})} \mathbb{E}_{\bar{\mathbf{a}}_{T-t_k} | \bar{\mathbf{a}}_0} \left[ \|\sigma_{T-t_k} \hat{\mathbf{s}}_\phi(\bar{\mathbf{a}}_{T-t_k}, \mathbf{s}, T-t_k) + \mathbf{z}_{T-t_k}\|_2^2 \right]. \quad (37)$$

We consider the next term contained in (37)

$$\begin{aligned} \hat{\mathbf{s}}_\phi(\bar{\mathbf{a}}_{T-t_k}, \mathbf{s}, T-t_k) &\stackrel{(33)}{=} \hat{\mathbf{s}}_\phi \left( e^{-(T-t_k)} \bar{\mathbf{a}}_0 + \sigma_{T-t_k} \mathbf{z}_{T-t_k}, \mathbf{s}, T-t_k \right) \\ &= \hat{\mathbf{s}}_\phi \left( e^{-(T-t_k)} \bar{\mathbf{a}}_0 + \sqrt{1 - e^{-2(T-t_k)}} \mathbf{z}_{T-t_k}, \mathbf{s}, T-t_k \right), \end{aligned}$$

where  $\mathbf{z}_{T-t_k} \sim \mathcal{N}(\mathbf{0}, \mathbf{I})$ , then obtain

$$\begin{aligned} &\mathbb{E}_{\bar{\mathbf{a}}_{T-t_k} | \bar{\mathbf{a}}_0} \left[ \|\hat{\mathbf{s}}_\phi(\bar{\mathbf{a}}_{T-t_k}, \mathbf{s}, T-t_k) + \mathbf{z}_{T-t_k}\|_2^2 \right] \\ &= \mathbb{E}_{\mathbf{z}_{T-t_k} \sim \mathcal{N}(\mathbf{0}, \mathbf{I})} \left[ \sigma_{T-t_k} \hat{\mathbf{s}}_\phi \left( e^{-(T-t_k)} \bar{\mathbf{a}}_0 + \sqrt{1 - e^{-2(T-t_k)}} \mathbf{z}_{T-t_k}, \mathbf{s}, T-t_k \right) \right]. \end{aligned}$$

Now, we rewrite (37) as the next expectation version,

$$\mathcal{L}(\phi) = \mathbb{E}_{k \sim \mathcal{U}([K]), \mathbf{z}_k \sim \mathcal{N}(\mathbf{0}, \mathbf{I}), \bar{\mathbf{a}}_0 \sim \pi(\cdot|\mathbf{s})} \left[ \sigma_{T-t_k} \hat{\mathbf{s}}_\phi \left( e^{-(T-t_k)} \bar{\mathbf{a}}_0 + \sqrt{1 - e^{-2(T-t_k)}} \mathbf{z}_{T-t_k}, \mathbf{s}, T-t_k \right) \right] \quad (38)$$

For  $k = 0, 1, \dots, K$ , and  $\alpha_0 = e^{-2T}$  and

$$\alpha_k = e^{2(-t_{k+1} + t_k)}. \quad (39)$$

Then we obtain

$$\bar{\alpha}_k = \prod_{k'=0}^{k-1} \alpha_{k'} = e^{-2(T-t_k)}.$$

With those notations, we rewrite (38) as follows,

$$\mathcal{L}(\phi) = \mathbb{E}_{k \sim \mathcal{U}([K]), \mathbf{z}_k \sim \mathcal{N}(\mathbf{0}, \mathbf{I}), \bar{\mathbf{a}}_0 \sim \pi(\cdot|\mathbf{s})} \left[ \sqrt{1 - \bar{\alpha}_k} \hat{\mathbf{s}}_\phi \left( \sqrt{\bar{\alpha}_k} \bar{\mathbf{a}}_0 + \sqrt{1 - \bar{\alpha}_k} \mathbf{z}_k, \mathbf{s}, T-t_k \right) + \mathbf{z}_k \right]. \quad (40)$$

Finally, we define a function  $\epsilon_\phi(\cdot, \cdot, \cdot) : \mathcal{S} \times \mathcal{A} \times [K] \rightarrow \mathbb{R}^p$ , and

$$\epsilon_\phi \left( \sqrt{\bar{\alpha}_k} \bar{\mathbf{a}}_0 + \sqrt{1 - \bar{\alpha}_k} \mathbf{z}_k, \mathbf{s}, k \right) =: -\sqrt{1 - \bar{\alpha}_k} \hat{\mathbf{s}}_\phi \left( \sqrt{\bar{\alpha}_k} \bar{\mathbf{a}}_0 + \sqrt{1 - \bar{\alpha}_k} \mathbf{z}_k, \mathbf{s}, T-t_k \right), \quad (41)$$

i.e. we estimate the score function via an estimator  $\epsilon_\phi$  as follows,

$$\hat{\mathbf{s}}_\phi \left( \sqrt{\bar{\alpha}_k} \bar{\mathbf{a}}_0 + \sqrt{1 - \bar{\alpha}_k} \mathbf{z}_k, \mathbf{s}, T-t_k \right) = -\frac{\epsilon_\phi \left( \sqrt{\bar{\alpha}_k} \bar{\mathbf{a}}_0 + \sqrt{1 - \bar{\alpha}_k} \mathbf{z}_k, \mathbf{s}, k \right)}{\sqrt{1 - \bar{\alpha}_k}}. \quad (42)$$

Then we rewrite (40) as follows,

$$\mathcal{L}(\phi) = \mathbb{E}_{k \sim \mathcal{U}([K]), \mathbf{z}_k \sim \mathcal{N}(\mathbf{0}, \mathbf{I}), \bar{\mathbf{a}}_0 \sim \pi(\cdot|\mathbf{s})} \left[ \mathbf{z}_k - \epsilon_\phi \left( \sqrt{\bar{\alpha}_k} \bar{\mathbf{a}}_0 + \sqrt{1 - \bar{\alpha}_k} \mathbf{z}_k, \mathbf{s}, k \right) \right].$$

This concludes the proof.  $\square$

---

**Algorithm 4:** Diffusion Policy (A Backward Version [Ho et al., 2020])
 

---

- 1: input state  $\mathbf{s}$ ; parameter  $\phi$ ; reverse length  $K$ ;
  - 2: initialize  $\{\beta_i\}_{i=1}^K$ ;  $\alpha_i =: 1 - \beta_i$ ,  $\bar{\alpha}_k =: \prod_{i=1}^k \alpha_i$ ,  $\sigma_k =: \sqrt{\frac{1 - \bar{\alpha}_{k-1}}{1 - \bar{\alpha}_k}} \beta_k$ ;
  - 3: initial  $\hat{\mathbf{a}}_K \sim \mathcal{N}(\mathbf{0}, \mathbf{I})$ ;
  - 4: **for**  $k = K, \dots, 1$  **do**
  - 5:    $\mathbf{z}_k \sim \mathcal{N}(\mathbf{0}, \mathbf{I})$ , if  $k > 1$ ; else  $\mathbf{z}_k = \mathbf{0}$ ;
  - 6:    $\hat{\mathbf{a}}_{k-1} \leftarrow \frac{1}{\sqrt{\alpha_k}} \left( \hat{\mathbf{a}}_k - \frac{\beta_k}{\sqrt{1 - \bar{\alpha}_k}} \epsilon_\phi(\hat{\mathbf{a}}_k, \mathbf{s}, k) \right) + \sigma_k \mathbf{z}_k$ ;
  - 7: **end for**
  - 8: return  $\hat{\mathbf{a}}_0$
- 

### C.2.2 Learning from Samples

According to the expectation version of loss (31), we know, for each pair  $(\mathbf{s}, \mathbf{a})$  sampled from experience memory, let  $k \sim \text{Uniform}(\{1, \dots, K\})$  and  $\mathbf{z} \sim \mathcal{N}(\mathbf{0}, \mathbf{I})$ , the following empirical loss

$$\ell_d(\phi) = \|\mathbf{z} - \epsilon_\phi(\sqrt{\alpha_k} \mathbf{a} + \sqrt{1 - \bar{\alpha}_k} \mathbf{z}, \mathbf{s}, k)\|_2^2$$

is a unbiased estimator of  $\mathcal{L}(\phi)$  defined in (31).

Finally, we learn the parameter  $\phi$  by minimizing the empirical loss  $\ell_d(\phi)$  according to gradient decent method:

$$\phi \leftarrow \phi - \eta_\phi \nabla_\phi \|\mathbf{z} - \epsilon_\phi(\sqrt{\alpha_k} \mathbf{a} + \sqrt{1 - \bar{\alpha}_k} \mathbf{z}, \mathbf{s}, k)\|_2^2,$$

where  $\epsilon_\phi$  is the step-size. For the implementation, see lines 25-28 in Algorithm 3.

### C.3 Playing Actions of DIPO

In this section, we present all the details of #update experience with diffusion policy presented in Algorithm 3.

Let  $\beta_k = 1 - \alpha_k$ , then according to Taylor formulation, we know

$$\sqrt{\alpha_k} = 1 - \frac{1}{2} \beta_k + o(\beta_k). \quad (43)$$

Recall the exponential integrator discretization (25), we know

$$\hat{\mathbf{a}}_{t_{k+1}} - \hat{\mathbf{a}}_{t_k} = (e^{t_{k+1} - t_k} - 1) (\hat{\mathbf{a}}_{t_k} + 2\hat{\mathbf{s}}_\phi(\hat{\mathbf{a}}_{t_k}, \mathbf{s}, T - t_k)) + \sqrt{2} \int_{t_k}^{t_{k+1}} e^{t' - t_k} d\mathbf{w}_{t'},$$

which implies

$$\begin{aligned} \hat{\mathbf{a}}_{t_{k+1}} &= \hat{\mathbf{a}}_{t_k} + (e^{t_{k+1} - t_k} - 1) (\hat{\mathbf{a}}_{t_k} + 2\hat{\mathbf{s}}_\phi(\hat{\mathbf{a}}_{t_k}, \mathbf{s}, T - t_k)) + \sqrt{e^{2(t_{k+1} - t_k)} - 1} \mathbf{z}_{t_k} \\ &\stackrel{(39)}{=} \hat{\mathbf{a}}_{t_k} + \left( \frac{1}{\sqrt{\alpha_k}} - 1 \right) (\hat{\mathbf{a}}_{t_k} + 2\hat{\mathbf{s}}_\phi(\hat{\mathbf{a}}_{t_k}, \mathbf{s}, T - t_k)) + \sqrt{\frac{1 - \alpha_k}{\alpha_k}} \mathbf{z}_{t_k} \\ &\stackrel{(42)}{=} \frac{1}{\sqrt{\alpha_k}} \hat{\mathbf{a}}_{t_k} - 2 \left( \frac{1}{\sqrt{\alpha_k}} - 1 \right) \frac{1}{\sqrt{1 - \bar{\alpha}_k}} \epsilon_\phi(\hat{\mathbf{a}}_{t_k}, \mathbf{s}, k) + \sqrt{\frac{1 - \alpha_k}{\alpha_k}} \mathbf{z}_{t_k} \\ &= \frac{1}{\sqrt{\alpha_k}} \hat{\mathbf{a}}_{t_k} - \frac{\beta_k}{\sqrt{\alpha_k}} \cdot \frac{1}{\sqrt{1 - \bar{\alpha}_k}} \epsilon_\phi(\hat{\mathbf{a}}_{t_k}, \mathbf{s}, k) + \sqrt{\frac{1 - \alpha_k}{\alpha_k}} \mathbf{z}_{t_k}, \end{aligned} \quad (44)$$

where  $\mathbf{z}_{t_k} \sim \mathcal{N}(\mathbf{0}, \mathbf{I})$ , Eq.(44) holds since we use the fact (43), which implies

$$2 \left( \frac{1}{\sqrt{\alpha_k}} - 1 \right) = 2 \left( \frac{1 - \sqrt{\alpha_k}}{\sqrt{\alpha_k}} \right) = \frac{\beta_k}{\sqrt{\alpha_k}} + o \left( \frac{\beta_k}{\sqrt{\alpha_k}} \right).$$

To simplify the expression, we rewrite (44) as follows,

$$\hat{\mathbf{a}}_{k+1} = \frac{1}{\sqrt{\alpha_k}} \hat{\mathbf{a}}_k - \frac{\beta_k}{\sqrt{\alpha_k}} \cdot \frac{1}{\sqrt{1 - \bar{\alpha}_k}} \boldsymbol{\epsilon}_\phi(\hat{\mathbf{a}}_k, \mathbf{s}, k) + \sqrt{\frac{1 - \alpha_k}{\alpha_k}} \mathbf{z}_k \quad (45)$$

$$= \frac{1}{\sqrt{\alpha_k}} \left( \hat{\mathbf{a}}_k - \frac{\beta_k}{\sqrt{1 - \bar{\alpha}_k}} \boldsymbol{\epsilon}_\phi(\hat{\mathbf{a}}_k, \mathbf{s}, k) \right) + \sqrt{\frac{1 - \alpha_k}{\alpha_k}} \mathbf{z}_k \quad (46)$$

$$= \frac{1}{\sqrt{\alpha_k}} \left( \hat{\mathbf{a}}_k - \frac{1 - \alpha_k}{\sqrt{1 - \bar{\alpha}_k}} \boldsymbol{\epsilon}_\phi(\hat{\mathbf{a}}_k, \mathbf{s}, k) \right) + \sqrt{\frac{1 - \alpha_k}{\alpha_k}} \mathbf{z}_k, \quad (47)$$

where  $k = 0, 1, \dots, K - 1$  runs forward in time,  $\mathbf{z}_k \sim \mathcal{N}(\mathbf{0}, \mathbf{I})$ . The agent plays the last action  $\hat{\mathbf{a}}_K$ .

Since we consider the SDE of the reverse process (4) that runs forward in time, while most diffusion probability model literature (e.g., [Ho et al., 2020, Song et al., 2021]) consider the backward version for sampling. To coordinate the relationship between the two versions, we also present the backward version in Algorithm 4, which is essentially identical to the iteration (47) but rewritten in the running in backward time version.

## D Time Derivative of KL Divergence Between Diffusion Policy and True Reverse Process

In this section, we provide the time derivative of KL divergence between diffusion policy (Algorithm 1) and true reverse process (defined in (4)).

### D.1 Time Derivative of KL Divergence at Reverse Time $k = 0$

In this section, we consider the case  $k = 0$  of diffusion policy (see Algorithm 1 or the iteration (9)). If  $k = 0$ , then for  $0 \leq t \leq h$ , the SDE (8) is reduced as follows,

$$d\hat{\mathbf{a}}_t = \left( \hat{\mathbf{a}}_t + 2\hat{\mathbf{S}}(\hat{\mathbf{a}}_0, \mathbf{s}, T) \right) dt + \sqrt{2}d\mathbf{w}_t, \quad t \in [0, h], \quad (48)$$

where  $\mathbf{w}_t$  is the standard Wiener process starting at  $\mathbf{w}_0 = \mathbf{0}$ .

Let the action  $\hat{\mathbf{a}}_t \sim \hat{\pi}_t(\cdot|\mathbf{s})$  follows the process (48). The next Proposition D.1 considers the distribution difference between the diffusion policy  $\hat{\pi}_t(\cdot|\mathbf{s})$  and the true distribution of backward process (4)  $\tilde{\pi}_t(\cdot|\mathbf{s})$  on the time interval  $t \in [0, h]$ .

**Proposition D.1.** *Under Assumption 4.1 and 4.2, let  $\tilde{\pi}_t(\cdot|\mathbf{s})$  be the distribution at time  $t$  with the process (4), and let  $\hat{\pi}_t(\cdot|\mathbf{s})$  be the distribution at time  $t$  with the process (48). Let*

$$\tau_0 =: \sup \left\{ t : te^t \leq \frac{\sqrt{5\nu}}{96L_sL_p} \right\}, \quad \tau =: \min \left\{ \tau_0, \frac{1}{12L_s} \right\}, \quad (49)$$

$$\epsilon_{\text{score}} =: \sup_{(k,t) \in [K] \times [t_k, t_{k+1}]} \left\{ \log \mathbb{E}_{\mathbf{a} \sim \tilde{\pi}_t(\cdot|\mathbf{s})} \left[ \exp \left\| \hat{\mathbf{S}}(\mathbf{a}, \mathbf{s}, T - hk) - \nabla \log \tilde{\pi}_t(\mathbf{a}|\mathbf{s}) \right\|_2^2 \right] \right\}, \quad (50)$$

and  $0 \leq t \leq h \leq \tau$ , then the following equation holds,

$$\frac{d}{dt} \text{KL}(\hat{\pi}_t(\cdot|\mathbf{s}) \| \tilde{\pi}_t(\cdot|\mathbf{s})) \leq -\frac{\nu}{4} \text{KL}(\hat{\pi}_t(\cdot|\mathbf{s}) \| \tilde{\pi}_t(\cdot|\mathbf{s})) + \frac{5}{4} \nu \epsilon_{\text{score}} + 12pL_s \sqrt{5\nu} t. \quad (51)$$

Before we show the details of the proof, we need to define some notations, which is useful later. Let

$$\hat{\pi}_t(\hat{\mathbf{a}}|\mathbf{s}) =: p(\hat{\mathbf{a}}_t = \hat{\mathbf{a}}|\mathbf{s}, t) \quad (52)$$

denote the distribution of the action  $\hat{\mathbf{a}}_t = \hat{\mathbf{a}}$  be played at time  $t$  along the process (48), where  $t \in [0, h]$ . For each  $t > 0$ , let  $\rho_{0,t}(\hat{\mathbf{a}}_0, \hat{\mathbf{a}}_t|\mathbf{s})$  denote the joint distribution of  $(\hat{\mathbf{a}}_0, \hat{\mathbf{a}}_t)$  conditional on the state  $\mathbf{s}$ , which can be written in terms of the conditionals and marginals as follows,

$$\rho_{0|t}(\hat{\mathbf{a}}_0|\hat{\mathbf{a}}_t, \mathbf{s}) = \frac{\rho_{0,t}(\hat{\mathbf{a}}_0, \hat{\mathbf{a}}_t|\mathbf{s})}{p(\hat{\mathbf{a}}_t = \hat{\mathbf{a}}|\mathbf{s}, t)} = \frac{\rho_{0,t}(\hat{\mathbf{a}}_0, \hat{\mathbf{a}}_t|\mathbf{s})}{\hat{\pi}_t(\hat{\mathbf{a}}_t|\mathbf{s})}.$$

### D.2 Auxiliary Results For Reverse Time $k = 0$

**Lemma D.2.** *Let  $\hat{\pi}_t(\hat{\mathbf{a}}|\mathbf{s})$  be the distribution at time  $t$  along interpolation SDE (48), where  $\hat{\pi}_t(\hat{\mathbf{a}}|\mathbf{s})$  is short for  $p(\hat{\mathbf{a}}_t = \hat{\mathbf{a}}|\mathbf{s}, t)$ , which is the distribution of the action  $\hat{\mathbf{a}}_t = \hat{\mathbf{a}}$  be played at time  $t$  alongs the process (48) among the time  $t \in [0, h]$ . Then its derivation with respect to time satisfies*

$$\frac{\partial}{\partial t} \hat{\pi}_t(\hat{\mathbf{a}}|\mathbf{s}) = -\hat{\pi}_t(\hat{\mathbf{a}}|\mathbf{s}) \text{div} \cdot \left( \hat{\mathbf{a}} + 2\mathbb{E}_{\hat{\mathbf{a}}_0 \sim \rho_{0|t}(\cdot|\hat{\mathbf{a}}, \mathbf{s})} [\hat{\mathbf{S}}(\hat{\mathbf{a}}_0, \mathbf{s}, T)|\hat{\mathbf{a}}_t = \hat{\mathbf{a}}] \right) + \Delta \hat{\pi}_t(\hat{\mathbf{a}}|\mathbf{s}). \quad (53)$$

Before we show the details of the proof, we need to clear the divergence term  $\mathbf{div}$ . In this section, all the notation is defined according to (17), and its value is at the point  $\hat{\mathbf{a}}$ .

For example, in Eq.(53), the divergence term  $\mathbf{div}$  is defined as follows,

$$\begin{aligned}\mathbf{div} \cdot \left( \hat{\mathbf{a}} + 2\mathbb{E}_{\hat{\mathbf{a}}_0 \sim \rho_{0|t}(\cdot|\hat{\mathbf{a}},\mathbf{s})} [\hat{\mathbf{S}}(\hat{\mathbf{a}}_0, \mathbf{s}, T) | \hat{\mathbf{a}}_t = \hat{\mathbf{a}}] \right) &= (\mathbf{div} \cdot \mathbf{p})(\hat{\mathbf{a}}), \\ \mathbf{p}(\mathbf{a}) &= \mathbf{a} + 2\mathbb{E}_{\hat{\mathbf{a}}_0 \sim \rho_{0|t}(\cdot|\mathbf{a},\mathbf{s})} [\hat{\mathbf{S}}(\hat{\mathbf{a}}_0, \mathbf{s}, T) | \hat{\mathbf{a}}_t = \mathbf{a}].\end{aligned}\quad (54)$$

For example, in Eq.(58), the divergence term  $\mathbf{div}$  is defined as follows,

$$\begin{aligned}\mathbf{div} \cdot \left( p(\hat{\mathbf{a}}|\hat{\mathbf{a}}_0, \mathbf{s}, t) \left( \hat{\mathbf{a}} + 2\hat{\mathbf{S}}(\hat{\mathbf{a}}_0, \mathbf{s}, T) \right) \right) &= (\mathbf{div} \cdot \mathbf{p})(\hat{\mathbf{a}}), \\ \mathbf{p}(\mathbf{a}) &= p(\mathbf{a}|\hat{\mathbf{a}}_0, \mathbf{s}, t) \left( \mathbf{a} + 2\hat{\mathbf{S}}(\hat{\mathbf{a}}_0, \mathbf{s}, T) \right).\end{aligned}\quad (55)$$

Similar definitions are parallel in Eq.(63), from Eq.(66) to Eq.(69).

*Proof.* First, for a given state  $\mathbf{s}$ , conditioning on the initial action  $\hat{\mathbf{a}}_0$ , we introduce a notation

$$p(\cdot|\hat{\mathbf{a}}_0, \mathbf{s}, t) : \mathbb{R}^p \rightarrow [0, 1], \quad (56)$$

and each

$$p(\hat{\mathbf{a}}|\hat{\mathbf{a}}_0, \mathbf{s}, t) =: p(\hat{\mathbf{a}}_t = \hat{\mathbf{a}}|\hat{\mathbf{a}}_0, \mathbf{s}, t)$$

that denotes the conditional probability distribution starting from  $\hat{\mathbf{a}}_0$  to the action  $\hat{\mathbf{a}}_t = \hat{\mathbf{a}}$  at time  $t$  under the state  $\mathbf{s}$ . Besides, we also know,

$$\hat{\pi}_t(\cdot|\mathbf{s}) = \mathbb{E}_{\hat{\mathbf{a}}_0 \sim \mathcal{N}(\mathbf{0}, \mathbf{I})} [p(\cdot|\hat{\mathbf{a}}_0, \mathbf{s}, t)] = \int_{\mathbb{R}^p} \rho_0(\hat{\mathbf{a}}_0) p(\cdot|\hat{\mathbf{a}}_0, \mathbf{s}, t) d\hat{\mathbf{a}}_0, \quad (57)$$

where  $\rho_0(\cdot) = \mathcal{N}(\mathbf{0}, \mathbf{I})$  is the initial action distribution for reverse process.

For each  $t > 0$ , let  $\rho_{0,t}(\hat{\mathbf{a}}_0, \hat{\mathbf{a}}_t|\mathbf{s})$  denote the joint distribution of  $(\hat{\mathbf{a}}_0, \hat{\mathbf{a}}_t)$  conditional on the state  $\mathbf{s}$ , which can be written in terms of the conditionals and marginals as follows,

$$\rho_{0,t}(\hat{\mathbf{a}}_0, \hat{\mathbf{a}}_t|\mathbf{s}) = p(\hat{\mathbf{a}}_0|\mathbf{s})\rho_{t|0}(\hat{\mathbf{a}}_t|\hat{\mathbf{a}}_0, \mathbf{s}) = p(\hat{\mathbf{a}}_t|\mathbf{s})\rho_{0|t}(\hat{\mathbf{a}}_0|\hat{\mathbf{a}}_t, \mathbf{s}).$$

Then we obtain the Fokker–Planck equation for the distribution  $p(\cdot|\hat{\mathbf{a}}_0, \mathbf{s}, t)$  as follows,

$$\frac{\partial}{\partial t} p(\hat{\mathbf{a}}|\hat{\mathbf{a}}_0, \mathbf{s}, t) = -\mathbf{div} \cdot \left( p(\hat{\mathbf{a}}|\hat{\mathbf{a}}_0, \mathbf{s}, t) \left( \hat{\mathbf{a}} + 2\hat{\mathbf{S}}(\hat{\mathbf{a}}_0, \mathbf{s}, T) \right) \right) + \Delta p(\hat{\mathbf{a}}|\hat{\mathbf{a}}_0, \mathbf{s}, t), \quad (58)$$

where the  $\mathbf{div}$  term is defined according to (16) and (17) if  $\mathbf{p}(\mathbf{a}) = p(\mathbf{a}|\hat{\mathbf{a}}_0, \mathbf{s}, t) \left( \mathbf{a} + 2\hat{\mathbf{S}}(\hat{\mathbf{a}}_0, \mathbf{s}, T) \right)$ .

Furthermore, according to (57), we know

$$\frac{\partial}{\partial t} \hat{\pi}_t(\hat{\mathbf{a}}|\mathbf{s}) = \frac{\partial}{\partial t} \int_{\mathbb{R}^p} \rho_0(\hat{\mathbf{a}}_0) p(\hat{\mathbf{a}}|\hat{\mathbf{a}}_0, \mathbf{s}, t) d\hat{\mathbf{a}}_0 = \int_{\mathbb{R}^p} \rho_0(\hat{\mathbf{a}}_0) \frac{\partial}{\partial t} p(\hat{\mathbf{a}}|\hat{\mathbf{a}}_0, \mathbf{s}, t) d\hat{\mathbf{a}}_0 \quad (59)$$

$$= \int_{\mathbb{R}^p} \rho_0(\hat{\mathbf{a}}_0) \left( -\mathbf{div} \cdot \left( p(\hat{\mathbf{a}}|\hat{\mathbf{a}}_0, \mathbf{s}, t) \left( \hat{\mathbf{a}} + 2\hat{\mathbf{S}}(\hat{\mathbf{a}}_0, \mathbf{s}, T) \right) \right) + \Delta p(\hat{\mathbf{a}}|\hat{\mathbf{a}}_0, \mathbf{s}, t) \right) d\hat{\mathbf{a}}_0 \quad (60)$$

$$= -\hat{\pi}_t(\hat{\mathbf{a}}|\mathbf{s}) \mathbf{div} \cdot \hat{\mathbf{a}} - 2\mathbf{div} \cdot \left( \hat{\pi}_t(\hat{\mathbf{a}}|\mathbf{s}) \mathbb{E}_{\hat{\mathbf{a}}_0 \sim \rho_{0|t}(\cdot|\hat{\mathbf{a}},\mathbf{s})} [\hat{\mathbf{S}}(\hat{\mathbf{a}}_0, \mathbf{s}, T) | \hat{\mathbf{a}}_t = \hat{\mathbf{a}}] \right) + \Delta \hat{\pi}_t(\hat{\mathbf{a}}|\mathbf{s}) \quad (61)$$

$$= -\hat{\pi}_t(\hat{\mathbf{a}}|\mathbf{s}) \mathbf{div} \cdot \left( \hat{\mathbf{a}} + 2\mathbb{E}_{\hat{\mathbf{a}}_0 \sim \rho_{0|t}(\cdot|\hat{\mathbf{a}},\mathbf{s})} [\hat{\mathbf{S}}(\hat{\mathbf{a}}_0, \mathbf{s}, T) | \hat{\mathbf{a}}_t = \hat{\mathbf{a}}] \right) + \Delta \hat{\pi}_t(\hat{\mathbf{a}}|\mathbf{s}), \quad (62)$$

where Eq.(61) holds since: with the definition of  $\hat{\pi}_t(\hat{\mathbf{a}}|\mathbf{s}) =: p(\hat{\mathbf{a}}|\mathbf{s}, t)$ , we obtain

$$\int_{\mathbb{R}^p} \rho_0(\hat{\mathbf{a}}_0) \left( -\mathbf{div} \cdot \left( p(\hat{\mathbf{a}}|\hat{\mathbf{a}}_0, \mathbf{s}, t) \hat{\mathbf{a}} \right) \right) d\hat{\mathbf{a}}_0 = -\hat{\pi}_t(\hat{\mathbf{a}}|\mathbf{s}) \mathbf{div} \cdot \hat{\mathbf{a}}; \quad (63)$$

recall

$$\hat{\pi}_t(\hat{\mathbf{a}}|\mathbf{s}) =: p(\hat{\mathbf{a}}_t = \hat{\mathbf{a}}|\mathbf{s}, t), \quad (64)$$

we know

$$\begin{aligned} \rho_0(\hat{\mathbf{a}}_0) p(\hat{\mathbf{a}}|\hat{\mathbf{a}}_0, \mathbf{s}, t) &= p(\hat{\mathbf{a}}, \hat{\mathbf{a}}_0|\mathbf{s}, t), && \blacktriangleright \text{Bayes' theorem} \\ p(\hat{\mathbf{a}}, \hat{\mathbf{a}}_0|\mathbf{s}, t) &= p(\hat{\mathbf{a}}|\mathbf{s}, t) p(\hat{\mathbf{a}}_0|\hat{\mathbf{a}}_t = \hat{\mathbf{a}}, \mathbf{s}, t) = \hat{\pi}_t(\hat{\mathbf{a}}|\mathbf{s}) p(\hat{\mathbf{a}}_0|\hat{\mathbf{a}}_t = \hat{\mathbf{a}}, \mathbf{s}, t), \end{aligned} \quad (65)$$

then we obtain

$$- \int_{\mathbb{R}^p} \rho_0(\hat{\mathbf{a}}_0) \mathbf{div} \cdot \left( p(\hat{\mathbf{a}}|\hat{\mathbf{a}}_0, \mathbf{s}, t) \hat{\mathbf{S}}(\hat{\mathbf{a}}_0, \mathbf{s}, T) \right) d\hat{\mathbf{a}}_0 \quad (66)$$

$$= - \int_{\mathbb{R}^p} \mathbf{div} \cdot \left( p(\hat{\mathbf{a}}, \hat{\mathbf{a}}_0|\mathbf{s}, t) \hat{\mathbf{S}}(\hat{\mathbf{a}}_0, \mathbf{s}, T) \right) d\hat{\mathbf{a}}_0 \quad (67)$$

$$= - \int_{\mathbb{R}^p} \mathbf{div} \cdot \left( \hat{\pi}_t(\hat{\mathbf{a}}|\mathbf{s}) p(\hat{\mathbf{a}}_0|\hat{\mathbf{a}}_t = \hat{\mathbf{a}}, \mathbf{s}, t) \hat{\mathbf{S}}(\hat{\mathbf{a}}_0, \mathbf{s}, T) \right) d\hat{\mathbf{a}}_0 \quad \blacktriangleright \text{see Eq.(65)}$$

$$= - \mathbf{div} \cdot \left( \hat{\pi}_t(\hat{\mathbf{a}}|\mathbf{s}) \int_{\mathbb{R}^p} p(\hat{\mathbf{a}}_0|\hat{\mathbf{a}}_t = \hat{\mathbf{a}}, \mathbf{s}, t) \hat{\mathbf{S}}(\hat{\mathbf{a}}_0, \mathbf{s}, T) d\hat{\mathbf{a}}_0 \right) \quad (68)$$

$$= - \mathbf{div} \cdot \left( \hat{\pi}_t(\hat{\mathbf{a}}|\mathbf{s}) \mathbb{E}_{\hat{\mathbf{a}}_0 \sim \rho_{0|t}(\cdot|\hat{\mathbf{a}}, \mathbf{s})} [\hat{\mathbf{S}}(\hat{\mathbf{a}}_0, \mathbf{s}, T) | \hat{\mathbf{a}}_t = \hat{\mathbf{a}}] \right), \quad (69)$$

where the last equation holds since

$$\int_{\mathbb{R}^p} p(\hat{\mathbf{a}}_0|\hat{\mathbf{a}}_t = \hat{\mathbf{a}}, \mathbf{s}, t) \hat{\mathbf{S}}(\hat{\mathbf{a}}_0, \mathbf{s}, T) d\hat{\mathbf{a}}_0 = \mathbb{E}_{\hat{\mathbf{a}}_0 \sim \rho_{0|t}(\cdot|\hat{\mathbf{a}}, \mathbf{s})} [\hat{\mathbf{S}}(\hat{\mathbf{a}}_0, \mathbf{s}, T) | \hat{\mathbf{a}}_t = \hat{\mathbf{a}}]. \quad (70)$$

Finally, consider (60) with (63) and (69), we conclude the Lemma D.2.  $\square$

We consider the time derivative of KL-divergence between the distribution  $\hat{\pi}_t(\cdot|\mathbf{s})$  and  $\tilde{\pi}_t(\cdot|\mathbf{s})$ , and decompose it as follows.

**Lemma D.3.** *The time derivative of KL-divergence between the distribution  $\hat{\pi}_t(\cdot|\mathbf{s})$  and  $\tilde{\pi}_t(\cdot|\mathbf{s})$  can be decomposed as follows,*

$$\frac{d}{dt} \text{KL}(\hat{\pi}_t(\cdot|\mathbf{s}) \| \tilde{\pi}_t(\cdot|\mathbf{s})) = \int_{\mathbb{R}^p} \frac{\partial \hat{\pi}_t(\mathbf{a}|\mathbf{s})}{\partial t} \log \frac{\hat{\pi}_t(\mathbf{a}|\mathbf{s})}{\tilde{\pi}_t(\mathbf{a}|\mathbf{s})} d\mathbf{a} - \int_{\mathbb{R}^p} \frac{\hat{\pi}_t(\mathbf{a}|\mathbf{s})}{\tilde{\pi}_t(\mathbf{a}|\mathbf{s})} \frac{\partial \tilde{\pi}_t(\mathbf{a}|\mathbf{s})}{\partial t} d\mathbf{a}. \quad (71)$$

*Proof.* We consider the time derivative of KL-divergence between the distribution  $\hat{\pi}_t(\cdot|\mathbf{s})$  and  $\tilde{\pi}_t(\cdot|\mathbf{s})$ , and we know

$$\begin{aligned} \frac{d}{dt} \text{KL}(\hat{\pi}_t(\cdot|\mathbf{s}) \| \tilde{\pi}_t(\cdot|\mathbf{s})) &= \frac{d}{dt} \int_{\mathbb{R}^p} \hat{\pi}_t(\mathbf{a}|\mathbf{s}) \log \frac{\hat{\pi}_t(\mathbf{a}|\mathbf{s})}{\tilde{\pi}_t(\mathbf{a}|\mathbf{s})} d\mathbf{a} \\ &= \int_{\mathbb{R}^p} \frac{\partial \hat{\pi}_t(\mathbf{a}|\mathbf{s})}{\partial t} \log \frac{\hat{\pi}_t(\mathbf{a}|\mathbf{s})}{\tilde{\pi}_t(\mathbf{a}|\mathbf{s})} d\mathbf{a} + \int_{\mathbb{R}^p} \hat{\pi}_t(\mathbf{a}|\mathbf{s}) \frac{\partial}{\partial t} \left( \frac{\hat{\pi}_t(\mathbf{a}|\mathbf{s})}{\tilde{\pi}_t(\mathbf{a}|\mathbf{s})} \right) d\mathbf{a} \\ &= \int_{\mathbb{R}^p} \frac{\partial \hat{\pi}_t(\mathbf{a}|\mathbf{s})}{\partial t} \log \frac{\hat{\pi}_t(\mathbf{a}|\mathbf{s})}{\tilde{\pi}_t(\mathbf{a}|\mathbf{s})} d\mathbf{a} + \int_{\mathbb{R}^p} \left( \cancel{\frac{\partial \hat{\pi}_t(\mathbf{a}|\mathbf{s})}{\partial t}} - \frac{\hat{\pi}_t(\mathbf{a}|\mathbf{s})}{\tilde{\pi}_t(\mathbf{a}|\mathbf{s})} \frac{\partial \tilde{\pi}_t(\mathbf{a}|\mathbf{s})}{\partial t} \right) d\mathbf{a} \\ &= \int_{\mathbb{R}^p} \frac{\partial \hat{\pi}_t(\mathbf{a}|\mathbf{s})}{\partial t} \log \frac{\hat{\pi}_t(\mathbf{a}|\mathbf{s})}{\tilde{\pi}_t(\mathbf{a}|\mathbf{s})} d\mathbf{a} - \int_{\mathbb{R}^p} \frac{\hat{\pi}_t(\mathbf{a}|\mathbf{s})}{\tilde{\pi}_t(\mathbf{a}|\mathbf{s})} \frac{\partial \tilde{\pi}_t(\mathbf{a}|\mathbf{s})}{\partial t} d\mathbf{a}, \end{aligned} \quad (72)$$

where the last equation holds since

$$\int_{\mathbb{R}^p} \frac{\partial \hat{\pi}_t(\mathbf{a}|\mathbf{s})}{\partial t} d\mathbf{a} = \frac{d}{dt} \underbrace{\int_{\mathbb{R}^p} \hat{\pi}_t(\mathbf{a}|\mathbf{s}) d\mathbf{a}}_{=1} = 0.$$

That concludes the proof.  $\square$

The relative entropy and relative Fisher information  $\text{FI}(\hat{\pi}_t(\cdot|\mathbf{s})\|\tilde{\pi}_t(\cdot|\mathbf{s}))$  can be rewritten as follows.

**Lemma D.4.** *The relative entropy and relative Fisher information  $\text{FI}(\hat{\pi}_t(\cdot|\mathbf{s})\|\tilde{\pi}_t(\cdot|\mathbf{s}))$  can be rewritten as the following identity,*

$$\text{FI}(\hat{\pi}_t(\cdot|\mathbf{s})\|\tilde{\pi}_t(\cdot|\mathbf{s})) = \int_{\mathbb{R}^p} \left( \left\langle \nabla \hat{\pi}_t(\mathbf{a}|\mathbf{s}), \nabla \log \frac{\hat{\pi}_t(\mathbf{a}|\mathbf{s})}{\tilde{\pi}_t(\mathbf{a}|\mathbf{s})} \right\rangle - \left\langle \nabla \frac{\hat{\pi}_t(\mathbf{a}|\mathbf{s})}{\tilde{\pi}_t(\mathbf{a}|\mathbf{s})}, \nabla \tilde{\pi}_t(\mathbf{a}|\mathbf{s}) \right\rangle \right) d\mathbf{a}.$$

*Proof.* We consider the following identity,

$$\begin{aligned} & \int_{\mathbb{R}^p} \left( \left\langle \nabla \frac{\hat{\pi}_t(\mathbf{a}|\mathbf{s})}{\tilde{\pi}_t(\mathbf{a}|\mathbf{s})}, \nabla \tilde{\pi}_t(\mathbf{a}|\mathbf{s}) \right\rangle - \left\langle \nabla \hat{\pi}_t(\mathbf{a}|\mathbf{s}), \nabla \log \frac{\hat{\pi}_t(\mathbf{a}|\mathbf{s})}{\tilde{\pi}_t(\mathbf{a}|\mathbf{s})} \right\rangle \right) d\mathbf{a} \\ &= \int_{\mathbb{R}^p} \left( \left\langle \frac{\tilde{\pi}_t(\mathbf{a}|\mathbf{s}) \nabla \hat{\pi}_t(\mathbf{a}|\mathbf{s}) - \hat{\pi}_t(\mathbf{a}|\mathbf{s}) \nabla \tilde{\pi}_t(\mathbf{a}|\mathbf{s})}{\tilde{\pi}_t(\mathbf{a}|\mathbf{s})}, \nabla \log \tilde{\pi}_t(\mathbf{a}|\mathbf{s}) \right\rangle - \hat{\pi}_t(\mathbf{a}|\mathbf{s}) \left\langle \nabla \log \hat{\pi}_t(\mathbf{a}|\mathbf{s}), \nabla \log \frac{\hat{\pi}_t(\mathbf{a}|\mathbf{s})}{\tilde{\pi}_t(\mathbf{a}|\mathbf{s})} \right\rangle \right) d\mathbf{a} \\ &= \int_{\mathbb{R}^p} \hat{\pi}_t(\mathbf{a}|\mathbf{s}) \left\langle \nabla \log \frac{\hat{\pi}_t(\mathbf{a}|\mathbf{s})}{\tilde{\pi}_t(\mathbf{a}|\mathbf{s})}, \nabla \log \tilde{\pi}_t(\mathbf{a}|\mathbf{s}) \right\rangle d\mathbf{a} - \int_{\mathbb{R}^p} \hat{\pi}_t(\mathbf{a}|\mathbf{s}) \left\langle \nabla \log \hat{\pi}_t(\mathbf{a}|\mathbf{s}), \nabla \log \frac{\hat{\pi}_t(\mathbf{a}|\mathbf{s})}{\tilde{\pi}_t(\mathbf{a}|\mathbf{s})} \right\rangle d\mathbf{a} \\ &= - \int_{\mathbb{R}^p} \hat{\pi}_t(\mathbf{a}|\mathbf{s}) \left\langle \nabla \log \frac{\hat{\pi}_t(\mathbf{a}|\mathbf{s})}{\tilde{\pi}_t(\mathbf{a}|\mathbf{s})}, \nabla \log \frac{\hat{\pi}_t(\mathbf{a}|\mathbf{s})}{\tilde{\pi}_t(\mathbf{a}|\mathbf{s})} \right\rangle d\mathbf{a} \\ &= - \int_{\mathbb{R}^p} \hat{\pi}_t(\mathbf{a}|\mathbf{s}) \left\| \nabla \log \frac{\hat{\pi}_t(\mathbf{a}|\mathbf{s})}{\tilde{\pi}_t(\mathbf{a}|\mathbf{s})} \right\|_2^2 d\mathbf{a} =: -\text{FI}(\hat{\pi}_t(\cdot|\mathbf{s})\|\tilde{\pi}_t(\cdot|\mathbf{s})), \end{aligned}$$

which concludes the proof.  $\square$

Lemma D.4 implies the following identity, which is useful later,

$$\begin{aligned} & \int_{\mathbb{R}^p} \left( - \left\langle \nabla \frac{\hat{\pi}_t(\mathbf{a}|\mathbf{s})}{\tilde{\pi}_t(\mathbf{a}|\mathbf{s})}, \nabla \tilde{\pi}_t(\mathbf{a}|\mathbf{s}) \right\rangle - \left\langle \nabla \hat{\pi}_t(\mathbf{a}|\mathbf{s}), \nabla \log \frac{\hat{\pi}_t(\mathbf{a}|\mathbf{s})}{\tilde{\pi}_t(\mathbf{a}|\mathbf{s})} \right\rangle \right) d\mathbf{a} \\ &= \int_{\mathbb{R}^p} \left( \left\langle \nabla \frac{\hat{\pi}_t(\mathbf{a}|\mathbf{s})}{\tilde{\pi}_t(\mathbf{a}|\mathbf{s})}, \nabla \tilde{\pi}_t(\mathbf{a}|\mathbf{s}) \right\rangle - \left\langle \nabla \hat{\pi}_t(\mathbf{a}|\mathbf{s}), \nabla \log \frac{\hat{\pi}_t(\mathbf{a}|\mathbf{s})}{\tilde{\pi}_t(\mathbf{a}|\mathbf{s})} \right\rangle - 2 \left\langle \nabla \frac{\hat{\pi}_t(\mathbf{a}|\mathbf{s})}{\tilde{\pi}_t(\mathbf{a}|\mathbf{s})}, \nabla \tilde{\pi}_t(\mathbf{a}|\mathbf{s}) \right\rangle \right) d\mathbf{a} \\ &= -\text{FI}(\hat{\pi}_t(\cdot|\mathbf{s})\|\tilde{\pi}_t(\cdot|\mathbf{s})) - 2 \int_{\mathbb{R}^p} \hat{\pi}_t(\mathbf{a}|\mathbf{s}) \left\langle \nabla \log \frac{\hat{\pi}_t(\mathbf{a}|\mathbf{s})}{\tilde{\pi}_t(\mathbf{a}|\mathbf{s})}, \nabla \log \tilde{\pi}_t(\mathbf{a}|\mathbf{s}) \right\rangle d\mathbf{a}. \quad (73) \end{aligned}$$

**Lemma D.5.** *The time derivative of KL-divergence between the distribution  $\hat{\pi}_t(\cdot|\mathbf{s})$  and  $\tilde{\pi}_t(\cdot|\mathbf{s})$  can be further decomposed as follows,*

$$\frac{d}{dt} \text{KL}(\hat{\pi}_t(\cdot|\mathbf{s})\|\tilde{\pi}_t(\cdot|\mathbf{s})) = -\text{FI}(\hat{\pi}_t(\cdot|\mathbf{s})\|\tilde{\pi}_t(\cdot|\mathbf{s})) \quad (74)$$

$$+ 2 \int_{\mathbb{R}^p} \int_{\mathbb{R}^p} \rho_{0,t}(\hat{\mathbf{a}}_0, \mathbf{a}|\mathbf{s}) \left\langle \nabla \log \frac{\hat{\pi}_t(\mathbf{a}|\mathbf{s})}{\tilde{\pi}_t(\mathbf{a}|\mathbf{s})}, \hat{\mathbf{S}}(\hat{\mathbf{a}}_0, \mathbf{s}, T) - \nabla \log \tilde{\pi}_t(\mathbf{a}|\mathbf{s}) \right\rangle d\mathbf{a} d\hat{\mathbf{a}}_0. \quad (75)$$

*Proof.* According to Lemma D.3, we need to consider the two terms in (72) correspondingly.

**First term in (72).** Recall Lemma D.2, we know

$$\begin{aligned} \frac{\partial}{\partial t} \hat{\pi}_t(\mathbf{a}|\mathbf{s}) &= -\hat{\pi}_t(\mathbf{a}|\mathbf{s}) \mathbf{div} \cdot \left( \mathbf{a} + 2\mathbb{E}_{\hat{\mathbf{a}}_0 \sim \rho_{0|t}(\cdot|\mathbf{a},\mathbf{s})} [\hat{\mathbf{S}}(\hat{\mathbf{a}}_0, \mathbf{s}, T) | \hat{\mathbf{a}}_t = \mathbf{a}] \right) + \Delta \hat{\pi}_t(\mathbf{a}|\mathbf{s}) \\ &\stackrel{(18)}{=} \mathbf{div} \cdot \left( -\left( \mathbf{a} + 2\mathbb{E}_{\hat{\mathbf{a}}_0 \sim \rho_{0|t}(\cdot|\mathbf{a},\mathbf{s})} [\hat{\mathbf{S}}(\hat{\mathbf{a}}_0, \mathbf{s}, T) | \hat{\mathbf{a}}_t = \mathbf{a}] \right) \hat{\pi}_t(\mathbf{a}|\mathbf{s}) + \nabla \hat{\pi}_t(\mathbf{a}|\mathbf{s}) \right). \end{aligned}$$

To short the expression, we define a notation  $\mathbf{g}_t(\cdot, \cdot) : \mathcal{S} \times \mathcal{A} \rightarrow \mathbb{R}^p$  as follows,

$$\mathbf{g}_t(\mathbf{s}, \mathbf{a}) =: \mathbf{a} + 2\mathbb{E}_{\hat{\mathbf{a}}_0 \sim \rho_{0|t}(\cdot|\mathbf{a},\mathbf{s})} [\hat{\mathbf{S}}(\hat{\mathbf{a}}_0, \mathbf{s}, T) | \hat{\mathbf{a}}_t = \mathbf{a}],$$

then we rewrite the distribution at time  $t$  along interpolation SDE (48) as follows,

$$\frac{\partial}{\partial t} \hat{\pi}_t(\mathbf{a}|\mathbf{s}) = \mathbf{div} \cdot \left( -\mathbf{g}_t(\mathbf{s}, \mathbf{a}) \hat{\pi}_t(\mathbf{a}|\mathbf{s}) + \nabla \hat{\pi}_t(\mathbf{a}|\mathbf{s}) \right).$$

We consider the first term in (72), according to integration by parts formula (20), we know

$$\begin{aligned} \int_{\mathbb{R}^p} \frac{\partial \hat{\pi}_t(\mathbf{a}|\mathbf{s})}{\partial t} \log \frac{\hat{\pi}_t(\mathbf{a}|\mathbf{s})}{\tilde{\pi}_t(\mathbf{a}|\mathbf{s})} d\mathbf{a} &= \int_{\mathbb{R}^p} \mathbf{div} \cdot \left( -\mathbf{g}_t(\mathbf{s}, \mathbf{a}) \hat{\pi}_t(\mathbf{a}|\mathbf{s}) + \nabla \hat{\pi}_t(\mathbf{a}|\mathbf{s}) \right) \log \frac{\hat{\pi}_t(\mathbf{a}|\mathbf{s})}{\tilde{\pi}_t(\mathbf{a}|\mathbf{s})} d\mathbf{a} \\ &\stackrel{(20)}{=} \int_{\mathbb{R}^p} \left\langle \mathbf{g}_t(\mathbf{s}, \mathbf{a}) \hat{\pi}_t(\mathbf{a}|\mathbf{s}) - \nabla \hat{\pi}_t(\mathbf{a}|\mathbf{s}), \nabla \log \frac{\hat{\pi}_t(\mathbf{a}|\mathbf{s})}{\tilde{\pi}_t(\mathbf{a}|\mathbf{s})} \right\rangle d\mathbf{a} \\ &= \int_{\mathbb{R}^p} \hat{\pi}_t(\mathbf{a}|\mathbf{s}) \left\langle \mathbf{g}_t(\mathbf{s}, \mathbf{a}), \nabla \log \frac{\hat{\pi}_t(\mathbf{a}|\mathbf{s})}{\tilde{\pi}_t(\mathbf{a}|\mathbf{s})} \right\rangle d\mathbf{a} \\ &\quad - \int_{\mathbb{R}^p} \left\langle \nabla \hat{\pi}_t(\mathbf{a}|\mathbf{s}), \nabla \log \frac{\hat{\pi}_t(\mathbf{a}|\mathbf{s})}{\tilde{\pi}_t(\mathbf{a}|\mathbf{s})} \right\rangle d\mathbf{a}. \end{aligned} \quad (76)$$

**Second term in (72).** According to the Kolmogorov backward equation, we know

$$\frac{\partial \tilde{\pi}_t(\mathbf{a}|\mathbf{s})}{\partial t} = -\mathbf{div} \cdot (\tilde{\pi}_t(\mathbf{a}|\mathbf{s}) \mathbf{a}) - \Delta \tilde{\pi}_t(\mathbf{a}|\mathbf{s}) = -\mathbf{div} \cdot \left( \tilde{\pi}_t(\mathbf{a}|\mathbf{s}) \mathbf{a} + \nabla \tilde{\pi}_t(\mathbf{a}|\mathbf{s}) \right), \quad (77)$$

then we obtain

$$\begin{aligned} \int_{\mathbb{R}^p} \frac{\hat{\pi}_t(\mathbf{a}|\mathbf{s})}{\tilde{\pi}_t(\mathbf{a}|\mathbf{s})} \frac{\partial \tilde{\pi}_t(\mathbf{a}|\mathbf{s})}{\partial t} d\mathbf{a} &= - \int_{\mathbb{R}^p} \frac{\hat{\pi}_t(\mathbf{a}|\mathbf{s})}{\tilde{\pi}_t(\mathbf{a}|\mathbf{s})} \mathbf{div} \cdot \left( \tilde{\pi}_t(\mathbf{a}|\mathbf{s}) \mathbf{a} + \nabla \tilde{\pi}_t(\mathbf{a}|\mathbf{s}) \right) d\mathbf{a} \\ &\stackrel{(20)}{=} \int_{\mathbb{R}^p} \left\langle \nabla \frac{\hat{\pi}_t(\mathbf{a}|\mathbf{s})}{\tilde{\pi}_t(\mathbf{a}|\mathbf{s})}, \tilde{\pi}_t(\mathbf{a}|\mathbf{s}) \mathbf{a} + \nabla \tilde{\pi}_t(\mathbf{a}|\mathbf{s}) \right\rangle d\mathbf{a} \\ &= \int_{\mathbb{R}^p} \tilde{\pi}_t(\mathbf{a}|\mathbf{s}) \left\langle \nabla \frac{\hat{\pi}_t(\mathbf{a}|\mathbf{s})}{\tilde{\pi}_t(\mathbf{a}|\mathbf{s})}, \mathbf{a} \right\rangle d\mathbf{a} + \int_{\mathbb{R}^p} \left\langle \nabla \frac{\hat{\pi}_t(\mathbf{a}|\mathbf{s})}{\tilde{\pi}_t(\mathbf{a}|\mathbf{s})}, \nabla \tilde{\pi}_t(\mathbf{a}|\mathbf{s}) \right\rangle d\mathbf{a}. \end{aligned} \quad (78)$$

**Time derivative of KL-divergence.** We consider the next identity,

$$\int_{\mathbb{R}^p} \left( \hat{\pi}_t(\mathbf{a}|\mathbf{s}) \left\langle \mathbf{g}_t(\mathbf{s}, \mathbf{a}), \nabla \log \frac{\hat{\pi}_t(\mathbf{a}|\mathbf{s})}{\tilde{\pi}_t(\mathbf{a}|\mathbf{s})} \right\rangle - \tilde{\pi}_t(\mathbf{a}|\mathbf{s}) \left\langle \nabla \frac{\hat{\pi}_t(\mathbf{a}|\mathbf{s})}{\tilde{\pi}_t(\mathbf{a}|\mathbf{s})}, \mathbf{a} \right\rangle \right) d\mathbf{a}$$



$$\begin{aligned}
&= \int_{\mathbb{R}^p} \left( \hat{\pi}_t(\mathbf{a}|\mathbf{s}) \left\langle \mathbf{g}_t(\mathbf{s}, \mathbf{a}), \nabla \log \frac{\hat{\pi}_t(\mathbf{a}|\mathbf{s})}{\tilde{\pi}_t(\mathbf{a}|\mathbf{s})} \right\rangle - \hat{\pi}_t(\mathbf{a}|\mathbf{s}) \frac{\tilde{\pi}_t(\mathbf{a}|\mathbf{s})}{\hat{\pi}_t(\mathbf{a}|\mathbf{s})} \left\langle \nabla \frac{\hat{\pi}_t(\mathbf{a}|\mathbf{s})}{\tilde{\pi}_t(\mathbf{a}|\mathbf{s})}, \mathbf{a} \right\rangle \right) d\mathbf{a} \\
&= 2 \int_{\mathbb{R}^p} \hat{\pi}_t(\mathbf{a}|\mathbf{s}) \left\langle \mathbb{E}_{\hat{\mathbf{a}}_0 \sim \rho_{0|t}(\cdot|\mathbf{a}, \mathbf{s})} [\hat{\mathbf{S}}(\hat{\mathbf{a}}_0, \mathbf{s}, T) | \hat{\mathbf{a}}_t = \mathbf{a}], \nabla \log \frac{\hat{\pi}_t(\mathbf{a}|\mathbf{s})}{\tilde{\pi}_t(\mathbf{a}|\mathbf{s})} \right\rangle d\mathbf{a},
\end{aligned}$$

then according to (72), and with the results (76), (78), we obtain

$$\begin{aligned}
\frac{d}{dt} \text{KL}(\hat{\pi}_t(\cdot|\mathbf{s}) \| \tilde{\pi}_t(\cdot|\mathbf{s})) &= -\text{FI}(\hat{\pi}_t(\cdot|\mathbf{s}) \| \tilde{\pi}_t(\cdot|\mathbf{s})) \\
&+ 2 \int_{\mathbb{R}^p} \hat{\pi}_t(\mathbf{a}|\mathbf{s}) \left\langle \nabla \log \frac{\hat{\pi}_t(\mathbf{a}|\mathbf{s})}{\tilde{\pi}_t(\mathbf{a}|\mathbf{s})}, \mathbb{E}_{\hat{\mathbf{a}}_0 \sim \rho_{0|t}(\cdot|\mathbf{a}, \mathbf{s})} [\hat{\mathbf{S}}(\hat{\mathbf{a}}_0, \mathbf{s}, T) | \hat{\mathbf{a}}_t = \mathbf{a}] - \nabla \log \tilde{\pi}_t(\mathbf{a}|\mathbf{s}) \right\rangle d\mathbf{a}.
\end{aligned} \tag{79}$$

Furthermore, we consider

$$\begin{aligned}
&\int_{\mathbb{R}^p} \hat{\pi}_t(\mathbf{a}|\mathbf{s}) \left\langle \nabla \log \frac{\hat{\pi}_t(\mathbf{a}|\mathbf{s})}{\tilde{\pi}_t(\mathbf{a}|\mathbf{s})}, \mathbb{E}_{\hat{\mathbf{a}}_0 \sim \rho_{0|t}(\cdot|\mathbf{a}, \mathbf{s})} [\hat{\mathbf{S}}(\hat{\mathbf{a}}_0, \mathbf{s}, T) | \hat{\mathbf{a}}_t = \mathbf{a}] - \nabla \log \tilde{\pi}_t(\mathbf{a}|\mathbf{s}) \right\rangle d\mathbf{a} \\
&= \int_{\mathbb{R}^p} \int_{\mathbb{R}^p} \rho_{0,t}(\hat{\mathbf{a}}_0, \mathbf{a}|\mathbf{s}) \left\langle \nabla \log \frac{\hat{\pi}_t(\mathbf{a}|\mathbf{s})}{\tilde{\pi}_t(\mathbf{a}|\mathbf{s})}, \hat{\mathbf{S}}(\hat{\mathbf{a}}_0, \mathbf{s}, T) - \nabla \log \tilde{\pi}_t(\mathbf{a}|\mathbf{s}) \right\rangle d\mathbf{a} d\hat{\mathbf{a}}_0,
\end{aligned} \tag{80}$$

where Eq.(80) holds due to  $\rho_{0,t}(\hat{\mathbf{a}}_0, \hat{\mathbf{a}}_t|\mathbf{s})$  denotes the joint distribution of  $(\hat{\mathbf{a}}_0, \hat{\mathbf{a}}_t)$  conditional on the state  $\mathbf{s}$ , which can be written in terms of the conditionals and marginals as follows,

$$\rho_{0|t}(\hat{\mathbf{a}}_0 | \hat{\mathbf{a}}_t, \mathbf{s}) = \frac{\rho_{0,t}(\hat{\mathbf{a}}_0, \hat{\mathbf{a}}_t|\mathbf{s})}{p_t(\hat{\mathbf{a}}_t|\mathbf{s})} = \frac{\rho_{0,t}(\hat{\mathbf{a}}_0, \hat{\mathbf{a}}_t|\mathbf{s})}{\hat{\pi}_t(\hat{\mathbf{a}}_t|\mathbf{s})}; \tag{81}$$

and in Eq.(80), we denote  $\hat{\mathbf{a}}_t = \mathbf{a}$ .

Finally, combining (79) and (80), we obtain the following equation,

$$\begin{aligned}
\frac{d}{dt} \text{KL}(\hat{\pi}_t(\cdot|\mathbf{s}) \| \tilde{\pi}_t(\cdot|\mathbf{s})) &= -\text{FI}(\hat{\pi}_t(\cdot|\mathbf{s}) \| \tilde{\pi}_t(\cdot|\mathbf{s})) \\
&+ 2 \int_{\mathbb{R}^p} \int_{\mathbb{R}^p} \rho_{0,t}(\hat{\mathbf{a}}_0, \mathbf{a}|\mathbf{s}) \left\langle \nabla \log \frac{\hat{\pi}_t(\mathbf{a}|\mathbf{s})}{\tilde{\pi}_t(\mathbf{a}|\mathbf{s})}, \hat{\mathbf{S}}(\hat{\mathbf{a}}_0, \mathbf{s}, T) - \nabla \log \tilde{\pi}_t(\mathbf{a}|\mathbf{s}) \right\rangle d\mathbf{a} d\hat{\mathbf{a}}_0,
\end{aligned} \tag{82}$$

which concludes the proof.  $\square$

**Lemma D.6.** *The time derivative of KL-divergence between the distribution  $\hat{\pi}_t(\cdot|\mathbf{s})$  and  $\tilde{\pi}_t(\cdot|\mathbf{s})$  is bounded as follows,*

$$\begin{aligned}
&\frac{d}{dt} \text{KL}(\hat{\pi}_t(\cdot|\mathbf{s}) \| \tilde{\pi}_t(\cdot|\mathbf{s})) \\
&\leq -\frac{3}{4} \text{FI}(\hat{\pi}_t(\cdot|\mathbf{s}) \| \tilde{\pi}_t(\cdot|\mathbf{s})) + 4 \int_{\mathbb{R}^p} \int_{\mathbb{R}^p} \rho_{0,t}(\hat{\mathbf{a}}_0, \mathbf{a}|\mathbf{s}) \left\| \hat{\mathbf{S}}(\hat{\mathbf{a}}_0, \mathbf{s}, T) - \nabla \log \tilde{\pi}_t(\mathbf{a}|\mathbf{s}) \right\|_2^2 d\mathbf{a} d\hat{\mathbf{a}}_0.
\end{aligned} \tag{84}$$

*Proof.* First, we consider

$$\int_{\mathbb{R}^p} \int_{\mathbb{R}^p} \rho_{0,t}(\hat{\mathbf{a}}_0, \mathbf{a}|\mathbf{s}) \left\langle \nabla \log \frac{\hat{\pi}_t(\mathbf{a}|\mathbf{s})}{\tilde{\pi}_t(\mathbf{a}|\mathbf{s})}, \hat{\mathbf{S}}(\hat{\mathbf{a}}_0, \mathbf{s}, T) - \nabla \log \tilde{\pi}_t(\mathbf{a}|\mathbf{s}) \right\rangle d\mathbf{a} d\hat{\mathbf{a}}_0$$

$$\leq \int_{\mathbb{R}^p} \int_{\mathbb{R}^p} \rho_{0,t}(\hat{\mathbf{a}}_0, \mathbf{a}|\mathbf{s}) \left( 2 \left\| \hat{\mathbf{S}}(\hat{\mathbf{a}}_0, \mathbf{s}, T) - \nabla \log \tilde{\pi}_t(\mathbf{a}|\mathbf{s}) \right\|_2^2 + \frac{1}{8} \left\| \nabla \log \frac{\hat{\pi}_t(\mathbf{a}|\mathbf{s})}{\tilde{\pi}_t(\mathbf{a}|\mathbf{s})} \right\|_2^2 \right) d\mathbf{a} d\hat{\mathbf{a}}_0 \quad (85)$$

$$= 2 \int_{\mathbb{R}^p} \int_{\mathbb{R}^p} \rho_{0,t}(\hat{\mathbf{a}}_0, \mathbf{a}|\mathbf{s}) \left\| \hat{\mathbf{S}}(\hat{\mathbf{a}}_0, \mathbf{s}, T) - \nabla \log \tilde{\pi}_t(\mathbf{a}|\mathbf{s}) \right\|_2^2 d\mathbf{a} d\hat{\mathbf{a}}_0 + \frac{1}{8} \text{FI}(\hat{\pi}_t(\cdot|\mathbf{s}) \|\tilde{\pi}_t(\cdot|\mathbf{s})), \quad (86)$$

where Eq.(85) holds since we consider  $\langle \mathbf{a}, \mathbf{b} \rangle \leq 2\|\mathbf{a}\|^2 + \frac{1}{8}\|\mathbf{b}\|^2$ .

Then, according to Lemma D.5, we obtain

$$\begin{aligned} \frac{d}{dt} \text{KL}(\hat{\pi}_t(\cdot|\mathbf{s}) \|\tilde{\pi}_t(\cdot|\mathbf{s})) &= -\text{FI}(\hat{\pi}_t(\cdot|\mathbf{s}) \|\tilde{\pi}_t(\cdot|\mathbf{s})) \\ &\quad + 2 \int_{\mathbb{R}^p} \int_{\mathbb{R}^p} \rho_{0,t}(\hat{\mathbf{a}}_0, \mathbf{a}|\mathbf{s}) \left\langle \nabla \log \frac{\hat{\pi}_t(\mathbf{a}|\mathbf{s})}{\tilde{\pi}_t(\mathbf{a}|\mathbf{s})}, \hat{\mathbf{S}}(\hat{\mathbf{a}}_0, \mathbf{s}, T) - \nabla \log \tilde{\pi}_t(\mathbf{a}|\mathbf{s}) \right\rangle d\mathbf{a} d\hat{\mathbf{a}}_0 \\ &\leq -\frac{3}{4} \text{FI}(\hat{\pi}_t(\cdot|\mathbf{s}) \|\tilde{\pi}_t(\cdot|\mathbf{s})) + 4 \int_{\mathbb{R}^p} \int_{\mathbb{R}^p} \rho_{0,t}(\hat{\mathbf{a}}_0, \mathbf{a}|\mathbf{s}) \left\| \hat{\mathbf{S}}(\hat{\mathbf{a}}_0, \mathbf{s}, T) - \nabla \log \tilde{\pi}_t(\mathbf{a}|\mathbf{s}) \right\|_2^2 d\mathbf{a} d\hat{\mathbf{a}}_0, \end{aligned} \quad (87)$$

which concludes the proof.  $\square$

Before we provide further analysis to show the boundedness of (87), we need to consider SDE (8). Let  $h > 0$  be the step-size, assume  $K = \frac{T}{h} \in \mathbb{N}$ , and  $t_k =: hk, k = 0, 1, \dots, K$ . SDE (8) considers as follows, for  $t \in [hk, h(k+1)]$ ,

$$d\hat{\mathbf{a}}_t = \left( \hat{\mathbf{a}}_t + 2\hat{\mathbf{S}}(\hat{\mathbf{a}}_{t_k}, \mathbf{s}, T - t_k) \right) dt + \sqrt{2}d\mathbf{w}_t, \quad (88)$$

Recall the SDE (88), in this section, we only consider  $k = 0$ , and we obtain the following SDE,

$$d\hat{\mathbf{a}}_t = \left( \hat{\mathbf{a}}_t + 2\hat{\mathbf{S}}(\hat{\mathbf{a}}_0, \mathbf{s}, T) \right) dt + \sqrt{2}d\mathbf{w}_t, \quad (89)$$

where  $\mathbf{w}_t$  is the standard Wiener process starting at  $\mathbf{w}_0 = \mathbf{0}$ , and  $t$  is from 0 to  $h$ .

Integration with (89), we obtain

$$\hat{\mathbf{a}}_t - \hat{\mathbf{a}}_0 = (e^t - 1) \left( \hat{\mathbf{a}}_0 + 2\hat{\mathbf{S}}(\hat{\mathbf{a}}_0, \mathbf{s}, T) \right) + \sqrt{2} \int_0^t e^t d\mathbf{w}_t, \quad (90)$$

which implies

$$\hat{\mathbf{a}}_t = e^t \hat{\mathbf{a}}_0 + 2(e^t - 1)\hat{\mathbf{S}}(\hat{\mathbf{a}}_0, \mathbf{s}, T) + \sqrt{e^t - 1} \mathbf{z}, \quad \mathbf{z} \sim \mathcal{N}(\mathbf{0}, \mathbf{I}). \quad (91)$$

**Lemma D.7.** Under Assumption 4.1, for all  $0 \leq t \leq \frac{1}{12L_s}$ , then the following holds,

$$\begin{aligned} &\int_{\mathbb{R}^p} \int_{\mathbb{R}^p} \rho_{0,t}(\hat{\mathbf{a}}_0, \mathbf{a}|\mathbf{s}) \left\| \hat{\mathbf{S}}(\hat{\mathbf{a}}_0, \mathbf{s}, T) - \nabla \log \tilde{\pi}_t(\mathbf{a}|\mathbf{s}) \right\|_2^2 d\mathbf{a} d\hat{\mathbf{a}}_0 \\ &\leq 36pt(1+t)L_s^2 + 144t^2L_s^2 \int_{\mathbb{R}^p} \hat{\pi}_t(\mathbf{a}|\mathbf{s}) \left( \left\| \hat{\mathbf{S}}(\mathbf{a}, \mathbf{s}, T) - \nabla \log \tilde{\pi}_t(\mathbf{a}|\mathbf{s}) \right\|_2^2 + \left\| \nabla \log \tilde{\pi}_t(\mathbf{a}|\mathbf{s}) \right\|_2^2 \right) d\mathbf{a}, \end{aligned}$$

where  $\hat{\mathbf{a}}_t$  updated according to (91).

*Proof.* See Section F.2.  $\square$

### D.3 Proof for Result at Reverse Time $k = 0$

*Proof.* According to the definition of diffusion policy, we know  $\hat{\pi}_t(\cdot|\mathbf{s}) = \bar{\pi}_{T-t}(\cdot|\mathbf{s})$ . Then according to Proposition B.4, we know  $\hat{\pi}_t(\cdot|\mathbf{s})$  is  $\nu_{T-t}$ -LSI, where

$$\nu_{T-t} = \frac{\nu}{\nu + (1 - \nu)e^{-2(T-t)}}.$$

Since we consider the time-step  $0 \leq t \leq T$ , then

$$\nu_{T-t} = \frac{\nu}{\nu + (1 - \nu)e^{-2(T-t)}} \geq 1, \quad \forall t \in [0, T]. \quad (92)$$

According to Proposition B.5, we know under Assumption 4.1,  $\nabla \log \hat{\pi}_t(\cdot|\mathbf{s})$  is  $L_p e^t$ -Lipschitz on the time interval  $[0, T_0]$ , where

$$T_0 =: \sup_{t \geq 0} \left\{ t : 1 - e^{-2t} \leq \frac{e^t}{L_p} \right\}.$$

Then according to Proposition B.6, we obtain

$$\int_{\mathbb{R}^p} \hat{\pi}_t(\mathbf{a}|\mathbf{s}) \left\| \nabla \log \hat{\pi}_t(\mathbf{a}|\mathbf{s}) \right\|_2^2 d\mathbf{a} \leq \frac{4L_p^2 e^{2t}}{\nu_{T-t}} \text{KL}(\hat{\pi}_t(\cdot|\mathbf{s}) \|\bar{\pi}_t(\cdot|\mathbf{s})) + 2pL_p e^t. \quad (93)$$

Furthermore, according to Donsker-Varadhan representation (see Section B.5), let

$$f(\mathbf{a}) =: \beta_t \left\| \hat{\mathbf{S}}(\mathbf{a}, \mathbf{s}, T) - \nabla \log \hat{\pi}_t(\mathbf{a}|\mathbf{s}) \right\|_2^2,$$

the positive constant  $\beta_t$  will be special later, see Eq.(98). With the result (29), we know

$$\text{KL}(\hat{\pi}_t(\cdot|\mathbf{s}) \|\bar{\pi}_t(\cdot|\mathbf{s})) \geq \int_{\mathbb{R}^p} \hat{\pi}_t(\mathbf{a}|\mathbf{s}) f(\mathbf{a}) d\mathbf{a} - \log \int_{\mathbb{R}^p} \bar{\pi}_t(\mathbf{a}|\mathbf{s}) \exp(f(\mathbf{a})) d\mathbf{a},$$

which implies

$$\begin{aligned} & \int_{\mathbb{R}^p} \hat{\pi}_t(\mathbf{a}|\mathbf{s}) \left\| \hat{\mathbf{S}}(\mathbf{a}, \mathbf{s}, T) - \nabla \log \hat{\pi}_t(\mathbf{a}|\mathbf{s}) \right\|_2^2 d\mathbf{a} \\ & \leq \frac{1}{\beta_t} \text{KL}(\hat{\pi}_t(\cdot|\mathbf{s}) \|\bar{\pi}_t(\cdot|\mathbf{s})) + \frac{1}{\beta_t} \log \int_{\mathbb{R}^p} \bar{\pi}_t(\mathbf{a}|\mathbf{s}) \exp \left( \left\| \hat{\mathbf{S}}(\mathbf{a}, \mathbf{s}, T) - \nabla \log \hat{\pi}_t(\mathbf{a}|\mathbf{s}) \right\|_2^2 \right) d\mathbf{a} \\ & = \frac{1}{\beta_t} \text{KL}(\hat{\pi}_t(\cdot|\mathbf{s}) \|\bar{\pi}_t(\cdot|\mathbf{s})) + \frac{1}{\beta_t} \log \mathbb{E}_{\mathbf{a} \sim \bar{\pi}_t(\cdot|\mathbf{s})} \left[ \exp \left\| \hat{\mathbf{S}}(\mathbf{a}, \mathbf{s}, T) - \nabla \log \hat{\pi}_t(\mathbf{a}|\mathbf{s}) \right\|_2^2 \right]. \end{aligned} \quad (94)$$

Finally, according to Lemma D.6-D.7, Eq.(93)-(94), we obtain

$$\begin{aligned} & \frac{d}{dt} \text{KL}(\hat{\pi}_t(\cdot|\mathbf{s}) \|\bar{\pi}_t(\cdot|\mathbf{s})) \\ & \stackrel{(87)}{\leq} -\frac{3}{4} \text{FI}(\hat{\pi}_t(\cdot|\mathbf{s}) \|\bar{\pi}_t(\cdot|\mathbf{s})) + 4 \int_{\mathbb{R}^p} \int_{\mathbb{R}^p} \rho_{0,t}(\hat{\mathbf{a}}_0, \mathbf{a}|\mathbf{s}) \left\| \hat{\mathbf{S}}(\hat{\mathbf{a}}_0, \mathbf{s}, T) - \nabla \log \hat{\pi}_t(\mathbf{a}|\mathbf{s}) \right\|_2^2 d\mathbf{a} d\hat{\mathbf{a}}_0 \\ & \stackrel{\text{Lemma D.7}}{\leq} -\frac{3}{4} \text{FI}(\hat{\pi}_t(\cdot|\mathbf{s}) \|\bar{\pi}_t(\cdot|\mathbf{s})) + 576t^2 L_s^2 \int_{\mathbb{R}^p} \hat{\pi}_t(\mathbf{a}|\mathbf{s}) \left\| \nabla \log \hat{\pi}_t(\mathbf{a}|\mathbf{s}) \right\|_2^2 d\mathbf{a} \end{aligned}$$

$$\begin{aligned}
& + 576t^2L_s^2 \int_{\mathbb{R}^p} \hat{\pi}_t(\mathbf{a}|\mathbf{s}) \left\| \hat{\mathbf{S}}(\mathbf{a}, \mathbf{s}, T) - \nabla \log \tilde{\pi}_t(\mathbf{a}|\mathbf{s}) \right\|_2^2 d\mathbf{a} \\
\leq & -\frac{3}{4} \text{FI}(\hat{\pi}_t(\cdot|\mathbf{s})\|\tilde{\pi}_t(\cdot|\mathbf{s})) + 576t^2L_s^2 \left( \frac{4L_p^2e^{2t}}{\nu_{T-t}} \text{KL}(\hat{\pi}_t(\cdot|\mathbf{s})\|\tilde{\pi}_t(\cdot|\mathbf{s})) + 2pL_p e^t \right) \\
& \quad \blacktriangleright \text{due to Eq. (93)} \\
& + \frac{576t^2L_s^2}{\beta_t} \left( \text{KL}(\hat{\pi}_t(\cdot|\mathbf{s})\|\tilde{\pi}_t(\cdot|\mathbf{s})) + \log \mathbb{E}_{\mathbf{a} \sim \tilde{\pi}_t(\cdot|\mathbf{s})} \left[ \exp \left\| \hat{\mathbf{S}}(\mathbf{a}, \mathbf{s}, T) - \nabla \log \tilde{\pi}_t(\mathbf{a}|\mathbf{s}) \right\|_2^2 \right] \right) \\
& \quad \blacktriangleright \text{due to Eq. (94)} \\
= & -\frac{3}{4} \text{FI}(\hat{\pi}_t(\cdot|\mathbf{s})\|\tilde{\pi}_t(\cdot|\mathbf{s})) + 576t^2L_s^2 \left( \frac{4L_p^2e^{2t}}{\nu_{T-t}} + \frac{1}{\beta_t} \right) \text{KL}(\hat{\pi}_t(\cdot|\mathbf{s})\|\tilde{\pi}_t(\cdot|\mathbf{s})) \\
& + \frac{576t^2L_s^2}{\beta_t} \log \mathbb{E}_{\mathbf{a} \sim \tilde{\pi}_t(\cdot|\mathbf{s})} \left[ \exp \left\| \hat{\mathbf{S}}(\mathbf{a}, \mathbf{s}, T) - \nabla \log \tilde{\pi}_t(\mathbf{a}|\mathbf{s}) \right\|_2^2 \right] + 1152t^2pL_s^2L_p e^t \\
\leq & \left( 576t^2L_s^2 \left( \frac{4L_p^2e^{2t}}{\nu_{T-t}} + \frac{1}{\beta_t} \right) - \frac{3}{2}\nu \right) \text{KL}(\hat{\pi}_t(\cdot|\mathbf{s})\|\tilde{\pi}_t(\cdot|\mathbf{s})) + \frac{576t^2L_s^2}{\beta_t} \epsilon_{\text{score}} + 1152t^2pL_s^2L_p e^t \\
& \quad \blacktriangleright \text{due to Assumption 4.2} \\
= & \left( 576t^2L_s^2 \left( 4c_t + \frac{1}{\beta_t} \right) - \frac{3}{2}\nu \right) \text{KL}(\hat{\pi}_t(\cdot|\mathbf{s})\|\tilde{\pi}_t(\cdot|\mathbf{s})) + \frac{576t^2L_s^2}{\beta_t} \epsilon_{\text{score}} + 1152t^2pL_s^2L_p e^t \\
& \quad \blacktriangleright \text{due to } \frac{L_p^2e^{2t}}{\nu_{T-t}} =: c_t \\
\stackrel{(98)}{=} & -\frac{\nu}{4} \text{KL}(\hat{\pi}_t(\cdot|\mathbf{s})\|\tilde{\pi}_t(\cdot|\mathbf{s})) + \frac{576t^2L_s^2}{\beta_t} \epsilon_{\text{score}} + 1152t^2pL_s^2L_p e^t \tag{95} \\
\stackrel{(99)}{\leq} & -\frac{\nu}{4} \text{KL}(\hat{\pi}_t(\cdot|\mathbf{s})\|\tilde{\pi}_t(\cdot|\mathbf{s})) + \frac{5}{4}\nu \epsilon_{\text{score}} + 1152t^2pL_s^2L_p e^t \tag{96}
\end{aligned}$$

where

$$\epsilon_{\text{score}} = \sup_{(k,t) \in [K] \times [kh, (k+1)h]} \left\{ \log \mathbb{E}_{\mathbf{a} \sim \tilde{\pi}_t(\cdot|\mathbf{s})} \left[ \exp \left\| \hat{\mathbf{S}}(\mathbf{a}, \mathbf{s}, T - hk) - \nabla \log \tilde{\pi}_t(\mathbf{a}|\mathbf{s}) \right\|_2^2 \right] \right\}; \tag{97}$$

Eq.(95) holds since we set  $\beta_t$  as follows, we set  $576t^2L_s^2 \left( 4c_t + \frac{1}{\beta_t} \right) = \frac{5\nu}{4}$ , i.e.,

$$\frac{1}{\beta_t} = \frac{5\nu}{2304t^2L_s^2} - 4c_t; \tag{98}$$

where Eq.(96) holds since

$$\frac{576t^2L_s^2}{\beta_t} = 576t^2L_s^2 \left( \frac{5\nu}{2304t^2L_s^2} - 4c_t \right) \leq \frac{5\nu}{4}. \tag{99}$$

Now, we consider the time-step  $t$  keeps the constant  $\beta_t$  positive, it is sufficient to consider the next condition due to the property (92),

$$\frac{5\nu}{2304t^2L_s^2} \geq 4L_p^2e^{2t}, \tag{100}$$

which implies  $te^t \leq \frac{\sqrt{5\nu}}{96L_sL_p}$ .

Formally, we define a notation

$$\tau_0 =: \sup \left\{ t : te^t \leq \frac{\sqrt{5\nu}}{96L_sL_p} \right\}, \quad (101)$$

$$\tau =: \min \left\{ \tau_0, T_0, \frac{1}{12L_s} \right\}. \quad (102)$$

Then with result of Eq.(100), if  $0 \leq t \leq h \leq \tau$ , we rewrite Eq.(96) as follows,

$$\begin{aligned} \frac{d}{dt} \text{KL}(\hat{\pi}_t(\cdot|\mathbf{s})\|\tilde{\pi}_t(\cdot|\mathbf{s})) &\leq -\frac{\nu}{4} \text{KL}(\hat{\pi}_t(\cdot|\mathbf{s})\|\tilde{\pi}_t(\cdot|\mathbf{s})) + \frac{5}{4} \nu \epsilon_{\text{score}} + 12pL_s\sqrt{5\nu}t \\ &= -\frac{\nu}{4} \text{KL}(\hat{\pi}_t(\cdot|\mathbf{s})\|\tilde{\pi}_t(\cdot|\mathbf{s})) + 12pL_s\sqrt{5\nu}t \\ &\quad + \frac{5}{4} \nu \sup_{(k,t) \in [K] \times [t_k, t_{k+1}]} \left\{ \log \mathbb{E}_{\mathbf{a} \sim \tilde{\pi}_t(\cdot|\mathbf{s})} \left[ \exp \left\| \hat{\mathbf{S}}(\mathbf{a}, \mathbf{s}, T - hk) - \nabla \log \tilde{\pi}_t(\mathbf{a}|\mathbf{s}) \right\|_2^2 \right] \right\}, \end{aligned} \quad (103)$$

which concludes the proof.  $\square$

**Remark D.8.** *The result of Proposition B.5 only depends on Assumption 4.1, thus the result (93) does not depend on additional assumption of the uniform  $L$ -smooth of  $\log \tilde{\pi}_t$  on the time interval  $[0, T]$ , e.g., Wibisono and Yang [2022]. Instead of the uniform  $L$ -smooth of  $\log \tilde{\pi}_t$ , we consider the  $L_p e^t$ -Lipschitz on the time interval  $[0, T_0]$ , which is one of the difference between our proof and [Wibisono and Yang, 2022]. Although we obtain a similar convergence rate from the view of Langevin-based algorithms, we need a weak condition.*

#### D.4 Proof for Result at Arbitrary Reverse Time $k$

**Proposition D.9.** *Under Assumption 4.1 and 4.2. Let  $\tilde{\pi}_k(\cdot|\mathbf{s})$  be the distribution at the time  $t = hk$  along the process (4) that starts from  $\tilde{\pi}_0(\cdot|\mathbf{s}) = \tilde{\pi}_T(\cdot|\mathbf{s})$ , then  $\tilde{\pi}_k(\cdot|\mathbf{s}) = \tilde{\pi}_{T-hk}(\cdot|\mathbf{s})$ . Let  $\hat{\pi}_k(\cdot|\mathbf{s})$  be the distribution of the iteration (9) at the  $k$ -th time  $t_k = hk$ , starting from  $\hat{\pi}_0(\cdot|\mathbf{s}) = \mathcal{N}(\mathbf{0}, \mathbf{I})$ . Let  $0 < h \leq \tau$ , then for all  $k = 0, 1, \dots, K-1$ ,*

$$\text{KL}(\hat{\pi}_{k+1}(\cdot|\mathbf{s})\|\tilde{\pi}_{k+1}(\cdot|\mathbf{s})) \leq e^{-\frac{1}{4}\nu h} \text{KL}(\hat{\pi}_k(\cdot|\mathbf{s})\|\tilde{\pi}_k(\cdot|\mathbf{s})) + \frac{5}{4} \nu \epsilon_{\text{score}} h + 12pL_s\sqrt{5\nu}h^2,$$

where  $\tau$  is defined in (102).

*Proof.* Recall Proposition D.1, we know for any  $0 \leq t \leq h \leq \tau$ , the following holds

$$\frac{d}{dt} \text{KL}(\hat{\pi}_t(\cdot|\mathbf{s})\|\tilde{\pi}_t(\cdot|\mathbf{s})) \leq -\frac{\nu}{4} \text{KL}(\hat{\pi}_t(\cdot|\mathbf{s})\|\tilde{\pi}_t(\cdot|\mathbf{s})) + \frac{5}{4} \nu \epsilon_{\text{score}} + 12pL_s\sqrt{5\nu}h, \quad (104)$$

where comparing to (51), we use the condition  $t \leq h$ .

We rewrite (104) as follows,

$$\frac{d}{dt} \left( e^{\frac{1}{4}\nu t} \text{KL}(\hat{\pi}_t(\cdot|\mathbf{s})\|\tilde{\pi}_t(\cdot|\mathbf{s})) \right) \leq e^{\frac{1}{4}\nu t} \left( \frac{5}{4} \nu \epsilon_{\text{score}} + 12pL_s\sqrt{5\nu}h \right).$$

Then, on the interval  $[0, h]$ , we obtain

$$\int_0^h \frac{d}{dt} \left( e^{\frac{1}{4}\nu t} \text{KL}(\hat{\pi}_t(\cdot|\mathbf{s})\|\tilde{\pi}_t(\cdot|\mathbf{s})) \right) dt \leq \int_0^h e^{\frac{1}{4}\nu t} \left( \frac{5}{4} \nu \epsilon_{\text{score}} + 12pL_s\sqrt{5\nu}h \right) dt,$$

which implies

$$e^{\frac{1}{4}\nu h} \text{KL}(\hat{\pi}_h(\cdot|\mathbf{s})\|\tilde{\pi}_h(\cdot|\mathbf{s})) \leq \text{KL}(\hat{\pi}_0(\cdot|\mathbf{s})\|\tilde{\pi}_0(\cdot|\mathbf{s})) + \frac{4}{\nu} \left( e^{\frac{1}{4}\nu h} - 1 \right) \left( \frac{5}{4}\nu\epsilon_{\text{score}} + 12pL_s\sqrt{5\nu h} \right).$$

Furthermore, we obtain

$$\begin{aligned} \text{KL}(\hat{\pi}_h(\cdot|\mathbf{s})\|\tilde{\pi}_h(\cdot|\mathbf{s})) &\leq e^{-\frac{1}{4}\nu h} \text{KL}(\hat{\pi}_0(\cdot|\mathbf{s})\|\tilde{\pi}_0(\cdot|\mathbf{s})) + \frac{4}{\nu} \left( 1 - e^{-\frac{1}{4}\nu h} \right) \left( \frac{5}{4}\nu\epsilon_{\text{score}} + 12pL_s\sqrt{5\nu h} \right) \\ &\leq e^{-\frac{1}{4}\nu h} \text{KL}(\hat{\pi}_0(\cdot|\mathbf{s})\|\tilde{\pi}_0(\cdot|\mathbf{s})) + \frac{5}{4}\nu\epsilon_{\text{score}}h + 12pL_s\sqrt{5\nu h^2}, \end{aligned} \quad (105)$$

where last equation holds since we use  $1 - e^{-x} \leq x$ , if  $x \geq 0$ .

Recall  $\tilde{\pi}_k(\cdot|\mathbf{s})$  is the distribution at the time  $t = hk$  along the process (4) that starts from  $\tilde{\pi}_0(\cdot|\mathbf{s}) = \bar{\pi}_T(\cdot|\mathbf{s})$ , then  $\tilde{\pi}_k(\cdot|\mathbf{s}) = \bar{\pi}_{T-hk}(\cdot|\mathbf{s})$ .

Recall  $\hat{\pi}_k(\cdot|\mathbf{s})$  is the distribution of the iteration (9) at the  $k$ -th time  $t_k = hk$ , starting from  $\hat{\pi}_0(\cdot|\mathbf{s}) = \mathcal{N}(\mathbf{0}, \mathbf{I})$ .

According to (105), we rename the  $\tilde{\pi}_0(\cdot|\mathbf{s})$  with  $\tilde{\pi}_k(\cdot|\mathbf{s})$ ,  $\tilde{\pi}_h(\cdot|\mathbf{s})$  with  $\tilde{\pi}_{k+1}(\cdot|\mathbf{s})$ ,  $\hat{\pi}_0(\cdot|\mathbf{s})$  with  $\hat{\pi}_k(\cdot|\mathbf{s})$  and  $\hat{\pi}_h(\cdot|\mathbf{s})$  with  $\hat{\pi}_{k+1}(\cdot|\mathbf{s})$ , then we obtain

$$\text{KL}(\hat{\pi}_{k+1}(\cdot|\mathbf{s})\|\tilde{\pi}_{k+1}(\cdot|\mathbf{s})) \leq e^{-\frac{1}{4}\nu h} \text{KL}(\hat{\pi}_k(\cdot|\mathbf{s})\|\tilde{\pi}_k(\cdot|\mathbf{s})) + \frac{5}{4}\nu\epsilon_{\text{score}}h + 12pL_s\sqrt{5\nu h^2},$$

which concludes the result.  $\square$

## E Proof of Theorem 4.3

**Theorem 4.3** (Finite-time Analysis of Diffusion Policy). *For a given state  $\mathbf{s}$ , let  $\{\bar{\pi}_t(\cdot|\mathbf{s})\}_{t=0:T}$  and  $\{\tilde{\pi}_t(\cdot|\mathbf{s})\}_{t=0:T}$  be the distributions along the Ornstein-Uhlenbeck flow (2) and (4) correspondingly, where  $\{\bar{\pi}_t(\cdot|\mathbf{s})\}_{t=0:T}$  starts at  $\bar{\pi}_0(\cdot|\mathbf{s}) = \pi(\cdot|\mathbf{s})$  and  $\{\tilde{\pi}_t(\cdot|\mathbf{s})\}_{t=0:T}$  starts at  $\tilde{\pi}_0(\cdot|\mathbf{s}) = \bar{\pi}_T(\cdot|\mathbf{s})$ . Let  $\hat{\pi}_k(\cdot|\mathbf{s})$  be the distribution of the exponential integrator discretization iteration (9) at the  $k$ -th time  $t_k = hk$ , i.e.,  $\hat{\mathbf{a}}_{t_k} \sim \hat{\pi}_k(\cdot|\mathbf{s})$  denotes the distribution of the diffusion policy (see Algorithms 1) at the time  $t_k = hk$ . Let  $\{\hat{\pi}_k(\cdot|\mathbf{s})\}_{k=0:K}$  be starting at  $\hat{\pi}_0(\cdot|\mathbf{s}) = \mathcal{N}(\mathbf{0}, \mathbf{I})$ , under Assumption 4.1 and 4.2, let the reverse length  $K$  satisfy*

$$K \geq T \cdot \max \left\{ \frac{1}{\tau_0}, \frac{1}{T_0}, 12L_s, \nu \right\},$$

where

$$\tau_0 =: \sup_{t \geq 0} \left\{ t : te^t \leq \frac{\sqrt{5\nu}}{96L_sL_p} \right\}, T_0 =: \sup_{t \geq 0} \left\{ t : 1 - e^{-2t} \leq \frac{e^t}{L_p} \right\}.$$

Then the KL-divergence between the diffusion policy  $\hat{\mathbf{a}}_K \sim \hat{\pi}_K(\cdot|\mathbf{s})$  and input policy  $\pi(\cdot|\mathbf{s})$  is upper-bounded as follows,

$$\begin{aligned} \text{KL}(\hat{\pi}_K(\cdot|\mathbf{s})\|\pi(\cdot|\mathbf{s})) &\leq \underbrace{e^{-\frac{9}{4}\nu hK} \text{KL}(\mathcal{N}(\mathbf{0}, \mathbf{I})\|\pi(\cdot|\mathbf{s}))}_{\text{convergence of forward process}} + \underbrace{64pL_s\sqrt{\frac{5}{\nu}} \cdot \frac{T}{K}}_{\text{errors from discretization}} \\ &\quad + \frac{20}{3} \underbrace{\sup_{(k,t) \in [K] \times [t_k, t_{k+1}]} \left\{ \log \mathbb{E}_{\mathbf{a} \sim \tilde{\pi}_t(\cdot|\mathbf{s})} \left[ \exp \left\| \hat{\mathbf{S}}(\mathbf{a}, \mathbf{s}, T - hk) - \nabla \log \tilde{\pi}_t(\mathbf{a}|\mathbf{s}) \right\|_2^2 \right] \right\}}_{\text{errors from score matching}}. \end{aligned}$$

*Proof.* Recall  $\tilde{\pi}_k(\cdot|\mathbf{s}) = \bar{\pi}_{T-hk}(\cdot|\mathbf{s})$ , then we know

$$\tilde{\pi}_K(\cdot|\mathbf{s}) = \bar{\pi}_{T-hK}(\cdot|\mathbf{s}) = \bar{\pi}_0(\cdot|\mathbf{s}) = \pi(\cdot|\mathbf{s}), \quad (106)$$

then according to Proposition D.9, we know

$$\begin{aligned} \text{KL}(\hat{\pi}_K(\cdot|\mathbf{s})\|\pi(\cdot|\mathbf{s})) &\stackrel{(106)}{=} \text{KL}(\hat{\pi}_K(\cdot|\mathbf{s})\|\tilde{\pi}_K(\cdot|\mathbf{s})) \\ &\leq e^{-\frac{1}{4}\nu K} \text{KL}(\hat{\pi}_0(\cdot|\mathbf{s})\|\tilde{\pi}_0(\cdot|\mathbf{s})) + \sum_{j=0}^{K-1} e^{-\frac{1}{4}\nu hj} \left( \frac{5}{4}\nu\epsilon_{\text{score}}h + 12pL_s\sqrt{5\nu}h^2 \right) \\ &\leq e^{-\frac{1}{4}\nu K} \text{KL}(\hat{\pi}_0(\cdot|\mathbf{s})\|\tilde{\pi}_0(\cdot|\mathbf{s})) + \frac{1}{1 - e^{-\frac{1}{4}\nu h}} \left( \frac{5}{4}\nu\epsilon_{\text{score}}h + 12pL_s\sqrt{5\nu}h^2 \right) \\ &\leq e^{-\frac{1}{4}\nu K} \text{KL}(\hat{\pi}_0(\cdot|\mathbf{s})\|\tilde{\pi}_0(\cdot|\mathbf{s})) + \frac{16}{3\nu h} \left( \frac{5}{4}\nu\epsilon_{\text{score}}h + 12pL_s\sqrt{5\nu}h^2 \right) \quad (107) \end{aligned}$$

$$= e^{-\frac{1}{4}\nu K} \text{KL}(\hat{\pi}_0(\cdot|\mathbf{s})\|\tilde{\pi}_0(\cdot|\mathbf{s})) + \frac{20}{3}\epsilon_{\text{score}} + 64\sqrt{\frac{5}{\nu}}pL_s h, \quad (108)$$

where Eq.(107) holds since we consider the

$$1 - e^{-x} \geq \frac{3}{4}x, \text{ if } 0 < x \leq \frac{1}{4}, \quad (109)$$

and we set the step-size  $h$  satisfies the next condition:

$$h\nu \leq 1, \text{ i.e., } h \leq \frac{1}{\nu}.$$

Let  $\xi(\cdot)$  be standard Gaussian distribution on  $\mathbb{R}^p$ , i.e.,  $\xi(\cdot) \sim \mathcal{N}(\mathbf{0}, \mathbf{I})$ , then we obtain the following result: for a given state  $\mathbf{s}$ ,

$$\begin{aligned} \frac{d}{dt} \text{KL}(\xi(\cdot)\|\bar{\pi}_t(\cdot|\mathbf{s})) &= \frac{d}{dt} \int_{\mathbb{R}^p} \xi(\mathbf{a}) \log \frac{\xi(\mathbf{a})}{\bar{\pi}_t(\mathbf{a}|\mathbf{s})} d\mathbf{a} \\ &= - \int_{\mathbb{R}^p} \frac{\xi(\mathbf{a})}{\bar{\pi}_t(\mathbf{a}|\mathbf{s})} \frac{\partial \bar{\pi}_t(\mathbf{a}|\mathbf{s})}{\partial t} d\mathbf{a} \\ &= - \int_{\mathbb{R}^p} \frac{\xi(\mathbf{a})}{\bar{\pi}_t(\mathbf{a}|\mathbf{s})} \left( \text{div} \cdot \left( \bar{\pi}_t(\mathbf{a}|\mathbf{s}) \nabla \log \frac{\bar{\pi}_t(\mathbf{a}|\mathbf{s})}{\xi(\mathbf{a})} \right) \right) d\mathbf{a} \\ &\quad \blacktriangleright \text{Fokker-Planck Equation} \\ &= \int_{\mathbb{R}^p} \left\langle \nabla \frac{\xi(\mathbf{a})}{\bar{\pi}_t(\mathbf{a}|\mathbf{s})}, \bar{\pi}_t(\mathbf{a}|\mathbf{s}) \nabla \log \frac{\bar{\pi}_t(\mathbf{a}|\mathbf{s})}{\xi(\mathbf{a})} \right\rangle d\mathbf{a} \quad \blacktriangleright \text{Integration by Parts} \\ &= \int_{\mathbb{R}^p} \left\langle \frac{\xi(\mathbf{a})}{\bar{\pi}_t(\mathbf{a}|\mathbf{s})} \nabla \log \frac{\xi(\mathbf{a})}{\bar{\pi}_t(\mathbf{a}|\mathbf{s})}, \bar{\pi}_t(\mathbf{a}|\mathbf{s}) \nabla \log \frac{\bar{\pi}_t(\mathbf{a}|\mathbf{s})}{\xi(\mathbf{a})} \right\rangle d\mathbf{a} \\ &= \int_{\mathbb{R}^p} \xi(\mathbf{a}) \left\langle \nabla \log \frac{\xi(\mathbf{a})}{\bar{\pi}_t(\mathbf{a}|\mathbf{s})}, \nabla \log \frac{\bar{\pi}_t(\mathbf{a}|\mathbf{s})}{\xi(\mathbf{a})} \right\rangle d\mathbf{a} \\ &= - \int_{\mathbb{R}^p} \xi(\mathbf{a}) \left\| \nabla \log \frac{\xi(\mathbf{a})}{\bar{\pi}_t(\mathbf{a}|\mathbf{s})} \right\|_2^2 d\mathbf{a} = -\mathbb{E}_{\mathbf{a} \sim \xi(\cdot)} \left[ \left\| \nabla \log \frac{\xi(\mathbf{a})}{\bar{\pi}_t(\mathbf{a}|\mathbf{s})} \right\|_2^2 \right] \end{aligned}$$

$$\begin{aligned}
&= -\text{FI}(\xi(\cdot) \|\bar{\pi}_t(\cdot|\mathbf{s})) \\
&\leq -2\nu_t \text{KL}(\xi(\cdot) \|\bar{\pi}_t(\cdot|\mathbf{s})) \quad \blacktriangleright \text{Assumption 4.2 and Proposition B.4} \\
&= -\frac{2\nu}{\nu + (1-\nu)e^{-2t}} \text{KL}(\xi(\cdot) \|\bar{\pi}_t(\cdot|\mathbf{s})) \\
&\leq -2\nu \text{KL}(\xi(\cdot) \|\bar{\pi}_t(\cdot|\mathbf{s})), \tag{110}
\end{aligned}$$

where the last equation holds since  $e^{-t} \leq 1$  with  $t \geq 0$ .

Eq.(110) implies

$$\frac{d}{dt} \log \text{KL}(\xi(\cdot) \|\bar{\pi}_t(\cdot|\mathbf{s})) \leq -2\nu,$$

integrating both sides of above equation on the interval  $[0, T]$ , we obtain

$$\text{KL}(\xi(\cdot) \|\bar{\pi}_T(\cdot|\mathbf{s})) \leq e^{-2\nu T} \text{KL}(\xi(\cdot) \|\bar{\pi}_0(\cdot|\mathbf{s})). \tag{111}$$

According to definition of diffusion policy, since:  $\hat{\mathbf{a}}_0 \sim \mathcal{N}(\mathbf{0}, \mathbf{I})$ , and  $\tilde{\pi}_0(\cdot|\mathbf{s}) \stackrel{(5)}{=} \bar{\pi}_T(\cdot|\mathbf{s})$ , then we know

$$\text{KL}(\hat{\pi}_0(\cdot|\mathbf{s}) \|\tilde{\pi}_0(\cdot|\mathbf{s})) = \text{KL}(\xi(\cdot) \|\bar{\pi}_T(\cdot|\mathbf{s})), \tag{112}$$

which implies

$$\text{KL}(\hat{\pi}_0(\cdot|\mathbf{s}) \|\tilde{\pi}_0(\cdot|\mathbf{s})) \stackrel{(112)}{=} \text{KL}(\xi(\cdot) \|\bar{\pi}_T(\cdot|\mathbf{s})) \stackrel{(111)}{\leq} e^{-2\nu T} \text{KL}(\xi(\cdot) \|\bar{\pi}_0(\cdot|\mathbf{s})). \tag{113}$$

Combining (108) and (113), we obtain

$$\begin{aligned}
\text{KL}(\hat{\pi}_K(\cdot|\mathbf{s}) \|\pi(\cdot|\mathbf{s})) &\leq e^{-\frac{1}{4}\nu h K - T} \text{KL}(\xi(\cdot) \|\bar{\pi}_0(\cdot|\mathbf{s})) + \frac{20}{3} \epsilon_{\text{score}} + 64 \sqrt{\frac{5}{\nu}} p L_s h \\
&\stackrel{(106)}{=} e^{-\frac{9}{4}\nu h K} \text{KL}(\mathcal{N}(\mathbf{0}, \mathbf{I}) \|\pi(\cdot|\mathbf{s})) + \frac{20}{3} \epsilon_{\text{score}} + 64 \sqrt{\frac{5}{\nu}} p L_s h. \tag{114}
\end{aligned}$$

Recall the following conditions (101), (102), and (109) on the step-size  $h$ ,

$$h \leq \min \left\{ \tau_0, \mathbb{T}_0, \frac{1}{12L_s}, \frac{1}{\nu} \right\},$$

which implies the reverse length  $K$  satisfy the following condition

$$K = \frac{T}{h} \geq T \cdot \max \left\{ \frac{1}{\tau_0}, \frac{1}{\mathbb{T}_0}, 12L_s, \nu \right\}.$$

Finally, recall the definition of  $\epsilon$  (97), we rewrite (114) as follows

$$\begin{aligned}
\text{KL}(\hat{\pi}_K(\cdot|\mathbf{s}) \|\pi(\cdot|\mathbf{s})) &\leq e^{-\frac{9}{4}\nu h K} \text{KL}(\mathcal{N}(\mathbf{0}, \mathbf{I}) \|\pi(\cdot|\mathbf{s})) + 64 p L_s \sqrt{\frac{5}{\nu}} \cdot \frac{T}{K} \\
&\quad + \frac{20}{3} \sup_{(k,t) \in [K] \times [t_k, t_{k+1}]} \left\{ \log \mathbb{E}_{\mathbf{a} \sim \tilde{\pi}_t(\cdot|\mathbf{s})} \left[ \exp \left\| \hat{\mathbf{S}}(\mathbf{a}, \mathbf{s}, T - hk) - \nabla \log \tilde{\pi}_t(\mathbf{a}|\mathbf{s}) \right\|_2^2 \right] \right\},
\end{aligned}$$

which concludes the proof.  $\square$



## F Additional Details

### F.1 Proof of Lemma F.1

**Lemma F.1.** *Under Assumption 4.1, for all  $0 \leq t' \leq T$ , if  $t \leq \frac{1}{12L_s}$ , then for any given state  $\mathbf{s}$*

$$\left\| \hat{\mathbf{S}}(\hat{\mathbf{a}}_t, \mathbf{s}, t') - \hat{\mathbf{S}}(\hat{\mathbf{a}}_0, \mathbf{s}, t') \right\| \leq 3L_s t \|\hat{\mathbf{a}}_0\| + 6L_s t \left\| \hat{\mathbf{S}}(\hat{\mathbf{a}}_t, \mathbf{s}, t') \right\| + 3L_s \sqrt{t} \|\mathbf{z}\|,$$

and

$$\left\| \hat{\mathbf{S}}(\hat{\mathbf{a}}_t, \mathbf{s}, t') - \hat{\mathbf{S}}(\hat{\mathbf{a}}_0, \mathbf{s}, t') \right\|_2^2 \leq 36L_s^2 t^2 \|\hat{\mathbf{a}}_0\|_2^2 + 72L_s^2 t^2 \left\| \hat{\mathbf{S}}(\hat{\mathbf{a}}_t, \mathbf{s}, t') \right\|_2^2 + 36L_s^2 t \|\mathbf{z}\|_2^2, \quad (115)$$

where  $\hat{\mathbf{a}}_t$  updated according to (91).

*Proof.* (of Lemma F.1). First, we consider

$$\begin{aligned} \left\| \hat{\mathbf{S}}(\hat{\mathbf{a}}_t, \mathbf{s}, t') - \hat{\mathbf{S}}(\hat{\mathbf{a}}_0, \mathbf{s}, t') \right\| &\leq L_s \|\hat{\mathbf{a}}_t - \hat{\mathbf{a}}_0\| \\ &= \left\| (e^t - 1)\hat{\mathbf{a}}_0 + 2(e^t - 1)\hat{\mathbf{S}}(\hat{\mathbf{a}}_0, \mathbf{s}, t') + \sqrt{e^t - 1}\mathbf{z} \right\| \\ &\leq 2L_s t \|\hat{\mathbf{a}}_0\|_2^2 + 4L_s t \left\| \hat{\mathbf{S}}(\hat{\mathbf{a}}_0, \mathbf{s}, t') \right\| + 2L_s \sqrt{t} \|\mathbf{z}\|, \end{aligned} \quad (116)$$

where the last equation holds due to  $e^t - 1 \leq 2t$ .

Furthermore, we consider the case with  $t \leq \frac{1}{12L_s}$ , then we obtain the boundedness of the term

$$\begin{aligned} \left\| \hat{\mathbf{S}}(\hat{\mathbf{a}}_0, \mathbf{s}, t') \right\| &\leq \left\| \hat{\mathbf{S}}(\hat{\mathbf{a}}_t, \mathbf{s}, t') \right\| + L_s \|\hat{\mathbf{a}}_t - \hat{\mathbf{a}}_0\| \\ &\leq \left\| \hat{\mathbf{S}}(\hat{\mathbf{a}}_t, \mathbf{s}, t') \right\| + 2L_s t \|\hat{\mathbf{a}}_0\| + 4L_s t \left\| \hat{\mathbf{S}}(\hat{\mathbf{a}}_0, \mathbf{s}, t') \right\| + 2L_s \sqrt{t} \|\mathbf{z}\| \\ &\leq \left\| \hat{\mathbf{S}}(\hat{\mathbf{a}}_t, \mathbf{s}, t') \right\| + 2L_s t \|\hat{\mathbf{a}}_0\| + \frac{1}{3} \left\| \hat{\mathbf{S}}(\hat{\mathbf{a}}_0, \mathbf{s}, t') \right\| + 2L_s \sqrt{t} \|\mathbf{z}\|, \end{aligned}$$

which implies

$$\left\| \hat{\mathbf{S}}(\hat{\mathbf{a}}_0, \mathbf{s}, t') \right\| \leq \frac{3}{2} \left\| \hat{\mathbf{S}}(\hat{\mathbf{a}}_t, \mathbf{s}, t') \right\| + 3L_s t \|\hat{\mathbf{a}}_0\|_2^2 + 3L_s \sqrt{t} \|\mathbf{z}\|. \quad (117)$$

Taking Eq.(117) into Eq.(116), and with  $t \leq \frac{1}{12L_s}$ , we obtain

$$\left\| \hat{\mathbf{S}}(\hat{\mathbf{a}}_t, \mathbf{s}, t') - \hat{\mathbf{S}}(\hat{\mathbf{a}}_0, \mathbf{s}, t') \right\| \leq 3L_s t \|\hat{\mathbf{a}}_0\| + 6L_s t \left\| \hat{\mathbf{S}}(\hat{\mathbf{a}}_t, \mathbf{s}, t') \right\| + 3L_s \sqrt{t} \|\mathbf{z}\|.$$

Finally, we know

$$\left\| \hat{\mathbf{S}}(\hat{\mathbf{a}}_t, \mathbf{s}, t') - \hat{\mathbf{S}}(\hat{\mathbf{a}}_0, \mathbf{s}, t') \right\|_2^2 \leq 36L_s^2 t^2 \|\hat{\mathbf{a}}_0\|_2^2 + 72L_s^2 t^2 \left\| \hat{\mathbf{S}}(\hat{\mathbf{a}}_t, \mathbf{s}, t') \right\|_2^2 + 36L_s^2 t \|\mathbf{z}\|_2^2, \quad (118)$$

which concludes the proof of Lemma F.1.  $\square$

## F.2 Proof of Lemma D.7

*Proof.*(Lemma D.7) Recall the update rule of  $\hat{\mathbf{a}}_t$  (91),

$$\hat{\mathbf{a}}_t = e^t \hat{\mathbf{a}}_0 + 2(e^t - 1) \hat{\mathbf{S}}(\hat{\mathbf{a}}_0, \mathbf{s}, T) + \sqrt{e^t - 1} \mathbf{z}, \quad \mathbf{z} \sim \mathcal{N}(\mathbf{0}, \mathbf{I}).$$

To simplify the expression, in this section, we introduce the following notation

$$\mathbf{z} \sim \rho_z(\cdot), \quad \text{where } \rho_z(\cdot) = \mathcal{N}(\mathbf{0}, \mathbf{I}). \quad (119)$$

According to the definition of  $\rho_{0,t}(\hat{\mathbf{a}}_0, \hat{\mathbf{a}}_t | \mathbf{s})$  (81), we denote  $\hat{\mathbf{a}}_t = \mathbf{a}$ , then we know,

$$\begin{aligned} & \int_{\mathbb{R}^p} \int_{\mathbb{R}^p} \rho_{0,t}(\hat{\mathbf{a}}_0, \mathbf{a} | \mathbf{s}) \left\| \hat{\mathbf{S}}(\hat{\mathbf{a}}_0, \mathbf{s}, T) - \nabla \log \tilde{\pi}_t(\mathbf{a} | \mathbf{s}) \right\|_2^2 d\mathbf{a} d\hat{\mathbf{a}}_0 \\ \leq & 2 \int_{\mathbb{R}^p} \int_{\mathbb{R}^p} \rho_{0,t}(\hat{\mathbf{a}}_0, \mathbf{a} | \mathbf{s}) \left( \left\| \hat{\mathbf{S}}(\hat{\mathbf{a}}_0, \mathbf{s}, T) - \hat{\mathbf{S}}(\hat{\mathbf{a}}_t, \mathbf{s}, T) \right\|_2^2 + \left\| \hat{\mathbf{S}}(\hat{\mathbf{a}}_t, \mathbf{s}, T) - \nabla \log \tilde{\pi}_t(\mathbf{a} | \mathbf{s}) \right\|_2^2 \right) d\mathbf{a} d\hat{\mathbf{a}}_0 \\ = & 2 \int_{\mathbb{R}^p} \int_{\mathbb{R}^p} \rho_{0,t}(\hat{\mathbf{a}}_0, \mathbf{a} | \mathbf{s}) \left( \left\| \hat{\mathbf{S}}(\hat{\mathbf{a}}_0, \mathbf{s}, T) - \hat{\mathbf{S}}(\mathbf{a}, \mathbf{s}, T) \right\|_2^2 + \left\| \hat{\mathbf{S}}(\mathbf{a}, \mathbf{s}, T) - \nabla \log \tilde{\pi}_t(\mathbf{a} | \mathbf{s}) \right\|_2^2 \right) d\mathbf{a} d\hat{\mathbf{a}}_0 \end{aligned}$$

Recall Lemma F.1, we know

$$\begin{aligned} & \int_{\mathbb{R}^p} \int_{\mathbb{R}^p} \rho_{0,t}(\hat{\mathbf{a}}_0, \mathbf{a} | \mathbf{s}) \left\| \hat{\mathbf{S}}(\hat{\mathbf{a}}_0, \mathbf{s}, T) - \hat{\mathbf{S}}(\mathbf{a}, \mathbf{s}, T) \right\|_2^2 d\mathbf{a} d\hat{\mathbf{a}}_0 \\ \stackrel{(115)}{\leq} & \int_{\mathbb{R}^p} \int_{\mathbb{R}^p} \int_{\mathbb{R}^p} \rho_{0,t}(\hat{\mathbf{a}}_0, \mathbf{a} | \mathbf{s}) \rho_z(\mathbf{z}) \left( 36L_s^2 t^2 \|\hat{\mathbf{a}}_0\|_2^2 + 72L_s^2 t^2 \left\| \hat{\mathbf{S}}(\mathbf{a}, \mathbf{s}, T) \right\|_2^2 + 36L_s^2 t \|\mathbf{z}\|_2^2 \right) d\mathbf{a} d\hat{\mathbf{a}}_0 d\mathbf{z} \\ = & \int_{\mathbb{R}^p} \int_{\mathbb{R}^p} \int_{\mathbb{R}^p} \rho_{0,t}(\hat{\mathbf{a}}_0, \mathbf{a} | \mathbf{s}) \rho_z(\mathbf{z}) \left( 36L_s^2 t^2 \|\hat{\mathbf{a}}_0\|_2^2 + 72L_s^2 t^2 \left\| \hat{\mathbf{S}}(\mathbf{a}, \mathbf{s}, T) \right\|_2^2 \right) d\mathbf{a} d\hat{\mathbf{a}}_0 d\mathbf{z} \end{aligned}$$

$$\begin{aligned} & + 36L_s^2 t \int_{\mathbb{R}^p} \int_{\mathbb{R}^p} \int_{\mathbb{R}^p} \rho_{0,t}(\hat{\mathbf{a}}_0, \mathbf{a} | \mathbf{s}) \rho_z(\mathbf{z}) \|\mathbf{z}\|_2^2 d\mathbf{a} d\hat{\mathbf{a}}_0 d\mathbf{z} \\ = & 36L_s^2 t^2 \int_{\mathbb{R}^p} \hat{\pi}_0(\hat{\mathbf{a}}_0 | \mathbf{s}) \|\hat{\mathbf{a}}_0\|_2^2 d\hat{\mathbf{a}}_0 + 72L_s^2 t^2 \int_{\mathbb{R}^p} \hat{\pi}_t(\mathbf{a} | \mathbf{s}) \left\| \hat{\mathbf{S}}(\mathbf{a}, \mathbf{s}, T) \right\|_2^2 d\mathbf{a} + 36L_s^2 p t \quad (120) \end{aligned}$$

$$= 36L_s^2 p t^2 + 72L_s^2 t^2 \int_{\mathbb{R}^p} \hat{\pi}_t(\mathbf{a} | \mathbf{s}) \left\| \hat{\mathbf{S}}(\mathbf{a}, \mathbf{s}, T) \right\|_2^2 d\mathbf{a} + 36L_s^2 p t \quad (121)$$

$$\leq 36p t (1+t) L_s^2 + 144t^2 L_s^2 \int_{\mathbb{R}^p} \hat{\pi}_t(\mathbf{a} | \mathbf{s}) \left( \left\| \hat{\mathbf{S}}(\mathbf{a}, \mathbf{s}, T) - \nabla \log \tilde{\pi}_t(\mathbf{a} | \mathbf{s}) \right\|_2^2 + \left\| \nabla \log \tilde{\pi}_t(\mathbf{a} | \mathbf{s}) \right\|_2^2 \right) d\mathbf{a}, \quad (122)$$

where the first term in Eq.(120) holds since:

$$\int_{\mathbb{R}^p} \int_{\mathbb{R}^p} \rho_{0,t}(\hat{\mathbf{a}}_0, \mathbf{a} | \mathbf{s}) \rho_z(\mathbf{z}) d\mathbf{a} d\mathbf{z} = \hat{\pi}_0(\hat{\mathbf{a}}_0 | \mathbf{s});$$

the second term in Eq.(120) holds since:

$$\int_{\mathbb{R}^p} \int_{\mathbb{R}^p} \int_{\mathbb{R}^p} \rho_{0,t}(\hat{\mathbf{a}}_0, \mathbf{a} | \mathbf{s}) \rho_z(\mathbf{z}) d\hat{\mathbf{a}}_0 d\mathbf{z} = \hat{\pi}_t(\mathbf{a} | \mathbf{s});$$

the third term in Eq.(120) holds since:  $\mathbf{z} \sim \mathcal{N}(\mathbf{0}, \mathbf{I})$ , then  $\|\mathbf{z}\|_2^2 \sim \chi^2(p)$ -distribution with  $p$  degrees of freedom, then

$$\int_{\mathbb{R}^p} \int_{\mathbb{R}^p} \int_{\mathbb{R}^p} \rho_{0,t}(\hat{\mathbf{a}}_0, \mathbf{a}|\mathbf{s}) \rho_z(\mathbf{z}) \|\mathbf{z}\|_2^2 d\mathbf{a} d\hat{\mathbf{a}}_0 d\mathbf{z} = p; \quad (123)$$

Eq.(121) holds with the same analysis of (123), since  $\hat{\mathbf{a}}_0 \sim \mathcal{N}(\mathbf{0}, \mathbf{I})$ , then  $\|\hat{\mathbf{a}}_0\|_2^2 \sim \chi^2(p)$ , which implies

$$\int_{\mathbb{R}^p} \hat{\pi}_0(\hat{\mathbf{a}}_0|\mathbf{s}) \|\hat{\mathbf{a}}_0\|_2^2 d\hat{\mathbf{a}}_0 = p;$$

Eq.(122) holds since we use the fact:  $\|\langle \boldsymbol{\alpha} + \boldsymbol{\beta} \rangle\|_2^2 \leq 2\|\boldsymbol{\alpha}\|_2^2 + 2\|\boldsymbol{\beta}\|_2^2$ . □

## G Details and Discussions for multimodal Experiments

In this section, we present all the implementation details and the plots of both 2D and 3D Visualization. Then we provide additional discussions for empirical results of the task of the multimodal environment in Section 3.2.

### G.1 Multimodal Environment

In this section, we clarify the task and reward of the multimodal environment.

#### G.1.1 Task

We design a simple “multi-goal” environment according to the *Didactic Example* [Haarnoja et al., 2017], in which the agent is a 2D point mass on the  $7 \times 7$  plane, and the agent tries to reach one of four points  $(0, 5)$ ,  $(0, -5)$ ,  $(5, 0)$  and  $(-5, 0)$  symmetrically placed goals.

#### G.1.2 Reward

The reward is defined according to the following three parts:

$$R = r_1 + r_2 + r_3,$$

where

- $r_1 \propto -\|\mathbf{a}\|_2^2$  if agent plays the action  $\mathbf{a}$ ;
- $r_2 = -\min\{\|(x, y) - \mathbf{target}\|_2^2\}$ ,  $\mathbf{target}$  denotes one of the target points  $(0, 5)$ ,  $(0, -5)$ ,  $(5, 0)$ , and  $(-5, 0)$ ;
- if the agent reaches one of the targets among  $\{(0, 5), (0, -5), (5, 0), (-5, 0)\}$ , then it receives a reward  $r_3 = 10$ .

Since the goal positions are symmetrically distributed at the four points  $(0, 5)$ ,  $(0, -5)$ ,  $(5, 0)$  and  $(-5, 0)$ , a reasonable policy should be able to take actions uniformly to those four goal positions with the same probability, which characters the capacity of exploration of a policy to understand the environment. Furthermore, we know that the shape of the reward curve should be symmetrical with four equal peaks.

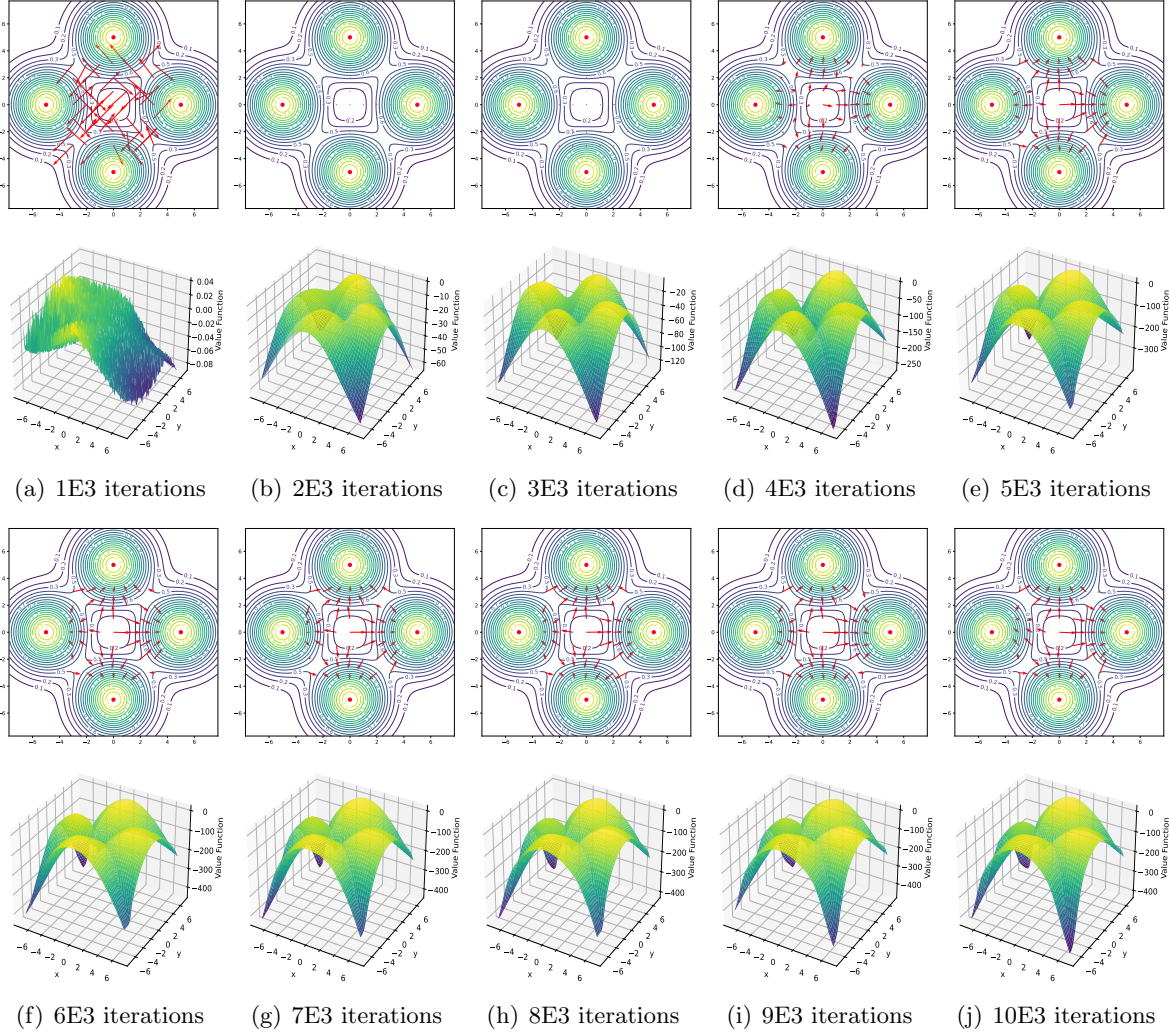


Figure 11: Policy representation comparison of diffusion policy with different iterations.

## G.2 Plots Details of Visualization

This section presents all the details of the 2D and 3D visualization for the multi-goal task. At the end of this section, we present the shape of the reward curve.

### G.2.1 2D Visualization

For the 2D visualization, the red arrowheads denote actions learned by the corresponding RL algorithms, where each action starts at one of the totals of  $7 \times 7 = 49$  points (corresponding to all the states) with horizontal and vertical coordinates ranges among  $\{-3, -2, -1, 0, 1, 2, 3\} \times \{-3, -2, -1, 0, 1, 2, 3\}$ . The length of the red arrowheads denotes the length of the action vector, and the direction of the red arrowheads denotes the direction of actions. This is to say; for each figure, we plot all the actions starting from the same coordinate points.

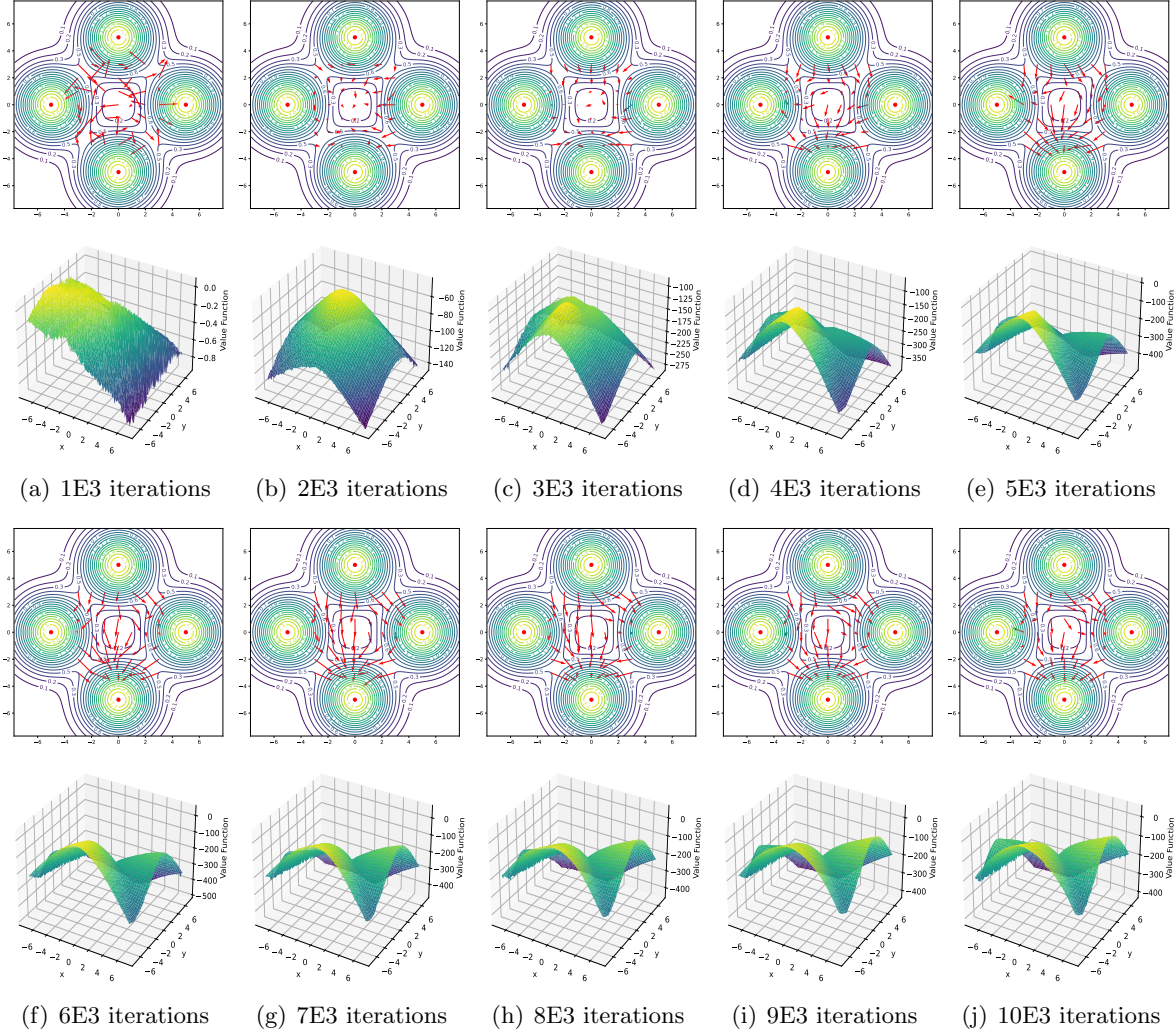


Figure 12: Policy representation comparison of SAC with different iterations.

### G.2.2 3D Visualization

For the 3D visualization, we provide a decomposition of the the region  $[-7, 7] \times [-7, 7]$  into  $100 \times 100 = 10000$  points, each point  $(x, y) \in [-7, 7] \times [-7, 7]$  denotes a state. For each state  $(x, y)$ , a corresponding action is learned by its corresponding RL algorithms, denoted as  $\mathbf{a}$ . Then according to the critic neural network, we obtain the state-action value function  $Q$  value of the corresponding point  $((x, y), \mathbf{a})$ . The 3D visualization shows the state-action  $Q$  (for PPO, is value function  $V$ ) with respect to the states.

### G.2.3 Shape of Reward Curve

Since the shape of the reward curve is symmetrical with four equal peaks, the 2D visualization presents the distribution of actions toward those four equal peaks. A good algorithm should take actions with a uniform distribution toward those four points  $(0, 5)$ ,  $(0, -5)$ ,  $(5, 0)$ , and  $(-5, 0)$  on the 2D visualization. The 3D visualization presents the learned shape according to the algorithm during the learning process. A good algorithm should fit the symmetrical reward

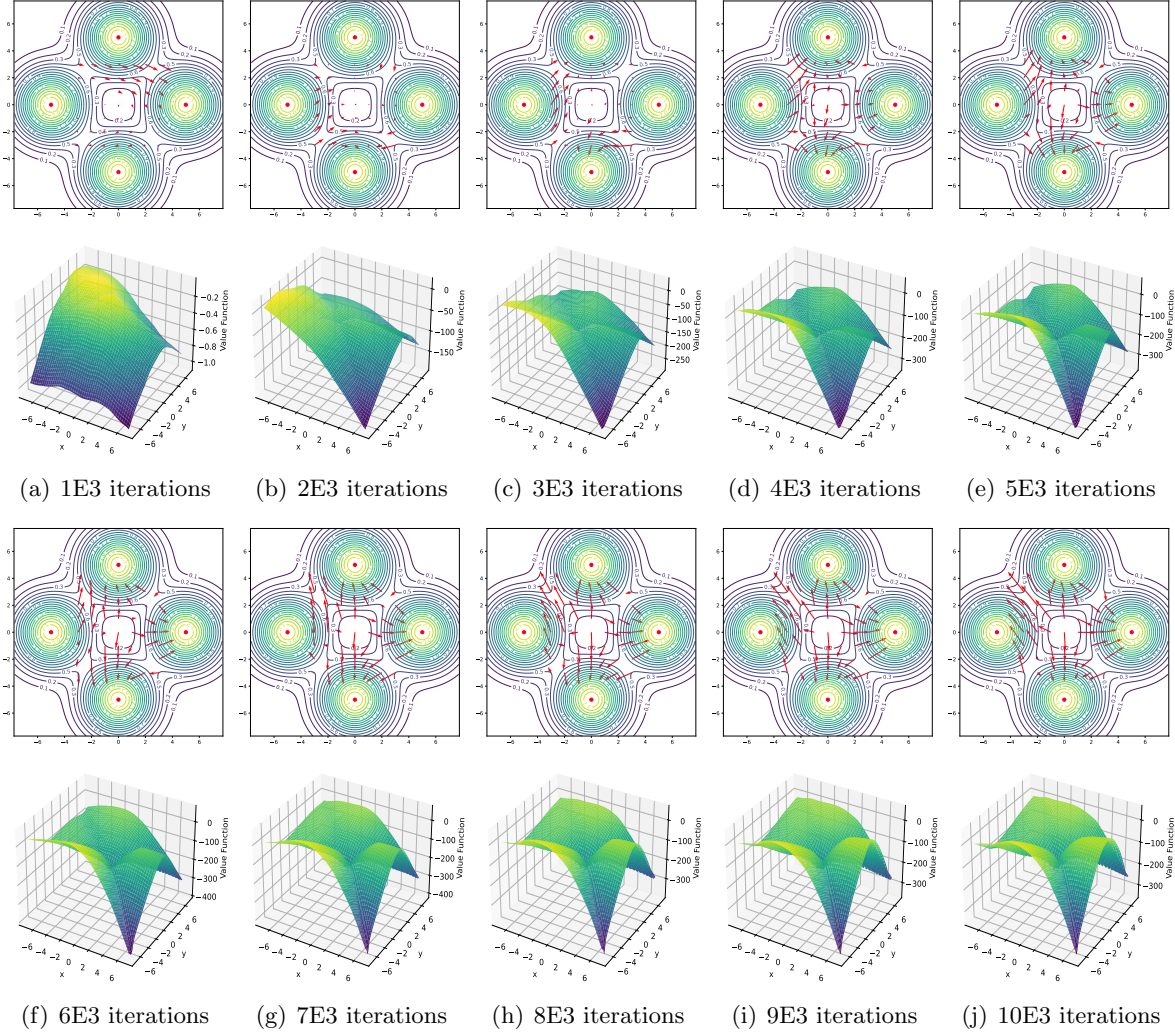


Figure 13: Policy representation comparison of TD3 with different iterations.

shape with four equal peaks. A multimodal policy distribution is efficient for exploration, which may lead an agent to learn a good policy and perform better. Thus, both 2D and 3D visualizations character the algorithm’s capacity to represent the multimodal policy distribution.

### G.3 Results Report

We have shown all the results in Figure 11 (for diffusion policy), 12 (for SAC), 13 (for TD3) and 14 (for PPO), where we train the policy with a total 10000 iterations, and show the 2D and 3D visualization every 1000 iteration.

Figure 11 shows that the diffusion policy accurately captures a multimodal distribution landscape of reward, while from Figure 12, 13, and 14, we know that both SAC, TD3, and PPO are not well suited to capture such multimodality. Comparing Figure 11 to Figure 12 and 13, we know that although SAC and TD3 share a similar best reward performance, where both diffusion policy and SAC and TD3 keep the highest reward around  $-20$ , diffusion policy matches the real environment and performance shape.

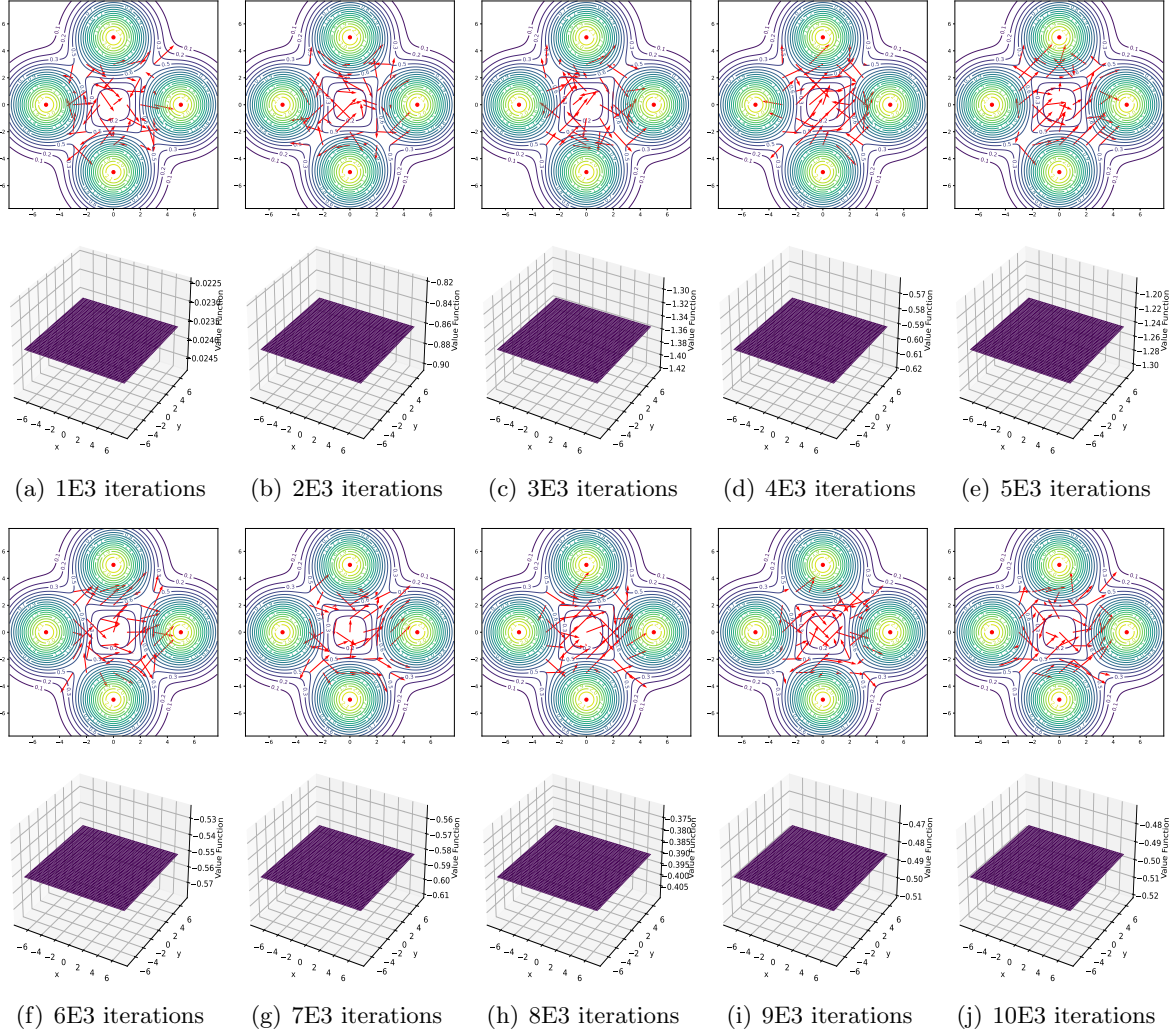


Figure 14: Policy representation comparison of PPO with different iterations.

From Figure 14, we also find PPO always runs around at the initial value, and it does not improve the reward performance, which implies PPO fails to fit multimodality. It does not learn any information about multimodality.

From the distributions of action directions and lengths, we also know the diffusion policy keeps a more gradual and steady action size than the SAC, TD3, and PPO to learn the multimodal reward performance. Thus, the diffusion model is a powerful policy representation that leads to a more sufficient exploration and better performance, which is our motivation to consider representing policy via the diffusion model.

## H Additional Experiments

In this section, we provide additional details about the experiments, including Hyper-parameters of all the algorithms; additional tricks for implementation of DIPO; details and additional reports for state-visiting; and ablation study on MLP and VAE.

The Python code for our implementation of DIPO is provided along with this submission in the supplementary material. SAC: <https://github.com/toshikwa/soft-actor-critic.pytorch> PPO: <https://github.com/ikostrikov/pytorch-a2c-ppo-acktr-gail> TD3: <https://github.com/sfujim/TD3>, which were official code library.

### H.1 Hyper-parameters for MuJoCo

Common Hyper-parameters:

Hyperparameter	DIPO	SAC	TD3	PPO
No. of hidden layers	2	2	2	2
No. of hidden nodes	256	256	256	256
Activation	mish	relu	relu	tanh
Batch size	256	256	256	256
Discount for reward $\gamma$	0.99	0.99	0.99	0.99
Target smoothing coefficient $\tau$	0.005	0.005	0.005	0.005
Learning rate for actor	$3 \times 10^{-4}$	$3 \times 10^{-4}$	$3 \times 10^{-4}$	$7 \times 10^{-4}$
Learning rate for critic	$3 \times 10^{-4}$	$3 \times 10^{-4}$	$3 \times 10^{-4}$	$7 \times 10^{-4}$
Actor Critic grad norm	2	N/A	N/A	0.5
Memeroy size	$1 \times 10^6$	$1 \times 10^6$	$1 \times 10^6$	$1 \times 10^6$
Entropy coefficient	N/A	0.2	N/A	0.01
Value loss coefficient	N/A	N/A	N/A	0.5
Exploration noise	N/A	N/A	$\mathcal{N}(0, 0.1)$	N/A
Policy noise	N/A	N/A	$\mathcal{N}(0, 0.2)$	N/A
Noise clip	N/A	N/A	0.5	N/A
Use gae	N/A	N/A	N/A	True

Table 2: Hyper-parameters for algorithms.

Additional Hyper-parameters of DIPO:

Hyperparameter	Hopper-v3	Walker2d-v3	Ant-v3	HalfCheetah-v3	Humanoid-v3
Learning rate for action	0.03	0.03	0.03	0.03	0.03
Actor Critic grad norm	1	2	0.8	2	2
Action grad norm ratio	0.3	0.08	0.1	0.08	0.1
Action gradient steps	20	20	20	40	20
Diffusion inference timesteps	100	100	100	100	100
Diffusion beta schedule	cosine	cosine	cosine	cosine	cosine
Update actor target every	1	1	1	2	1

Table 3: Hyper-parameters of DIPO.



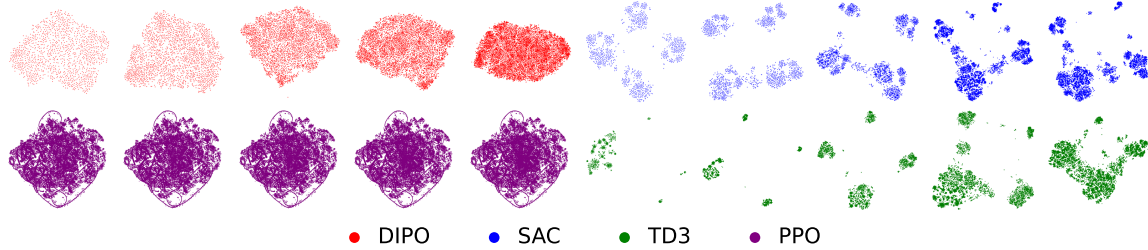


Figure 15: State-visiting distribution of Humanoid-v3, where states get dimension reduction by t-SNE. The points with different colors represent the states visited by the policy with the style. The distance between points represents the difference between states.

## H.2 Additional Tricks for Implementation of DIPO

We have provided the additional details for the Algorithm 3.

### H.2.1 Double Q-learning for Estimating Q-Value

We consider the double Q-learning [Hasselt, 2010] to update the  $Q$  value. We consider the two critic networks  $Q_{\psi_1}, Q_{\psi_2}$ , two target networks  $Q_{\psi'_1}, Q_{\psi'_2}$ . Let Bellman residual be as follows,

$$\mathcal{L}_Q(\psi) = \mathbb{E}_{(\mathbf{s}_t, \mathbf{a}_t, \mathbf{s}_{t+1}, \mathbf{a}_{t+1})} \left[ \left\| \left( r(\mathbf{s}_{t+1} | \mathbf{s}_t, \mathbf{a}_t) + \gamma \min_{i=1,2} Q_{\psi'_i}(\mathbf{s}_{t+1}, \mathbf{a}_{t+1}) \right) - Q_{\psi}(\mathbf{s}_t, \mathbf{a}_t) \right\|^2 \right].$$

Then, we update  $\psi_i$  as follows, for  $i \in \{1, 2\}$

$$\psi_i \leftarrow \psi_i - \eta \nabla \mathcal{L}_Q(\psi_i).$$

Furthermore, we consider the following soft update rule for  $\psi'_i$  as follows,

$$\psi'_i \leftarrow \rho \psi'_i + (1 - \rho) \psi_i.$$

Finally, for the action gradient step, we consider the following update rule: replacing each action  $\mathbf{a}_t \in \mathcal{D}_{\text{env}}$  as follows

$$\mathbf{a}_t \leftarrow \mathbf{a}_t + \eta_a \nabla_{\mathbf{a}} \left( \min_{i=1,2} \{Q_{\psi_i}(\mathbf{s}_t, \mathbf{a})\} \right) \Big|_{\mathbf{a}=\mathbf{a}_t}.$$

### H.2.2 Critic and Diffusion Model

We use a four-layer feedforward neural network of 256 hidden nodes, with activation function Mish [Misra, 2019] between each layer, to design the two critic networks  $Q_{\psi_1}, Q_{\psi_2}$  two target networks  $Q_{\psi'_1}, Q_{\psi'_2}$ , and the noise term  $\epsilon_\phi$ . We consider gradient normalization for critic and  $\epsilon_\phi$  to stabilize the training process.

For each reverse time  $k \in [K]$ , we consider the sinusoidal positional encoding [Vaswani et al., 2017] to encode each  $k \in [K]$  into a 32-dimensional vector.

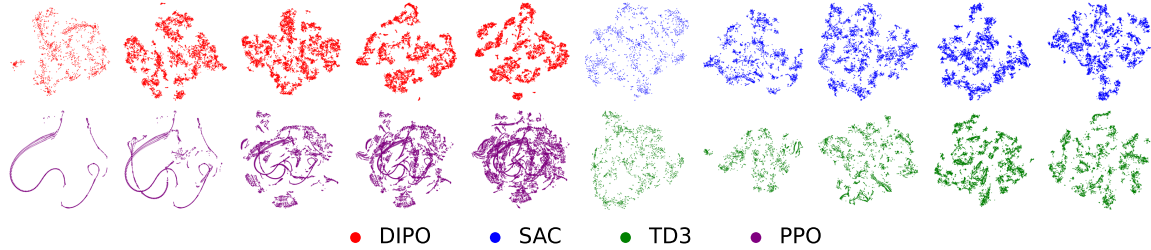


Figure 16: State-visiting distribution of Walker2d-v3, where states get dimension reduction by t-SNE. The points with different colors represent the states visited by the policy with the style. The distance between points represents the difference between states.

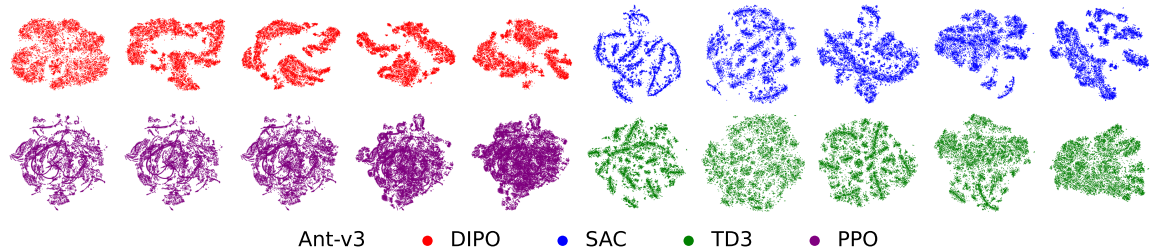


Figure 17: State-visiting visualization by each algorithm on the Ant-v3 task, where states get dimension reduction by t-SNE. The points with different colors represent the states visited by the policy with the style. The distance between points represents the difference between states.

### H.3 Details and Additional Reports for State-Visiting

In this section, we provide more details for Section 7.1, including the implementation details (see Appendix H.3.1), more comparisons and more insights for the empirical results. We provide the main discussions cover the following three observations:

- poor exploration results in poor initial reward performance;
- good final reward performance along with dense state-visiting;
- a counterexample: PPO violates the above two observations.

#### H.3.1 Implementation Details for 2D State-Visiting

We save the parameters for each algorithm during the training for each  $1E5$  iteration. Then we run the model with an episode with ten random seeds to compare fairly; those ten random seeds are the same among different algorithms. Thus, we collect a state set with ten episodes for each algorithm. Finally, we convert high-dimensional state data into two-dimensional state data by t-SNE [Van der Maaten and Hinton, 2008], and we show the visualization according to the open implementation [https://scikit-learn.org/stable/auto\\_examples/manifold/plot\\_t\\_sne\\_perplexity.html](https://scikit-learn.org/stable/auto_examples/manifold/plot_t_sne_perplexity.html) where we set the parameters as follows,

$$\text{perplexity} = 50, \text{early\_exaggeration} = 12, \text{random\_state} = 33.$$

We have shown all the results in Figure 15 (for Humanoid); Figure 16 (for Walker2d); Figure 17 (for Ant); Figure 18 (for HalfCheetah); and Figure 19 (for Hopper), where we plot the result after each  $E5$  iterations.

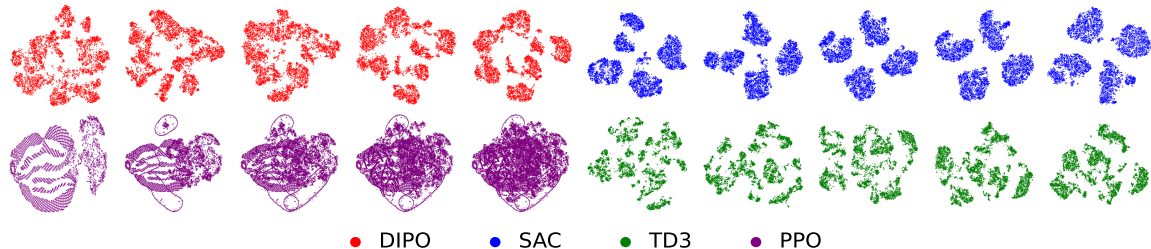


Figure 18: The state-visiting visualization by each algorithm on the HalfCheetah-v3 task, where states get dimension reduction by t-SNE. The points with different colors represent the states visited by the policy with the style. The distance between points represents the difference between states.

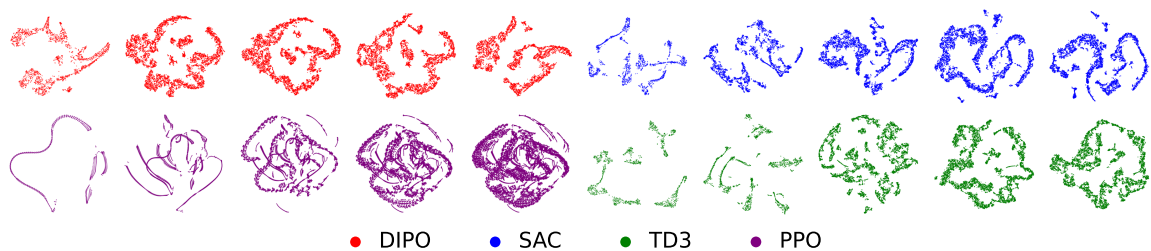


Figure 19: State-visiting distribution of Hopper-v3, where states get dimension reduction by t-SNE. The points with different colors represent the states visited by the policy with the style. The distance between points represents the difference between states.

### H.3.2 Observation 1: Poor Exploration Result in Poor Initial Reward Performance

From Figure 6, we know TD3 and PPO reach a worse initial reward performance than DIPO and SAC for the Hopper task, which coincides with the results appear in Figure 19. At the initial interaction, TD3 and PPO explore within a very sparse state-visiting region, which decays the reward performance. Such an empirical result also appears in the Walker2d task for PPO (see Figure 16), Humanoid task for TD3 and SAC (see Figure 15), where a sparse state-visiting is always accompanied by a worse initial reward performance. Those empirical results once again confirm a common sense: poor exploration results in poor initial reward performance.

Conversely, from Figure 6, we know DIPO and SAC obtain a better initial reward performance for the Hopper task, and Figure 19 shows that DIPO and SAC explore a wider range of state-visiting that covers than TD3 and PPO. That implies that a wide state visit leads to better initial reward performance. Such an empirical result also appears in the Walker2d task for DIPO, SAC, and TD3 (see Figure 16), Humanoid task for DIPO (see Figure 15), where the agent runs with a wider range state-visiting, which is helpful to the agent obtains a better initial reward performance.

In summary, poor exploration could make the agent make a poor decision and cause a poor initial reward performance. While if the agent explores a wider range of regions to visit more states, which is helpful for the agent to understand the environment and could lead to better initial reward performance.

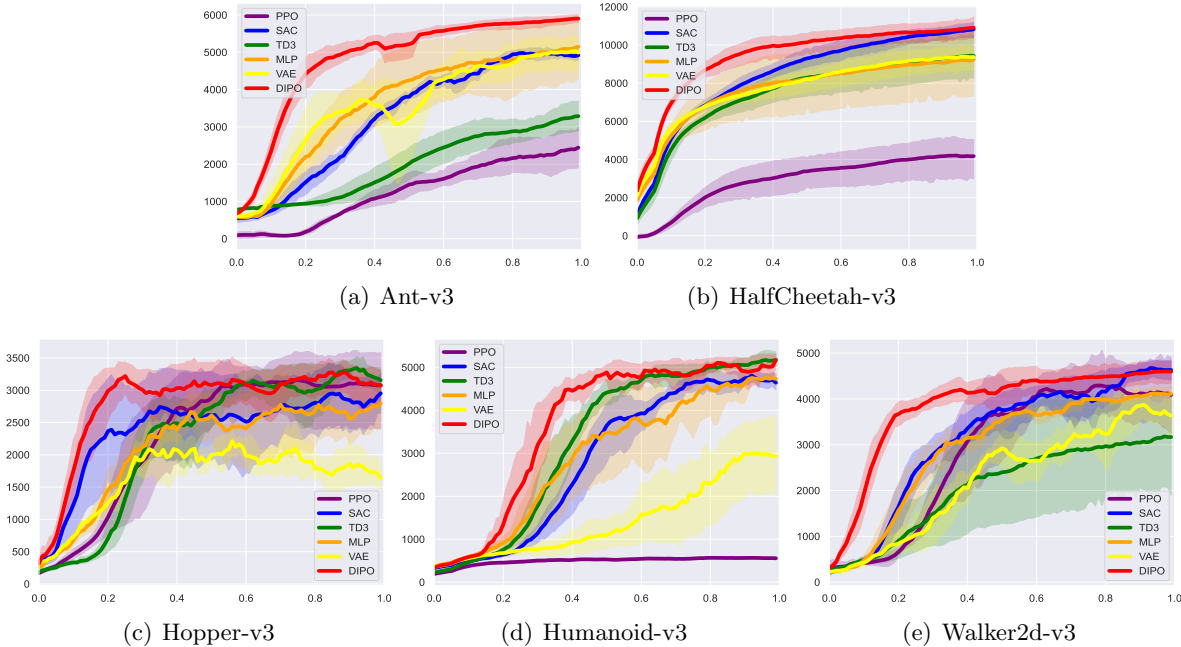


Figure 20: Average performances on MuJoCo Gym environments with  $\pm$  std shaded, where the horizontal axis of coordinate denotes the iterations ( $\times 10^6$ ), the plots smoothed with a window of 10.

### H.3.3 Observation 2: Good Final Reward Performance along with Dense State-Visiting

From Figure 19, we know DIPO, SAC, and TD3 achieve a more dense state-visiting for the Hopper task at the final iterations. Such an empirical result also appears in the Walker2d and Humanoid tasks for DIPO, SAC, and TD3 (see Figure 15 and 16). This is a reasonable result since after sufficient training, the agent identifies and avoids the "bad" states, and plays actions to transfer to "good" states. Besides, this observation is also consistent with the result that appears in Figure 6, the better algorithm (e.g., the proposed DIPO) usually visits a more narrow and dense state region at the final iterations. On the contrary, PPO shows an aimless exploration among the Ant-v3 task (see Figure 7) and HalfCheetah (see Figure 8), which provides a partial explanation for why PPO is not so good in the Ant-v3 and HalfCheetah task. This is a natural result for RL since a better algorithm should keep a better exploration at the beginning and a more sufficient exploitation at the final iterations.

### H.3.4 Observation 3: PPO Violates above Two Observations

From all of those 5 tasks (see Figure 15 to 19), we also find PPO violates the common sense of RL, where PPO usual with a narrow state-visiting at the beginning and wide state-visiting at the final iteration. For example, from Figure 6 and 19, we know PPO achieves an asymptotic reward performance as DIPO for the Hopper-v3, while the state-visiting distribution of PPO is fundamentally different from DIPO. DIPO shows a wide state-visiting region gradually turns into a narrow state-visiting region, while PPO shows a narrow state-visiting region gradually turns into a wide state-visiting region. We show the fair visualization with t-SNE by the same setting for all of those 5 tasks, the abnormal empirical results show that PPO may find some

new views different from DIPO/TD3/SAC to understand the environment.

#### H.4 Ablation Study on MLP and VAE

A fundamental question is why must we consider the diffusion model to learn a policy distribution. In fact, Both VAE and MLP are widely used to learn distribution in machine learning, can we replace the diffusion model with VAE and MLP in DIPO? In this section, we further analyze the empirical reward performance among DIPO, MLP, and VAE.

We show the answer in Figure 9 and Figure 20, where the VAE (or MLP) is the result we replace the diffusion policy of DIPO (see Figure 3) with VAE (or MLP), i.e., we consider VAE (or MLP)+action gradient (15) for the tasks.

Results of Figure 20 show that the diffusion model achieves the best reward performance among all 5 tasks. This implies the diffusion model is an expressive and flexible family to model a distribution, which is also consistent with the field of the generative model.

Additionally, from the results of Figure 20 we know MLP with action gradient also performs well among all 5 tasks, which implies the action gradient is a very promising way to improve reward performance. For example, Humanoid-v3 is the most challenging task among Mujoco tasks, MLP achieves a final reward performance near the PPO, SAC, DIPO, and TD3. We all know that these algorithms (PPO, SAC, DIPO, and TD3) are meticulously constructed mathematically, while MLP with action gradient is a simple model, but it achieves so good reward performance, which is a direction worth further in-depth research to search simple but efficient RL algorithm.